JAERI-M
93-073

EXPERIMENTAL AND ANALYTICAL STUDIES OF HIGH HEAT FLUX COMPONENTS FOR FUSION EXPERIMENTAL REACTOR

March 1993

Masanori ARAKI

日本原子力研究所
Japan Atomic Energy Research Institute

JAERI-Mレポートは，日本原子力研究所が不定期に公刊している研究報告書です。
入手の問合わせは，日本原子力研究所技術情報部情報資料課（〒319－11茨城県那珂郡東海村）あて，お申しこしください。なお，このほかに財団法人原子力弘済会資料センター（〒319-11茨城県那珂郡東海村日本原子力研究所内）で複写による実費頒布をおこなっております。

JAERI-M reports are issued irregularly.
Inquiries about availability of the reports should be addressed to Information Division, Department of Technical Information, Japan Atomic Energy Research Institute, Tokai-mura, Naka-gun, Ibaraki-ken 319-11, Japan.

編集兼発行　日本原子力研究所
印　　刷　日立高速印刷株式会社

JAERI-M 93-073

Experimental and Analytical Studies of High Heat Flux Components for Fusion Experimental Reactor

Masanori ARAKI

Department of Fusion Engineering Research
Naka-Fusion Research Establishment
Japan Atomic Energy Research Institute
Naka-machi, Naka-gun, Ibaraki-ken

(Received February 26, 1993)

As the second stage of research and development (R&D) for fusion experimental reactors, recent three large tokamaks, i.e., JT-60 in Japan, JET in the European Community, and TFTR in the United States of America, were designed and constructed. Break-even plasma condition which is defined that an output fusion power produced by D-T reaction is equal to an input power have been achieved in JET. Equivalent break-even plasma condition in hydrogen plasma operation has also been achieved in JT-60. These positive results elevate the importance of R&D efforts on the next stage of experimental reactors. These R&D efforts are currently being carried out under the International Thermonuclear Experimental Reactor (ITER) program, which is a collaborative enterprise between Japan, the European Community, the Russian Republic, and the United States. Since the ITER will be designed to handle the nuclear fusion power from the nuclear fusion of deuterium and tritium (D-T), reactor engineering R&D issues are very important for the ITER program. In particular, development of plasma facing components, i.e., components which the surfaces directly face the ITER plasma, is one of the key issues for the design of ITER.

R&D issues can be categorized into four developmental items : 1) the armor, 2) the heat removal structure, 3) the braze technology, and 4) the integrated performance. This report describe their experimental and analytical results.

With respect to developing high performance heat removal structures for the divertor plates, an externally-finned swirl tube was developed based on the results of critical heat flux experiments on various tube structures, i.e., a smooth, an internally-finned tube, an externally-finned and rectangular-faced tubes. This tube geometry has advantages of not only improvement of critical heat flux but also drastic reduction of thermal deformation. As the result, the burnout heat flux, which also indicates incident critical heat flux, of 41 $\pm$ 1 MW/m^2 was achieved in the externally-finned swirl tube.

The ability to predict the critical heat flux (CHF) with highly subcooled flow boiling under one-sided heating conditions is one of the key issues in the design of plasma facing components for the ITER. At a first step, applicability of the existing CHF correlations based on uniform heating conditions was evaluated by comparing of the CHF experimental data with the smooth and the externally-finned tubes under one-sided heating condition. As the results, 1) experimentally determined CHF data for straight tube show relatively good agreement with some correlations within an accuracy of $\pm$ 20%, 2) for the externally-finned tube, no existing correlations are available for prediction of the CHF, although this tube geometry more closely approximates uniform circumferential heating conditions. Further experiments are necessary to evaluate the applicability of the existing CHF correlations under one-sided heating conditions.

With respect to the evaluation of the bonds between carbon-based material and heat sink metal, results of the brazing tests were compared with the analytical results by three dimensional model with temperature-dependent thermal and mechanical properties. In particular, the adhesive property between the armor tile and the heat sink metal was concentrated in this report. Analytical results showed that residual stresses from brazing can be estimated by the analytical three directional stress values instead of the equivalent stress value applied. Based on the analytical results, divertor mock-ups with different armor tile materials have been successfully fabricated in order to investigate their overall performance. Thermal cycling tests of the divertor mock-ups have been carried out under ITER relevant heat flux conditions. Results of these tests confirmed that bonded carbon-fiber-composite/copper (CFC/OFHC-Cu) divertor mock-ups have withstood the ITER relevant heat flux condition without cracks.

In the analytical study on the separatrix sweeping for effectively reducing surface heat fluxes on the divertor plate, thermal response of the divertor plate has been analyzed under ITER relevant heat flux conditions and has been tested. The analytical results showed the application of the sweeping is very effective for reducing the surface temperature of the divertor plate. Based on the analytical results, thermal response experiments with a divertor mock-up were carried out. As the result, it has been experimentally demonstrated that application of the sweeping technique is very effective for improvement in the power handling capability of the divertor plate and that the divertor mock-up has withstood a large number of additional cyclic heat loads.

Keywords : ITER, High Heat Flux, Plasma Facing Components, Divertor Plate, Critical Heat Flux, One-sided Heating Condition

核融合実験炉用高熱流束受熱機器に関する開発研究

日本原子力研究所那珂研究所核融合工学部
荒木　政則

（1993年2月26日受理）

核融合炉開発の第2段階として、日本、欧州、米国のいわゆる3大トカマク（JT－60,JET,TFTR）の設計・建設を終え、臨界プラズマ条件を達成することに成功した。これに伴い、核融合炉の開発研究は新たな展開を迎え、国際共同で熱核融合実験炉（ITER；International Thermonuclear Experimental Reactor）の概念設計及び実験的基礎研究を行う段階、更には工学設計へと進展している。国際熱核融合実験炉ITERでは、核融合反応により生成する熱及び粒子エネルギーを利用するため、炉工学技術の研究・開発が重要な課題として指摘されるようになってきた。中でも、プラズマに直接面して高い熱・粒子負荷を定常的に受ける受熱機器（プラズマ対向機器）の開発は、ITER設計上最も重要な課題の1つとして上げられる。

このため、ITER用ダイバータ板を開発する上で、4つの重要な開発課題、つまり、1）表面材料開発、2）高性能除熱構造開発、3）異種材料接合技術及び4）総合評価に分類し、本研究を実施した。本稿では、これらの開発研究を通して得られた成果及び研究結果について述べる。

高性能冷却構造の開発では、円管、内部フィン付円管、外部フィン付管及び角管の限界熱流束結果をもとに限界熱流束増大及び熱変形抑制を図るために外部フィン付スワール管を考案した。外部フィン付スワール管の基本開発コンセプトは、高限界熱流束化を達成する目的でスワールテープを、また、熱変形抑制化を目的として外部フィンをそれぞれ採用したことにあり、これらの相乗効果でさらに高い限界熱流束が期待できるものである。実験結果は、冷却材流束及び圧力を変数としてまとめた。特に、外部フィン付スワール管において、ITERで要求される限界性能を大きく上回る限界熱流束41 ± 1MW／m^2を達成した。

那珂研究所：〒311－01 茨城県那珂郡那珂町大字向山801－1

また、ダイバータ板に使用される冷却管の片面加熱条件下における限界性能を予測することは、設計上重要であり、その第1段階として片面加熱条件下で行った円管及び外部フィン付管における限界熱流束実験結果を既存の均一全周加熱条件下の限界熱流束を与える予測式と比較し、その適応性評価を行った。比較評価の結果、1）円管では、いくつかの予測式は±20％の精度でよく一致した。2）外部フィン付管では、その受熱形態が全周加熱条件に近いにも拘らず、既存の予測式では予測できず、新たな予測式が必要である、3）片面加熱条件下における冷却管熱伝達特性の実験的評価が必要である等を明らかにした。また、本研究結果から、今後の研究課題を明かにした。

さらに、プラズマ対向機器表面材料候補材である炭素系材料と冷却構造体との接合性及びその接合体接合特性評価に関する研究では、金属との接合特性を評価することが重要であり、各種炭素系材料と銅との接合実験を実施するとともに異方性を考慮した3次元応力解析を実施し、比較評価した。この結果、炭素系材料と銅との接合において、一般に広く利用されている等価応力では、接合特性を評価できないことを明かにすると共に、新たに3軸応力成分で評価できることを明かにし、大幅な合理化設計を可能とした。また、本評価をもとに製作したダイバータ接合体の熱サイクル実験を実施し、ITERの概念設計条件をほぼ満足するダイバータ接合体開発に世界で初めて成功した。また、実験結果から、炭素系材料側に生ずる応力振幅で熱サイクル特性を評価することを新たに提案した。

また、ダイバータ板上の熱負荷を実行的に軽減できるダイバータセパラトリックススイーピングに関する解析的及び実験的研究では、周期的に熱負荷分布が変化することにより、周波数に応じた温度振幅数が付加されるため、熱サイクル特性評価上最重要項目となっていた。そこで、異方性を考慮した3次元熱解析を行うと共に解析的に明らかにできない熱サイクル特性を実験的に世界で初めて評価した。この結果、ダイバータセパラトリックススイーピングは、ダイバータ板上の熱負荷を大幅に軽減できることを解析的に明かにすると共に、熱サイクル特性は、周波数に応じて付加される温度振幅数に対して十分健全であることを実験的に立証した。

Contents

目　　次

1. INTRODUCTION

1.1 Backgrounds and Objectives

As the second stage of research and development (R&D) for fusion experimental reactors, recent three large tokamaks, i.e., JT-60 in Japan, JET in the European Community, and TFTR in the United States of America, were designed and constructed. Break-even plasma condition which is defined that an output fusion power produced by D-T reaction is equal to an input power have been achieved in JET. Equivalent break-even plasma condition in hydrogen plasma operation has also been achieved in JT-60. These positive results elevate the importance of R&D efforts on the next stage of experimental reactors. These R&D efforts are currently being carried out under the International Thermonuclear Experimental Reactor (ITER) program, which is a collaborative enterprise between Japan, the European Community, the Russian Republic, and the United States.

Figure 1-1 shows schematic of the ITER. Since the ITER will be designed to handle the nuclear fusion power from the nuclear fusion of deuterium and tritium (D-T), reactor engineering R&D issues are very important for the ITER program. In particular, development of plasma facing components, i.e., components which the surfaces directly face the ITER plasma, becomes one of the key issues to be overcome. The plasma facing components will be subjected to severe heat loads not only during steady state normal operation but also during off-normal events such as plasma disruptions. Table 1-1 summarizes the performance requirements for the ITER plasma facing components [1].

Divertor plates are the most important plasma facing components. For the ITER plasma which has a double null configuration, the divertor plates are installed at the upper and lower positions of the plasma as shown in Fig. 1-1. Each divertor plate will be subjected to radiation heat loads, high fluxes of energetic particles, and high energy neutrons from the plasma.

Figure 1-2 shows a cross sectional view of the lower part of the divertor plate. Each divertor plate has two high heat load regions in the poloidal direction. For high performance operation in ITER, it is necessary to use low-Z materials such as high performance carbon-based materials with high thermal conductivity and strong mechanical

properties as the armor tiles for plasma facing components. Furthermore, to facilitate the conduction of heat from the armor to the actively cooled heat sink structure, carbon-based material as the armor tile must be brazed to the heat sink structure. Therefore, it is very important to develop the braze technology because of poor compatibilities of thermomechanical properties. Since the ITER is also designed for high plasma current and steady state operation, the plasma facing components will be subjected to more severe heat loads than those for the existing fusion experimental machines such as the JT-60, JET, and TFTR. As summarized in table 1-1, the steady state heat flux on the surface of the divertor plate is expected to be 15 to 30 MW/m^2.

The ITER R&D program for the divertor plates is summarized in Fig. 1-3. R&D issues can be categorized into four developmental items: 1) the armor, 2) the heat removal structure, 3) the braze technology, and 4) the integrated performance . The detailed experimental issues are indicated in Figs. 1-4, 1-5, 1-6, and 1-7.

With respect to developing the armor materials, the most important issue is erosion damage by the tokamak plasma. This issue can be studied in parallel with other developmental issues because the erosion processes effect only the near surface region of the structure. Especially, they will enormously be damaged during plasma disruptions. For example, evaluations of the damage of divertor plates under disruption heat loads reveal that the surface of the armor material is enormously damaged but are essentially undamaged the interface and the substrate of the divertor plate during a disruption. The energy deposited on the divertor plate can be divided into two parts, i.e., a storage energy and an evaporation energy due to the sublimation of the armor materials. When the carbon-based material is exposed to heat fluxes higher than 2000 MW/m^2 for 2 ms, corresponding to a deposited energy of 4 MJ/m^2, analytical results show that the storage energy does not increase any longer with the deposited energy and saturates at a value of about 2 MJ/m^2. Even if all of the energy were used to heat the armor material, its temperature rise would be expected to be less than 200 K.

The second experimental issue is development of heat removal structures for the divertor plates under one-sided heating condition. In ITER, the divertor plate is exposed to stationary heat flux as high as 15 to 30 MW/m^2 described above. Since little developmental study of heat removal structure under one-sided heating conditions is available, high performance cooling structure is needed for the ITER divertor plates. The following thermal characteristics as shown in Fig. 1-5 becomes important; critical heat flux (CHF) of the cooling structure, critical heat flux (CHF) correlations, and heat transfer along the

circumference. There are many experimental and analytical studies on critical heat flux under uniform heating condition [2-7], but only a limited amount of literature under one-sided heating condition [8-10]. Since there is little literature for one-sided heating condition, systematic experimental evaluations based on experiments are necessary.

The third and the fourth experimental issues are shown in Figs. 1-6 and 1-7. Since high thermal response of the divertor plate will be required to handle the intense heat loads, carbon-based materials with high thermal conductivities are brazed to a metal cooling structures. However, poor compatibility of thermomechanical properties between the carbon-based materials and the metal will lead to residual stresses. Also the adhesive properties of the bond strongly depend upon braze materials, surface treatment before brazing, and configuration of the bond.

Since the divertor plate experiences periodic high heat flux variation, an evaluation of the thermal fatigue of the divertor plate will be important for the ITER design. In particular, the thermal fatigue induced in the bonds of the divertor plate, which is strongly affected by brazing process, is critical and therefore some experimental study is required from the viewpoint of lifetime evaluation. It is also very important to investigate applications of special techniques, such as separatrix sweeping which can be used to reduce the surface heat flux of the divertor plate, from the lifetime point of view.

In view of the above statement, this study focuses on the following subjects:

(1) critical heat flux experiments of various cooling tubes under one-sided heating condition,

(2) evaluation of critical heat flux correlations under one-sided heating condition,

(3) evaluation of the thermal response of the divertor plate under large numbers of cyclic high heat loads,

(4) analytical and experimental evaluation of sweeping effects on the reduction of the surface heat flux deposited to the divertor plate.

Table 1-1 Required Performances for Plasma Facing Components of ITER

Operation phase		Physics		Technology	
Component		First Wall	Diver-tor	First Wall	Diver-tor
Normal Operation					
- Aver. neutron wall load	MW/m^2	1	0.5	0.8	0.4
- Peak/aver. surface heat flux,	MW/m^2	0.6/0.15	15-30/0.6	0.6/0.15	15-30/0.6
- Peak volumetric heat load in structure	MW/m^3	20	5	15	4
- Number of pulses (full load)	10^4	1		2-5	
- Total burn time	h	400		10^4-$3x10^4$	
- Peak neutron damage (steel)	dpa	0.7	0.3	12-36	5-15
- Min. dwell time	s	200		200	
- Incident DT-ions:					
• peak flux	$10^{20}/m^2s$	1	4000	1	4000
• energy	eV	10-100	50-100	10-100	60-200
- Allowed water leak g/s	g/s	10^{-8}		10^{-8}	
Disruptions					
- Number (at full load)		500		200-500	
- Thermal quench:• time	ms	0.1-3		0.1-3	
• peak energy depos.,	MJ/m^2	2	10-20	2	10-20
- Current quench:• time	ms	5-100*		5-100*	
• radiative energy depos.	MJ/m^2	2		2	
• run-away elect. energy depos. (at ≤ 300 MeV)	MJ/m^2	30		30	

* 20 ms are used as reference value for the analysis

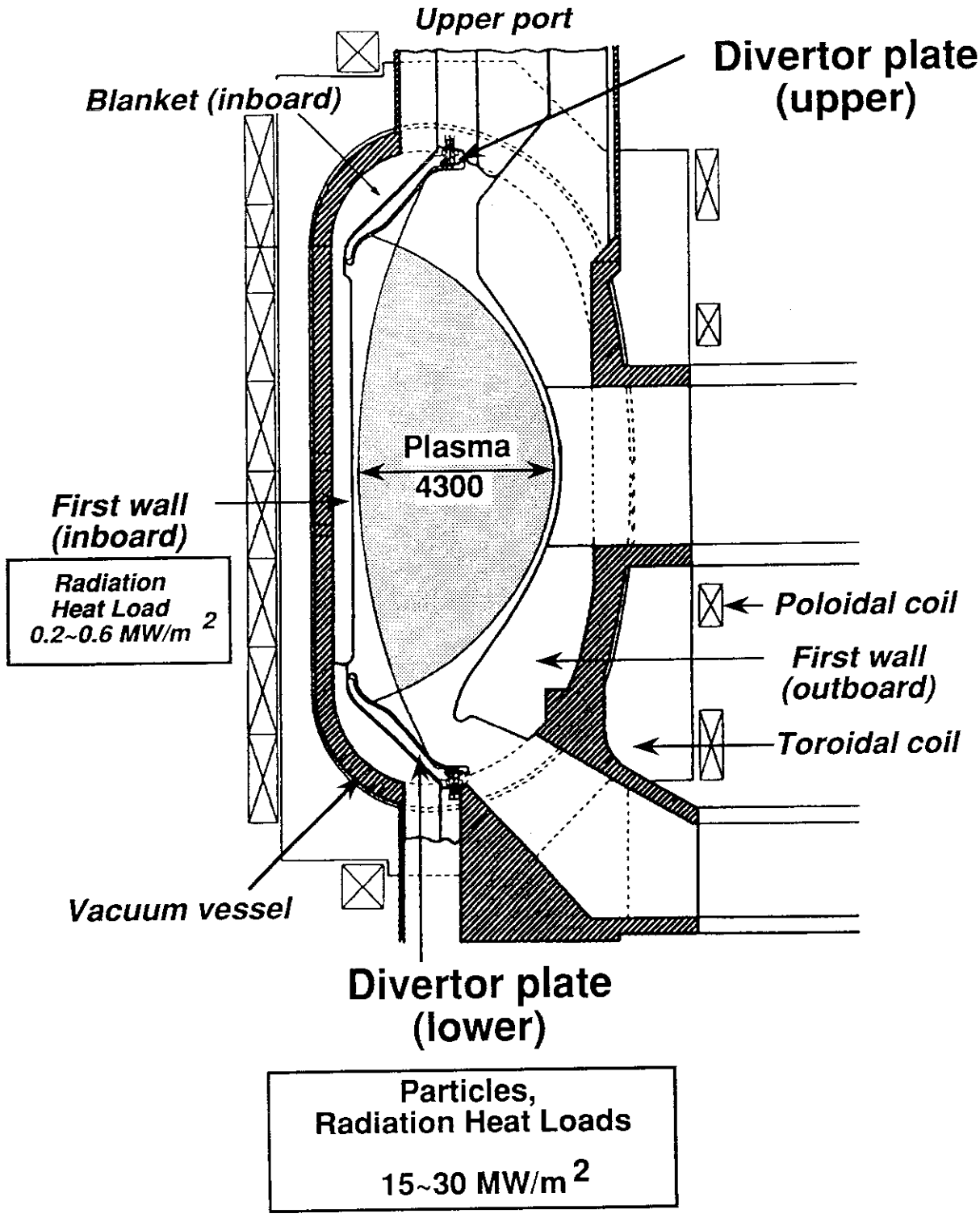

Figure 1-1 Schematic of ITER

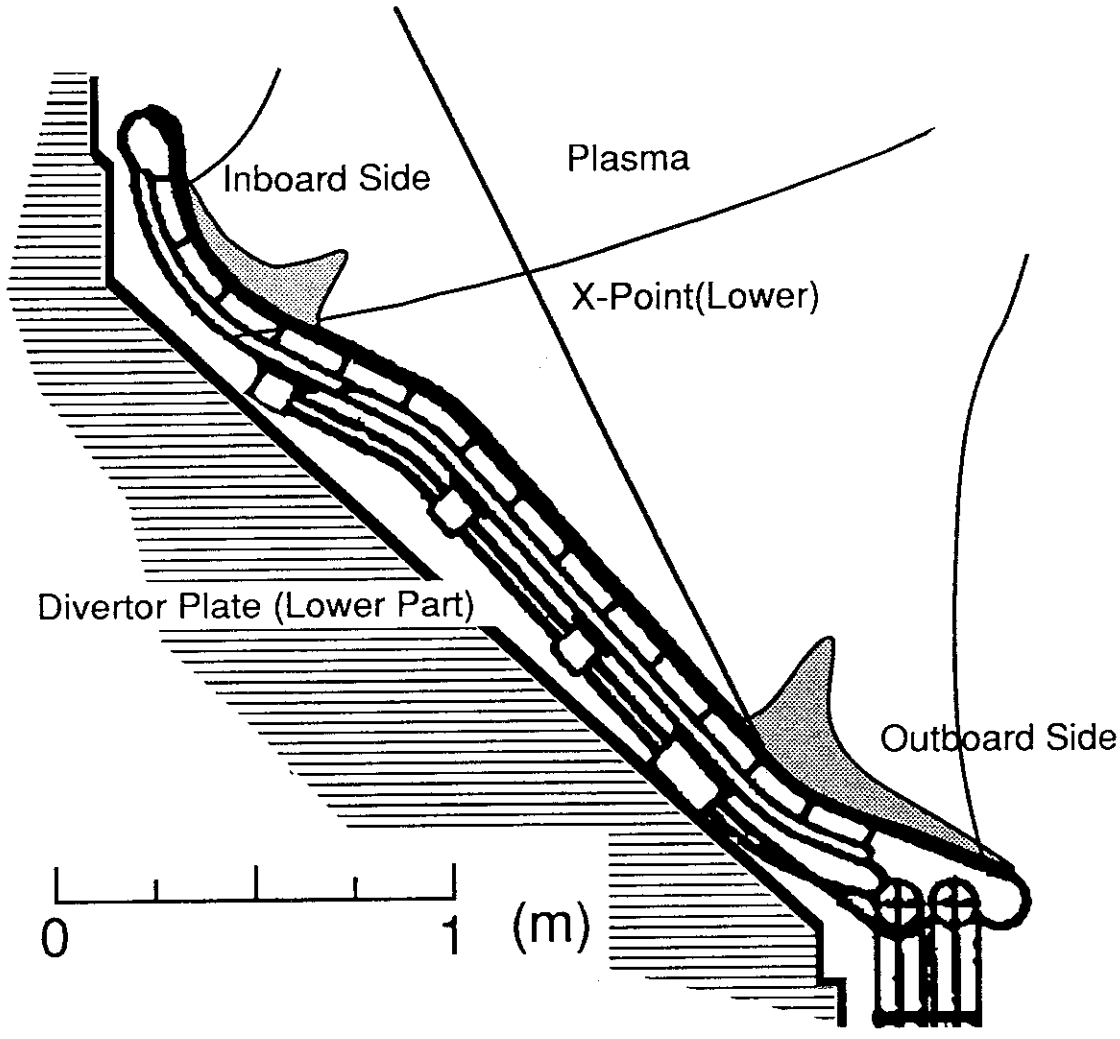

Figure 1-2 Cross Sectional View of Divertor Plate

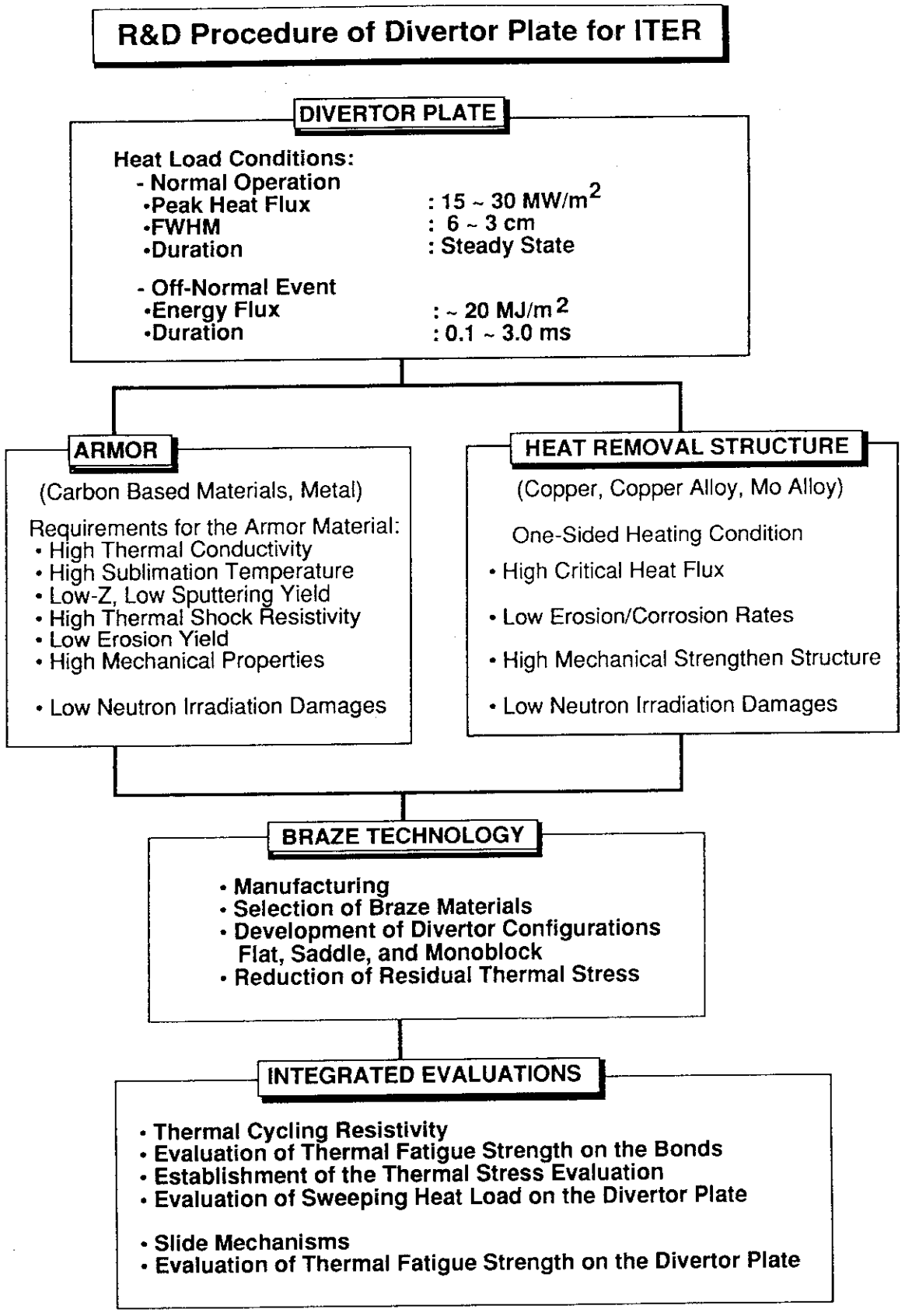

Figure 1-3 R&D Procedure of Divertor plate for ITER

Developmental Issues of the Armor

ARMOR

(Carbon Based Materials, Metal)

Requirements for the Armor Material:
- High Thermal Conductivity
- High Sublimation Temperature
- Low-Z, Low Supperting Yield
- High Thermal Shock Resistivity
- Low Erosion Yield
- High Mechanical Properties
- Low Neutron Irradiation Damages

- Development of Carbon Based Materials with High Thermal and Mechanical Properties

- **Graphite Based Materials**
- **Carbon Fiber Reinforced Carbon Composites 1-D, 2-D, 3-Dimensional CFCs**

- Experimental Evaluations on Thermal Shock Resistivity

- **Evaluation of Fracture and Erosion Mechanisms**
- **Ion Beam Irradiation Damage**
- **Heat Irradiation Damage (Electron Beam Irradiation)**
- **Plasma Irradiation Damage**

- Evaluations of Neutron Irradiation Damages

- **Neutron Irradiation Experiments of the Carbon Based Materials**

Figure 1-4 Developmental Issues of the Armor

Developmental Issues of the Heat Removal Structure

HEAT REMOVAL STRUCTURE

(Copper, Copper Alloy, Mo Alloy)

- High Critical Heat Flux
- Low Erosion/Corrosion Rates
- High Mechanical Strengthen Structure
- Low Neutron Irradiation Damages

- **Experimental Evaluation on Critical Heat Flux of Various Cooling Structures Under One-Sided Heating Condition**
  - **Development of the Cooling Structure with High Critical Heat Flux**

    Swirl Tube
    Swirl Tube with an External Fin
    Modified Swirl Tube
    Tubes with Internal Fins
  - **Flow Velocity Dependence**
  - **Water Pressure Dependence**
  - **Subcooling, Heated Length Dependence**

- **Evaluation of the Existing Critical Heat Flux Correlations on the Application for One-side Heating**
  - **Evaluation of Critical Heat Flux Defined at the Cooling Structure Inner Wall**

- **Evaluation of Heat Transfer Under One-Sided Heating Condition**
  - **in Nonboiling Region**
  - **in Subcooled Boiling Region**

- **Evaluations of Erosion/Corrosion Rates**
  - **Flow Velocity Dependence**
  - **Water Temperature Dependence**
  - **Structure Dependence**

Figure 1-5 Developmental Issues of the Heat Removal Structure

Braze Technology and Integrated Experimental Issues

BRAZE TECHNOLOGY

- Manufacturing the Bonds
- Adhesive Properties of the Bonds
  - Selection of Braze Materials
- Development of Divertor Configurations
  Flat, Saddle, and Monoblock
- Reduction of Residual Thermal Stress

Figure 1-6 Testing and Integrated Evaluating Issues

INTEGRATED EVALUATIONS

- Thermal Cycling Experiments of Various Types of
  Divertor Plate Mock-Ups
  - Thermal Cycling Resistivity
  - Evaluation of Thermal Fatigue Strength on the Bonds
  - Establishment of the Thermal Stress Evaluation
  - Evaluation of Thermal Fatigue Strength on the Divertor Plate
  - Slide Mechanisms
- Evaluation of Sweeping Heat Load on the Divertor Plate
  - Influence of Additional Minor-Temperature Change on the Bonds
  - Influence of Additional Minor-Temperature Change on the Bonds
  - Evaluation of Thermal Fatigue Strength on the Bonds

Figure 1-7 Testing and Integrated Evaluating Issues

1.2 Outline of this study

<Critical Heat Flux Experiments>

High heat flux components such as the divertor plate and beam dumps for NBI are subjected to particle and radiation heat loads under one-sided heating condition, which induces thermomechanical problems such as bending of the tube and large thermal stress. Further, extremely high heat flux is loaded on striking points of the divertor plate. In order to develop the cooling system, therefore, high heat flux removal system will be needed. Among many heat removal concepts, a swirl tube is considered one of the most promising candidates for the cooling system of high heat flux components and an experimental study to develop high heat flux components for the next generation of fusion experimental reactors has been started, using an ion source developed for JT-60 neutral beam injector (NBI).

In this study, a modified swirl tube, namely an externally-finned swirl tube, is developed and compared with a simple smooth tube, an externally-finned tube, an internally-finned tube, and a rectangular-faced tube with circular cooling line. The major dimensions of the externally-finned swirl tube are 10 mm in outer-diameter, 15 mm in external fin width, and 700 mm in length.

To evaluate quantitatively cooling capability of the swirl tubes, burnout heat flux is introduced which is defined at the tube outer surface in this study because of one-sided heating condition. The burnout heat flux, which also indicates incident critical heat flux, of 41 $\pm$ 1 MW/m^2 is achieved in the externally-finned swirl tube under the condition that water flow velocity, inlet pressure and temperature were 13 m/s, 0.9 MPa and 20 °C, respectively. The burnout heat fluxes of the externally-finned swirl tube and the internally-finned tube increased linearly with increasing the flow velocity.

On the other hand, the burnout heat fluxes of up to 30 MW/m^2 were obtained for tubes without a twist tape or internal fins, but their values saturated in spite of increasing the flow velocities.

The burnout data in the rectangular faced tube were similar to that in the smooth tube in the present experiment, although larger heat conduction along the circumference was expected compared to the smooth tube.

<Critical Heat Flux Correlation>

The ability to predict the critical heat flux (CHF) with highly subcooled flow boiling is one of the key issues in the design of plasma facing components for the next generation fusion machines such as the ITER and FER. In particular, the divertor plate is subjected to severe heat loads under one-sided heating conditions. Because there are no correlations predicting CHF for highly subcooled flow with heating on one side, experimental data obtained under one-sided heating condition have been compared to various existing CHF correlations for uniform circumferential heating conditions. Incident critical heat fluxes for various tubes were translated into the heat flux values at the tube inner wall by applying heat transfer correlation with highly subcooled boiling.

Experimentally determined CHF data for straight tube show relatively good agreement with some correlations within an accuracy of ± 20 %. On the other hand, all of the existing correlations systematically underpredict CHF values for over the range of the mass flow investigated in the present experimental conditions. The heat flux profile along the circumference of the rectangular faced tube inner wall is found to be similar to that for the straight tube. This is mainly attributable to the high degree of sensitivity of existing CHF correlations to the inner diameter.

For the externally-finned tube, no existing correlations are available for prediction of the CHF, although this tube geometry more closely approximates uniform circumferential heating conditions. Further experiments are necessary to evaluate the applicability of the existing CHF correlations under one-sided heating conditions.

<Thermal Cycling Experiments>

Plasma facing components for fusion experimental reactors such as the ITER/FER will be exposed to a large number of high heat flux and thermal cycles. From the engineering point of view, divertor mock-ups with different armor tile materials have been prepared in order to investigate their overall performance. In particular, the adhesive property between the armor tile and the heat sink metal was concentrated in this study. Thermal cycling tests of the divertor mock-ups have been carried out under ITER/FER relevant heat flux conditions in a particle beam engineering facility at Japan Atomic

Energy Research Institute (JAERI).

Results of these tests confirmed that bonded carbon-fiber-composite/copper (CFC/OFHC-Cu) divertor mock-ups have withstood 10.0 MW/m^2 for one thousand cycles without cracks. At this experimental condition, the integrity and the durability of the bonds have also been confirmed. Some bonded CFC/OFHC-Cu samples have withstood 12.5 MW/m^2 for one thousand cycles without an increase of the surface temperature, although a small crack was observed at a corner of the bonded layer.

For the bonded fine-grained graphite/OFHC copper (Gr/OFHC-Cu) divertor mock-ups with a molybdenum intermediate layer, the integrity of the bonds has also been confirmed after 1,000 thermal cycles under the heating condition of 16 MW/m^2 for 1.0 s, which corresponds to the steady state heat flux of 8 MW/m^2. A small Gr/OFHC-Cu sample has resisted up to 10 MW/m^2 for 1,000 cycles without an increase of the surface temperature, although many longer cracks appeared at the outer surface of the graphite close to the bonded layer.

Residual stresses from brazing have also been determined using three dimensional models. The analytical results confirmed the results of the test sample manufacture efforts, that is, no cracks or detachments were observed. Since no thermal plastic fatigue evaluation codes are available for the prediction of the lifetime, experimental data were correlated with numerical thermal stresses during heating.

<Evaluation of Separatrix Sweeping Effects>

Magnitude of the heat flux on the surface of the divertor plate of the ITER is one of the most limiting constraints on its lifetime. A technique for sweeping the separatrix across the divertor surface will be applied to reduce surface heat fluxes and erosion damages due to intense fluxes over 15 MW/m^2. As the first step for evaluation of the sweeping effects, thermal response of the divertor plate has been analyzed under ITER relevant heat flux conditions that a peak heat flux on the divertor plate and full width at half maximum are expected to be 30 MW/m^2 and 3 cm, respectively.

The analytical results show the application of the sweeping is very effective for reducing the surface temperature of the divertor plate. To realize these benefits for ITER, the divertor separatrix must be swept with a frequency of higher than 3.0 Hz over a distance of ± 10 cm.

Based on the analytical results, thermal response experiments with a divertor mock-up are carried out using the JAERI Electron Beam Irradiation Stand (JEBIS). The condition for this experiment was a peak heat flux of 30 MW/m^2 with a sweeping frequency of 1.0 Hz over a distance of ± 10 cm for a 30 second long cycle. Experimental results show that the divertor mock-up has successfully endured for >1,000 major thermal cycles without increase of the surface temperature. Therefore, it has been experimentally demonstrated that application of the sweeping technique is very effective for improvement in the power handling capability of the divertor plate. Experimental results showed good agreement with analytical results.

2. CRITICAL HEAT FLUX EXPERIMENTS FOR VARIOUS TUBE CONFIGURATIONS

2.1 Introduction

Steady state and high heat flux heat removals will be required in the next generation of fusion devices such as the international thermonuclear experimental reactor (ITER) or fusion experimental reactor (FER). The high heat flux components in these devices are exposed to severe heat loads from tokamak plasma or intense ion beams under one-sided heating condition. The peak heat flux on the surface of the components such as divertor plates and beam dumps for neutral beam injectors will amount to a few tens of megawatts per square meter. By introducing tilted surface for the beam dumps, it is still difficult to reduce the heat flux below 30 MW/m^2 on the surface of the beam stops. This value is several to ten times larger than the design value for JT-60 NBI [11]. With respect to the cooling structure of the divertor plate for ITER/FER, similar deposited heat flux is expected.

Various kinds of beam stops for high heat flux and steady state heat removal with one-sided heating condition have been investigated so far [8, 12-17]. Table 2-1 shows a summary of recent results on developing high heat flux components. There are two types of beam stop elements, i.e., either a panel or a tube structures. In the beam stops based on the panel structure, the heat removal per panel area is relatively large and water flow rate per heat loading is small [12, 13]. However, the maximum heat flux on the surface of the panel seems to be limited to 20 MW/m^2 because of low heat transfer coefficient and large thermal stress across the panel. On the other hand, the maximum heat flux which can be handled by the tube structure will be higher than 50 MW/m^2 [15]. There are several types of the tube structure depending on the cross section of the tube. Tubes with a twisted tape or internal fins are used in order to increase the equivalent heat transfer coefficient for forced convection. In particular, swirl tube has a higher performance on the heat removal compared with other types of the tube.

The beam stops based on a tube with twisted tape inserted have already achieved the burnout heat flux of 54 MW/m^2 with a pulse length of 30 s, though the beam irradiated area is small in the test [15]. In order to reduce the thermal stress, a tube with external fins was proposed to decrease the temperature gradient across the tube [8]. Hence, the externally-finned swirl tube is proposed for the beam stop elements of the ITER-NBI

which is now designed in the international collaboration. A reliable data base of burnout heat flux for many cooling tubes is required for the design of beam stops.

2.2 Experimental set-up and test samples

The JT-60 prototype neutral beam injection system was used for the present burnout experiments. The experimental set-up and performances in this system are shown in Fig. 2-1 and Table 2-2, respectively. A test sample was installed normal to the beam axis at the position of 3.04 m from the ion source. Six kinds of the test samples shown in Fig. 2-2 were tested. Major dimensions of the test samples shown in Figs. 2-2 and 2-3 are 10.0 mm in outer diameter, 1.5 mm in wall thickness, and 700 mm in length. Dimension of a rectangular faced tube with circle cooling line is 10 mm in inner diameter and 16 mm in width and height. The tube material is oxygen-free copper with 0.2 % silver content because it has a higher softening point and greater mechanical strength than pure oxygen-free copper.

A tape twist ratio is defined as the number of internal diameters for 180° of twist. In the present experiment, the externally-finned swirl tubes with the tape twist ratios of 2.0 and 2.5 were fabricated in order to evaluate CHF performance for the different tape twist ratios. The binding force between a twisted tape and an inside wall of the tube, which is the amount of the friction force divided by the tape insertion length, was measured and was more than 2000 kg/m at temperatures in the range of 20 to 400 °C. This value is large enough to be fit for a water pressure of up to 2 MPa. Furthermore, even if the binding force is reduced, sleeves which protrude from the inside wall at both ends of the tube will prevent the twisted tape from slipping off.

Surface temperatures at five positions for each test sample were measured by thermocouples. The thermocouples were chromel-alumel type (K-type) with 0.5 mm-diameter sheath and were buried in grooves cut on the surface with silver brazing. The positions of the thermocouples along the water flow direction were determined by two-dimensional thermal conduction analysis. Inlet and outlet temperatures of the cooling water were also measured with thermocouples which were inserted into the tubes as shown in Fig. 2-3. The flow rates were measured by a gauge pressure transmitter with a diaphragm. The flow rate and the pressure were controlled by two throttles at the inlet and outlet of the test sample.

Performances of the ion source are summarized in Table 2-2. With an accuracy of ± 1 MW/m^2, beam intensity profiles were measured with a multi-channel copper calorimeter which was installed at the same position as that of the test sample. Figure 2-4 shows typical heat flux distributions normal to the beam axis. The value of heat flux are presented in terms of the incident ion beam flux normal to the tube. Heat fluxes up to 100 MW/m^2 were measured calorimetrically at the beam energy and current of 60 kV and 31 A. However, heat flux more than 100 MW/m^2 could not be measured owing to the deformation of the calorimeter.

The experiment was conducted at the flow rate of 10 to 30 l/min with an inlet pressure of up to 1 MPa (gauge). Their flow rates corresponds to axial flow velocities of about 4 to 13 m/s. The temperature of inlet cooling water was kept to be 20 °C during a beam pulse. In addition, a beam dump for the long pulse beam (beam dump 1) was developed and installed as shown in Fig. 2-1 because the beam dump 2 was designed to handle a short pulse beam up to 0.5 s. The beam dump 1 consists of an array of 16 externally-finned swirl tubes. All experimental data were interpolated by a multi-channel data logger system whose sampling and interval times are set 30 ms/ch and 10 ms, respectively.

2.3 Results and discussion

2.3-1 Burnout data

A typical temperature variation with time in the externally-finned swirl tube with the tape twist ratio of 2.5 is shown in Fig. 2-5. The numbers on each curve (labelled 1 to 7) correspond to locations of thermocouples which are indicated in Fig. 2-3. A test sample was bombarded by an ion beam of 19 A at 45 kV. The water flow rate is 30 l/min which corresponds to the axial flow velocity of 13 m/s. Inlet and outlet reading pressures are 0.9 and 0.2 MPa, respectively.

The surface temperature at point 4, which is located 10 mm downstream from the beam center, rises very quickly to the equilibrium value of 400 °C within 0.3 s after beam-on and then rises very slowly with a small fluctuation between the temperatures of 390 and 405 °C and starts to rise very quickly at 2.0 s due to burnout. It seems that a vapor layer or a small hot region forms and spreads from 0.5 s after beam-on. Surface

temperatures of location 3 and 5 at the positions of 70 mm upstream and downstream from the beam center also rise quickly within 0.2 s and reach 250 and 325 °C, respectively. The ion beam was stopped at 2.0 s due to the beam cut-off interlock triggered by the thermocouple output which was set at 500 °C.

In the externally-finned swirl tube, no influence of burnout at point 4 on other points was observed in all burnout tests. This result was different from that of other tubes. In the tubes without the twisted tape inserted, which were also studied by Horiike et al. [17], the hot region spread widely along the flow direction. This phenomenon is also observed in the burnout tests on the externally-finned tube, the internally-finned tube, the rectangular faced tube, and smooth tube. In our early burnout experiments, the surface of these tubes melted and water leakage occurred from a crack whose size was about 0.7 mm in width and 2.6 mm in length. A concavely melted region was 5 mm in width and 25 to 30 mm in length. On the other hand, in the externally-finned swirl tube, the melted region was 5 mm in width and 17 mm in length. This region corresponds to the pitch length of the externally-finned swirl tube, which means limitation of the melting to the pitch length of the inserted twist tape.

2.3-2 Dependence of CHF on the flow rate

Dependences of the burnout heat flux on the axial flow velocity are summarized in Fig. 2-6. Burnout data of the rectangular face tube is also shown in Fig. 2-7. Although the burnout heat flux increases with the flow rate in general, in the tubes without a twisted tape or internal fins, the burnout heat flux saturated around 10 m/s axial flow velocity as shown in Figs. 2-6 and 2-7. This phenomenon, called 'Burnout Upper Limit', may indicate that the heat transfer coefficient in the boundary layer between the tube wall and the coolant does not increase and then large hot region or dry layer in the top of the tube already forms well.

In the externally-finned swirl tube, the burnout heat flux ratio, which is defined by the ratio of the burnout heat flux of the externally-finned swirl tube to that of the externally-finned tube, was about 1.1 at the equivalent axial flow velocity of 4.0 to 6.0 m/s and improved up to 1.4 with an increase of the axial flow velocity of more than 10 m/s. This result agrees well with the report by Tompson et al. [18], but differs from the results of Gambill et al. [19] who investigated the burnout experiments on the swirl tube under a

uniform heat flux distribution in both peripheral and axial directions. The reason of this difference may be attributable to difference of heat conditions and existence of the external fin. It can be seen from Fig. 2-6 that the burnout heat flux of the externally-finned swirl tube is a factor of 1.5 higher than that of the smooth tube at the same heating and cooling flow conditions.

Two-dimensional thermal conduction analyses of tubes with and without an external fin was carried out to evaluate effects of the external fin. Figure 2-7 shows their temperature distributions under conditions that the equivalent axial flow velocity is 13 m/s and heat flux is 30 MW/m^2 for the externally-finned tube and 20 MW/m^2 for the smooth tube, respectively. In the externally-finned tube, numerical results indicate that the wall temperature of the tube with an external fin reaches more than 200 °C and that a small hot region on the tube wall may be formed to the nucleate boiling and/or quasi-stable film boiling states all around the inner wall of the tube. It should be noted that a small temperature gradient between the heated region and the rear region is expected in the tube with an external fin. On the other hand, the wall temperature of the tube without an external fin at the heated side reaches more than 300 °C, but the temperature in the rear wall does not reach a saturation temperature of 160 °C. Therefore, the tube with an external fin will induce not only reducing the thermal stress across the tube, but also improving the characteristics of boiling heat transfer along the circumference.

Measured burnout heat fluxes of the internally-finned tube are also presented in Fig. 2-6. Compared of burnout heat fluxes of this tube with those of the smooth tube under the same cooling condition, an improvement of burnout heat flux by 32 % was observed at higher velocities but at velocities below 11 m/s, the improvement was not observed. The tube with internal fins, however, needs supplying with a large amount of cooling water in order to obtain the same performance of the swirl tube.

Comparing CHF data of the smooth tube with the rectangular faced tube, no differences were observed, although heat deposition profile seemed to be slightly different from each other. These results are discussed in next paragraph in detail.

2.3-3 Dependence of CHF on the pressure

Dependences of the burnout heat flux on the pressure are also indicated in Figs. 2-6 and 2-8. Its dependence on the inlet water pressure of from 0.5 to 0.9 MPa was small in

all the samples and this result agrees with other results [8, 18, 19]. For evaluation of CHF on the pressure, further experiments will be necessary for relatively wide pressure ranges.

2.3-4 Dependence of CHF on the tape twist ratio

A small burnout heat flux dependence for different tape twist ratios was observed in every burnout test. This result was slightly different to that of Gambill due mainly to different heating conditions.

2.3-5 Effect of external fin

Many burnout tests were finally conducted in order to evaluate the effect of the external fin on the thermal deformation. Deformations of tubes with and without the external fins were measured, and these values were about 3 mm and 8 to 15 mm at the center of the tube, respectively. It is clear that external fins have the effect of reducing the thermal stress across the tube and this effect can be applied to the cases of the swirl tube, internally-finned tube, etc.

2.3-6 Pressure drop

Figure 2-9 shows pressure drops of various type of the tubes at the inlet pressure range of 0.5 to 0.9 MPa. In general, pressure drops of tubes with a twist tape and internal fins are slightly higher than that of the smooth tube. In particular, measured pressure drop of the externally-finned swirl tube was a little bit higher than that predicted by Gambill [19]. This reason is as follow; a twist tape has straight tapes at both end regions to fix it to the tube wall. During the manufacturing process of the externally-finned swirl tube, the straight part of the tape might slightly be deviated from the center of the tube in the bend region since test sample was bent at both end regions as shown in Fig.2-3.

2.4 Conclusions

Through the critical heat flux experiments under a non-uniform and one-sided heating conditions by intense hydrogen beams, the following results were obtained:

1. A swirl tube with an external fin was developed for the cooling tube element of high heat flux components. Major dimension of the tube was 10 mm in outer diameter, 1.5 mm in wall thickness, 700 mm in length, and a tape twist ratio of 2.5
2. An incident critical heat flux of 41 ± 1 MW/m^2 was obtained in the case of the externally-finned swirl tube whose outer diameter, wall thickness, length, and tape twist ratio are 10 mm, 1.5 mm, 700 mm, and 2.5, respectively. The hydraulic conditions as to the flow rate and the inlet pressure were 30 l/min and 0.9 MPa (gauge), respectively.
3. The critical heat flux increases linearly with an increase of the flow rate. However, the heat flux of the tubes without a twist tape or internal fins saturates at some flow rate.
4. It was found that the critical heat flux of the tube with an external fin is a factor of 1.5 higher than that of the smooth tube at the same conditions. However, same CHF values were obtained in the smooth tube and the rectangular faced tube.
5. The effect of water pressure on the critical heat flux was small.
6. It was confirmed that the tubes with an external fin have the effect of reducing the thermal stress across the tube.

Table 2-1 Recent High Heat Flux Component Developments

	HYPER-VAPOTRON [1] (JET)	Beam dump for [2] NBETF-NBI (LBL)	(DESIGN) Steady-state [3] beam dump for TFTR-NBI (PPPL)	Beam target for [4] METF-NBI (ORNL)	Beam dump for [5] MFSTF-NBI (LLNL)	Rotating target
Max. heat flux (kW/cm^2)	1.2 - 1.6 (1.0 - 2.0)	~1.6 (1.0)	1.0 - 2.0	~5.4 (3MW-30s)	~1.33 (8.0)	(20.0)
Material	1% Cr + Cu	0.2% Zr + Cu	Zr + OFHC or INCONEL	OFHC (tape : INCONEL)	Mo	
Size width	112	215	OD : 19.1	OD : 9.5	OD : 5.0	
Size height	30	–	t : 1.6	t : 1.6	t : 0.25	
Size length	940 (540)	200	Int. finned tubes	Swirl-tubes	Int. finned tubes	
Cooling water: Press. inlet	–	16.5	–	16.0	–	
Cooling water: Press. outlet	–	6.5	–	4.0	–	
Cooling water: Press. operat	7.0	–	22.0	–	54.0	
Cooling water: Flow rate (l/min/tube)	166	220	29 (average) (max. 60)	20	5.4 (total : 2700)	
Cooling water: Press. drop (kg/cm^2)	~0.5	~7.2	–	~11.0	–	
Pulse length (sec)	>10 (10)	30 (30)	>30	30 (30)	~0.4 (30)	
Life time (cycle)	(100000)	(>25000)	–	30000 1000 (LP)	(300000)	
Structure of surface	 V - shape	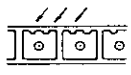 V - shape	 Bowl - shape	 V - shape	V - shape	
Remarks	ION SOURCE 75keV, 10MW, D-BEAM (TOMSON CSF)	ION SOURCE 120keV, 50A, 30s, D (170keV, 65A, 30s) (MDAC)	ION SOURCE 120 keV, D-BEAM	ION SOURCE 75 keV, 40A, 30s (UNITED TECH.)	(UNITED TECH.)	

	JT-60 NBI (JAERI)			Active diagnostics for JT-60 (JAERI) [7]		(DESIGN) [8] Beam dump for FER NBI (JAERI)
	Beam dump [6]	Water jacket	Calorimeter	Beam dump	Calorimeter	
Max. heat flux (kW/cm^2)	0.5 (0.5)	0.4 - 0.5 (0.45)	~1.0 (1.0)	~7.5 (9.0)	3.7 (4.0)	(4.0) (17MW)
Material	0.2% Ag + OFHC	0.2% Ag + OFHC	0.2% Ag + OFHC	W/ OFHC	0.2% Ag + OFHC	0.2% Ag + OFHC (tape : INCONEL) (or Ni)
Size width	OD : 14.0	16 x 16	30	49	140	(OD : 10.0)
Size height	t : 2.0		36	50	260	(t : 1.5)
Size length	Ext. finned tubes		30	49	20	Ext. finned swirl-tubes
Cooling water: Press. inlet	10.0	9.0	9.0	8.0	8.0	(20.0)
Cooling water: Press. outlet	9.0	5.0	5.0	–	–	–
Cooling water: Press. operat	11.5	–	–	–	–	–
Cooling water: Flow rate (l/min/tube)	22.6 (max 27) (total : 2400)	16.1 (average) (total : 1000)	9.3 (average) (total : 250)	4.5 - 11.0 (series)	1.6 - 2.0 (series)	(20.0 - 30.0)
Cooling water: Press. drop (kg/cm^2)	0.5 - 1.0	0.5 - 1.0	0.5 - 2.0	–	–	(10.0 - 15.0)
Pulse length (sec)	10 (10)	10 (10)	0.5 - 1.0 (0.5)	~ 0.1 (0.1)	~ 0.1 (0.1)	Continuous
Life time (cycle)	(10^6)	(10^6)	(10^6)			–
Structure of surface	 Bowl - shape	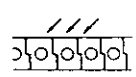 Flat	 V - shape	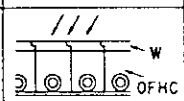 Flat	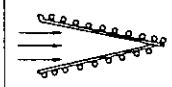 V - shape	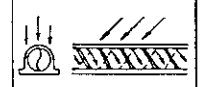 Flat
Remarks	ION SOURCE 100 keV, 70A, 10s H - BEAM			ION SOURCE 200keV, 3.5A, 0.1s He - BEAM		ION SOURCE 500keV, 100A, Cont. D - BEAM

Table 2-2. Performance of the JT-60 Prototype Neutral Beam Injection System

Power Supply System		
Acceleration Voltage	, kV	; 20 ~ 100
Acceleration Current	, A	; max. 80
Pulse Length	, s	; max. 10
Ion Source		
Work Gas		; H_2
Acceleration Voltage	, kV	; max. 100
Acceleration Current	, A	; max. 50
Pulse Length	, s	; max. 10
Half Width at e-holding	, cm	; 6 x 9
Beam Extraction Area	, cm	; 12 x 27
Pressure in the Beamline	, Pa	; about 0.053
Beam Target 1 (for long pulse beam)		
Active Cooling Method		
Tube Type		; Externally-finned Swirl Tube
Number of Tubes		; 16
Angle to the Beam Axis		; 45 °
Max. Heat Removal, kW		; 900
Permissible Pulse Length, s		; > 5
Beam Target 2 (for short pulse beam)		
Passive Cooling Method		
Max. Heat Removal, kW		; 4000
Max. Heat Flux Normal, to the Beam Axis	MW/m^2	; 250
Permissible Pulse Length, s		; ~ 0.1

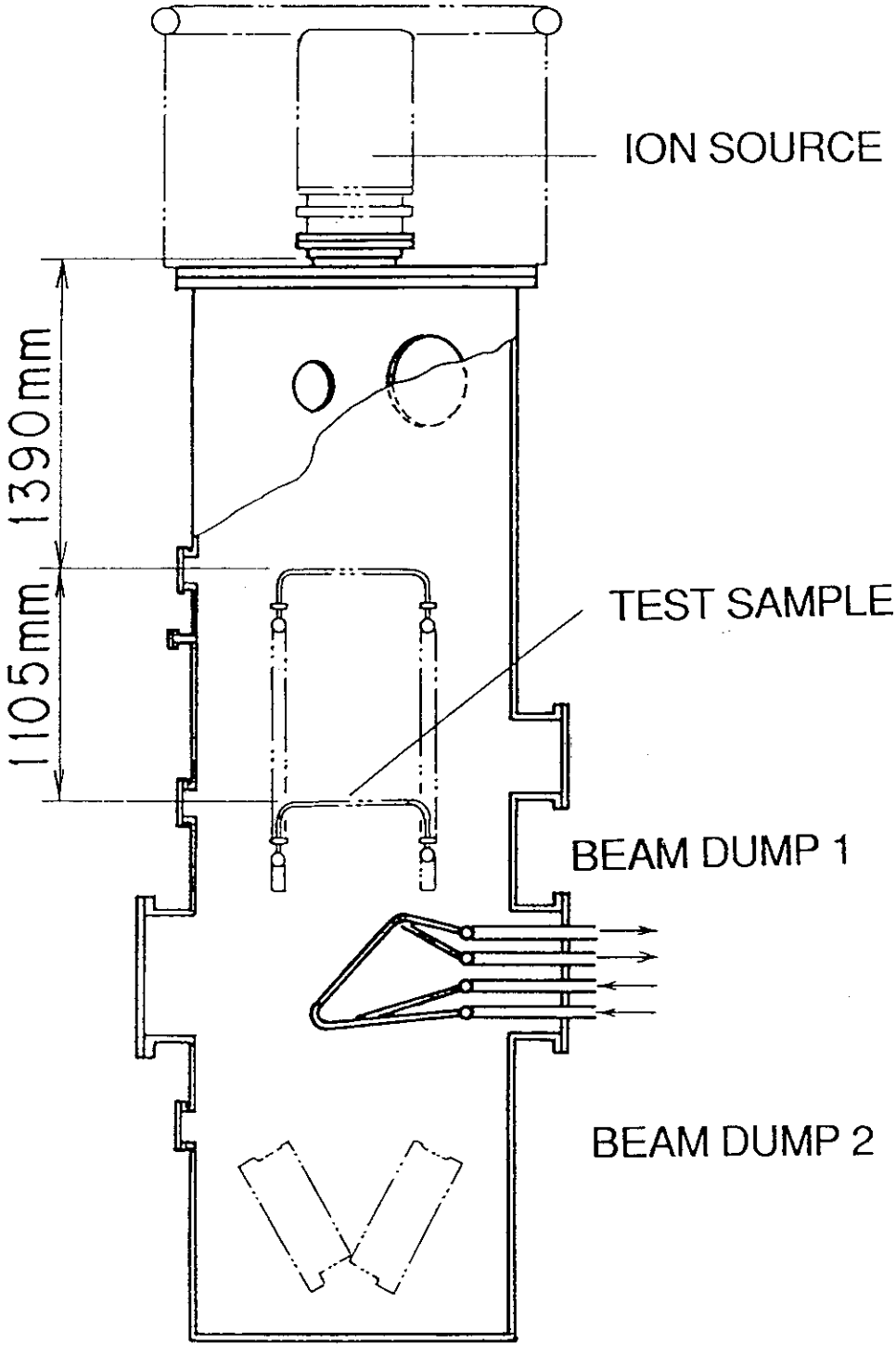

Figure 2-1 Schematic of the JT-60 Prototype Neutral Beam Injector System

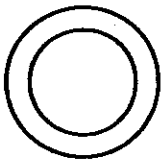

SMOOTH TUBE

MATERIAL	: OFHC Copper with 0.2 % Ag Content
OD/ID	: 10 mm/ 7 mm
LENGTH	: 500 mm

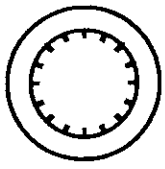

INTERNALLY-FINNED TUBE

MATERIAL	: OFHC Copper with 0.2 % Ag Content
OD/ID	: 10 mm/ 7 mm
LENGTH	: 500 mm
INTERNAL FIN HEIGHT	: ~ 1.2 mm
NUMBER OF FINS	: 16
HELIX ANGLE	: 5 °

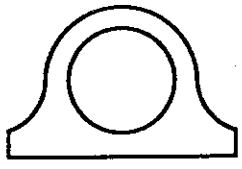

EXTERNALLY-FINNED TUBE

MATERIAL	: OFHC Copper with 0.2 % Ag Content
OD/ID	: 10 mm/ 7 mm
LENGTH	: 500 mm
EXTERNAL FIN WIDTH	: 15 mm

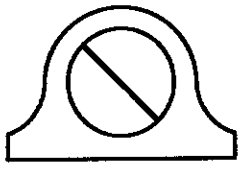

EXTERNALLY-FINNED SWIRL TUBE

MATERIAL(TUBE)	: OFHC Copper with 0.2 % Ag Content
MATERIAL(TAPE)	: INCONEL
OD/ID	: 10 mm/ 7 mm
LENGTH	: 500 mm
EXTERNAL FIN WIDTH	: 15 mm
TWIST RATIO*	: 2.0, 2.5

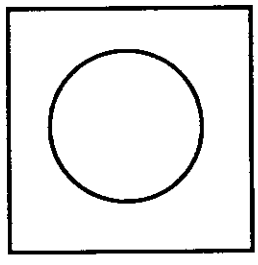

RECTANCULAR FACED TUBE WITH CIRCLE COOLING LINE

MATERIAL(TUBE)	: OFHC Copper with 0.2 % Ag Content
HEIGHT/WIDTH/ID	: 16 mm/ 16 mm/10 mm
LENGTH	: 500 mm

Figure 2-2. Cross Sectional View of Test Samples.

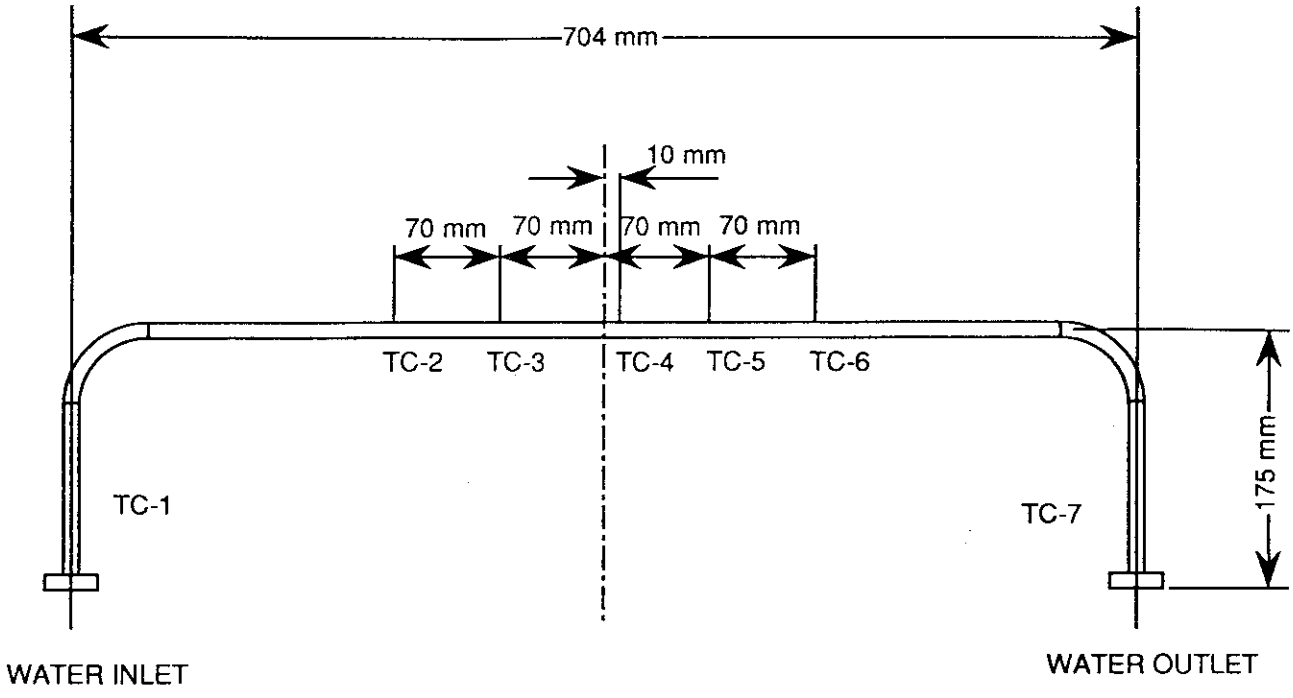

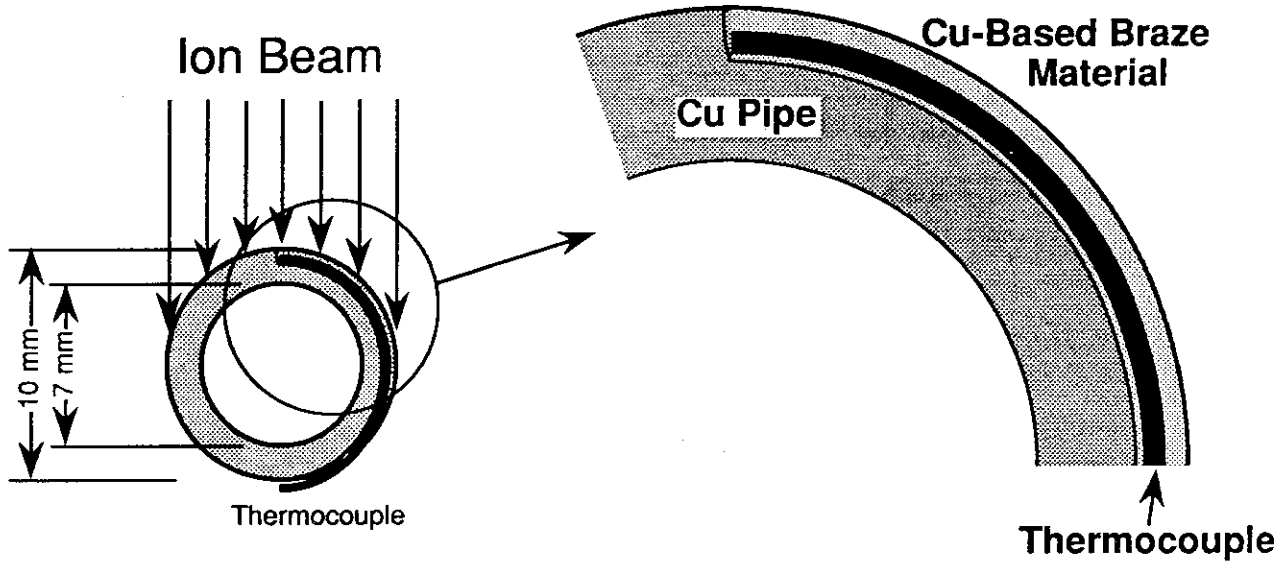

Figure 2-3. An Illustration of the Test Sample

Five thermocouples were brazed on the top surface of the test sample for detection of CHF and two thermocouples were also inserted to the tube to measure water temperature variations during heating.

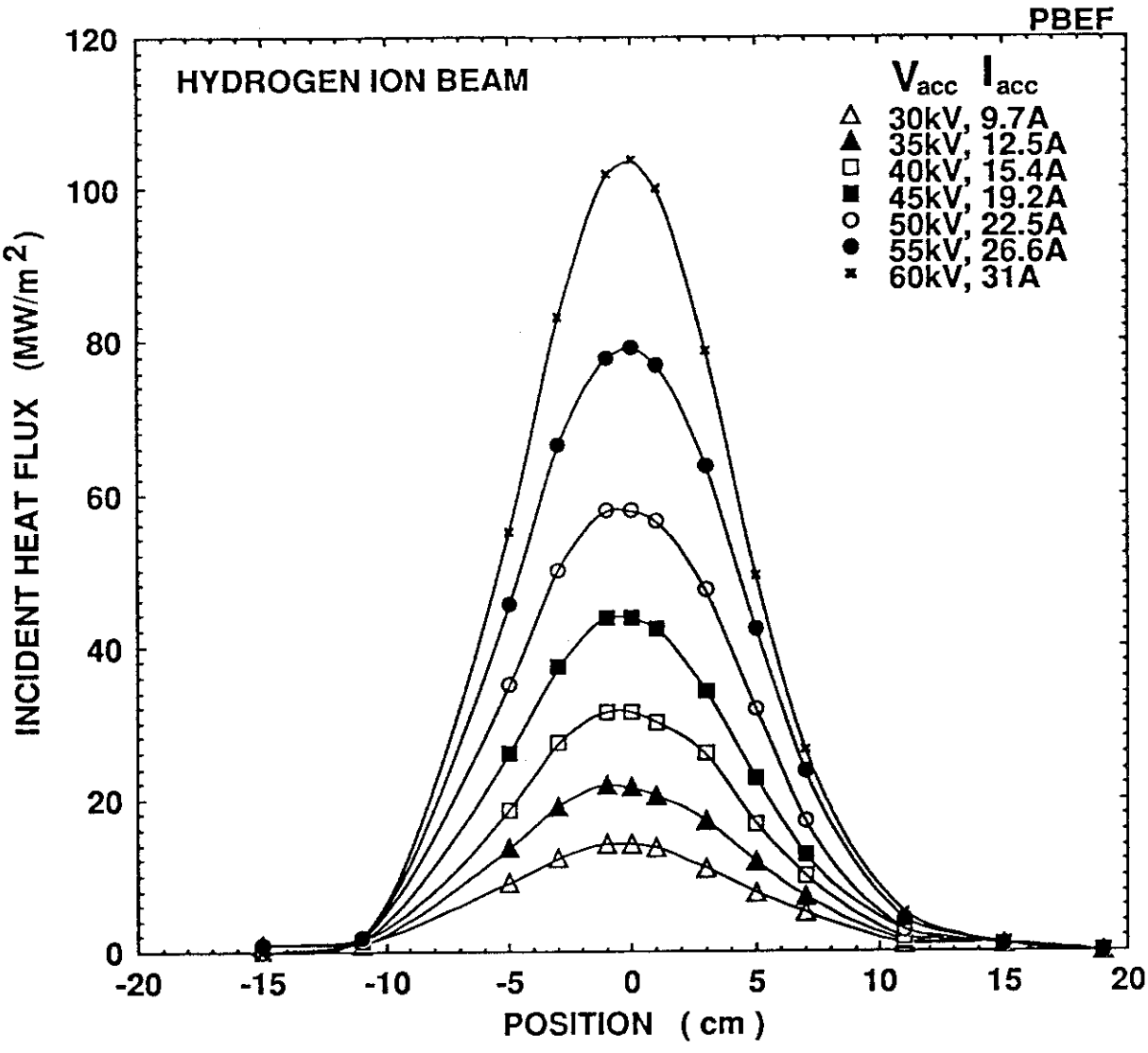

Figure 2-4. Intensity Profiles of the Ion Beam.

In the figure, V_{acc} and I_{acc} are acceleration voltage and beam acceleration current, respectively. Each profile shows quasi-Gaussian curve in the flow direction, while almost flat profile in perpendicular to the flow direction is obtained.

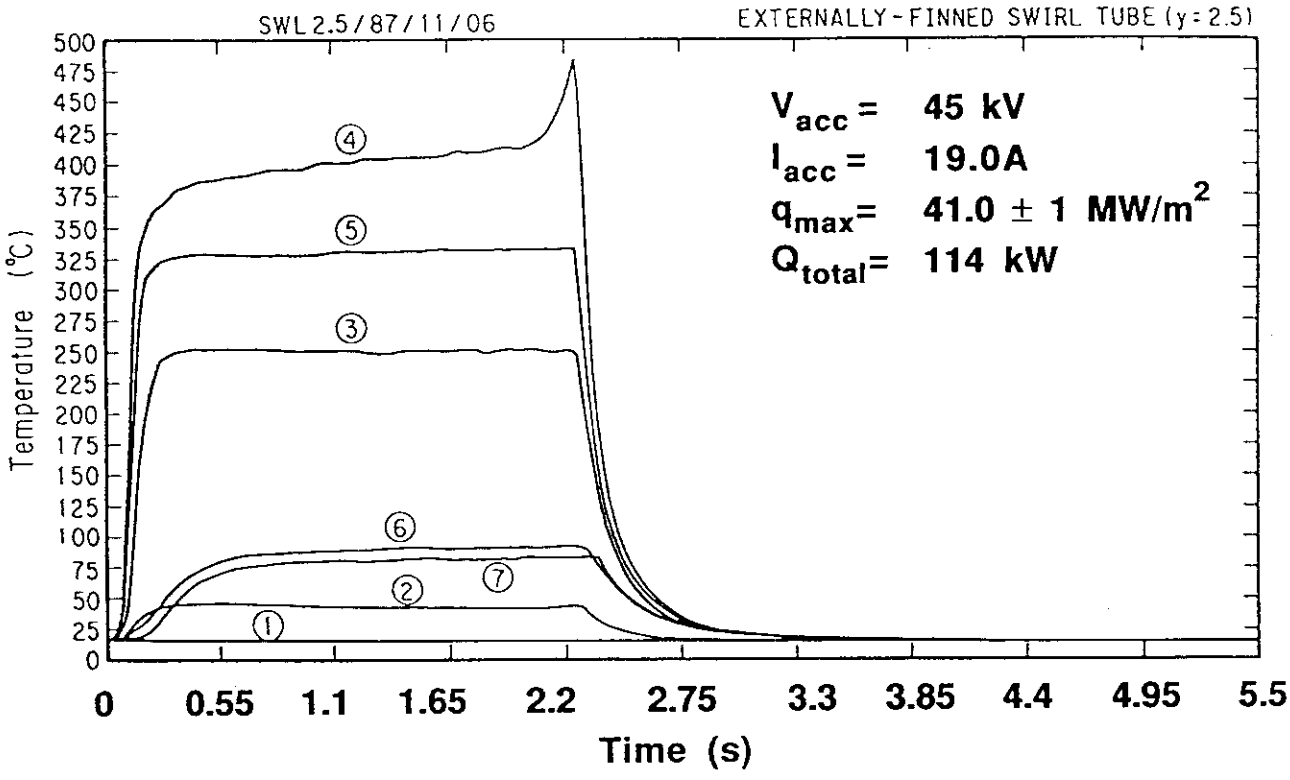

Figure 2-5 A Typical Example of Measured Temperatures in the Case of the Externally-Finned Swirl Tube

The number on each curve (labeled 1 to 7) corresponds to the thermocouples which are indicated in Fig. 2-3.

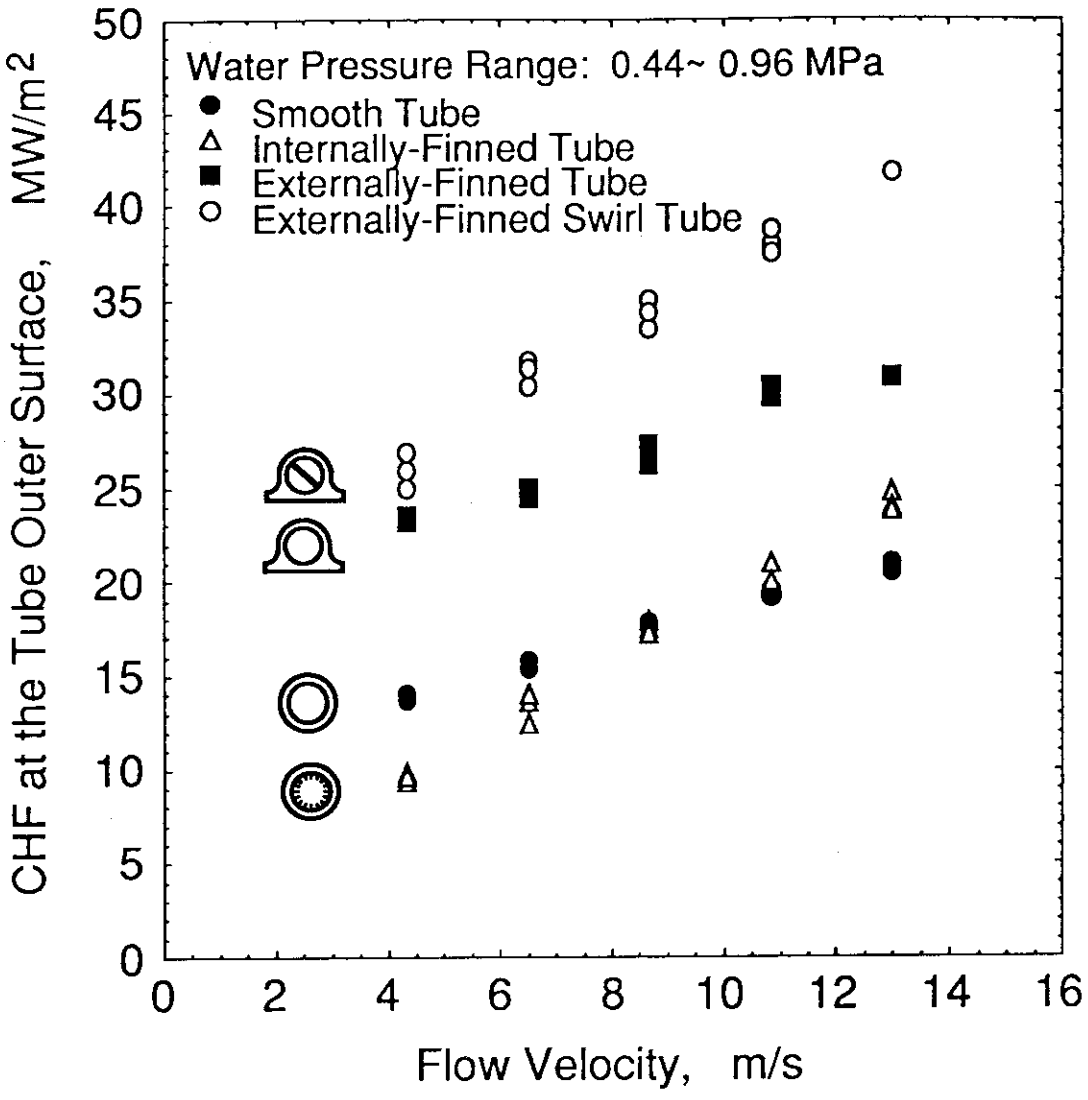

Figure 2-6 Experimental CHF Data as a Function of Flow Velocity

It is noted that the ordinate shows CHF at the tube outer surface, but not that at the tube inner surface.

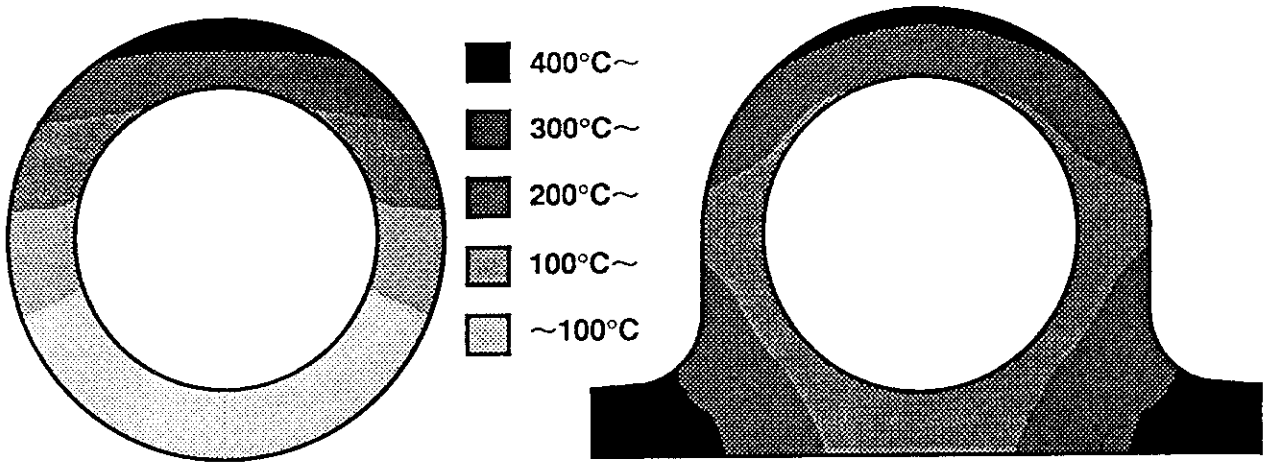

Surface Heat Flux	; 20 MW/m ^{2}
Flow Velocity	; 10 m/s
Inlet Temperature	; 20 °C
Outer Diameter	; 10 mm
Inner Diameter	; 7 mm

Surface Heat Flux	; 30 MW/m ^{2}
Flow Velocity	; 10 m/s
Inlet Temperature	; 20 °C
Outer Diameter	; 10 mm
Inner Diameter	; 7 mm
Width of an Fin	; 15 mm

Figure 2-7 Temperature Distributions of Tubes with and without the External Fin Under One-Sided Heating Condition

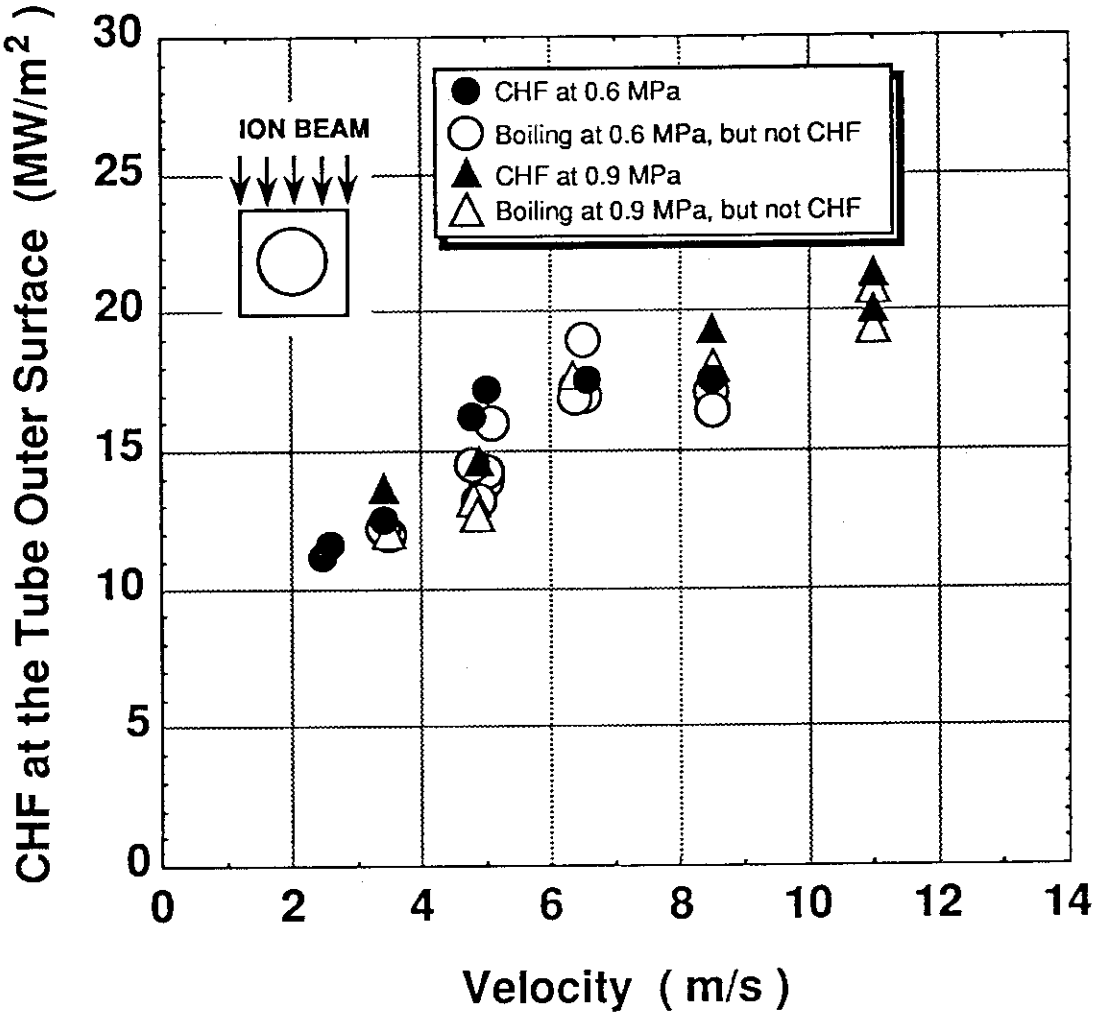

Figure 2-8 CHF Data of the Rectangular Faced Tube as a Function Flow Velocity

Symbols with a close circle and close traiangle show CHF points for different water inlet pressure and those with an open circle and an open traiangle show nucleate boiling regions without CHF, respectively.

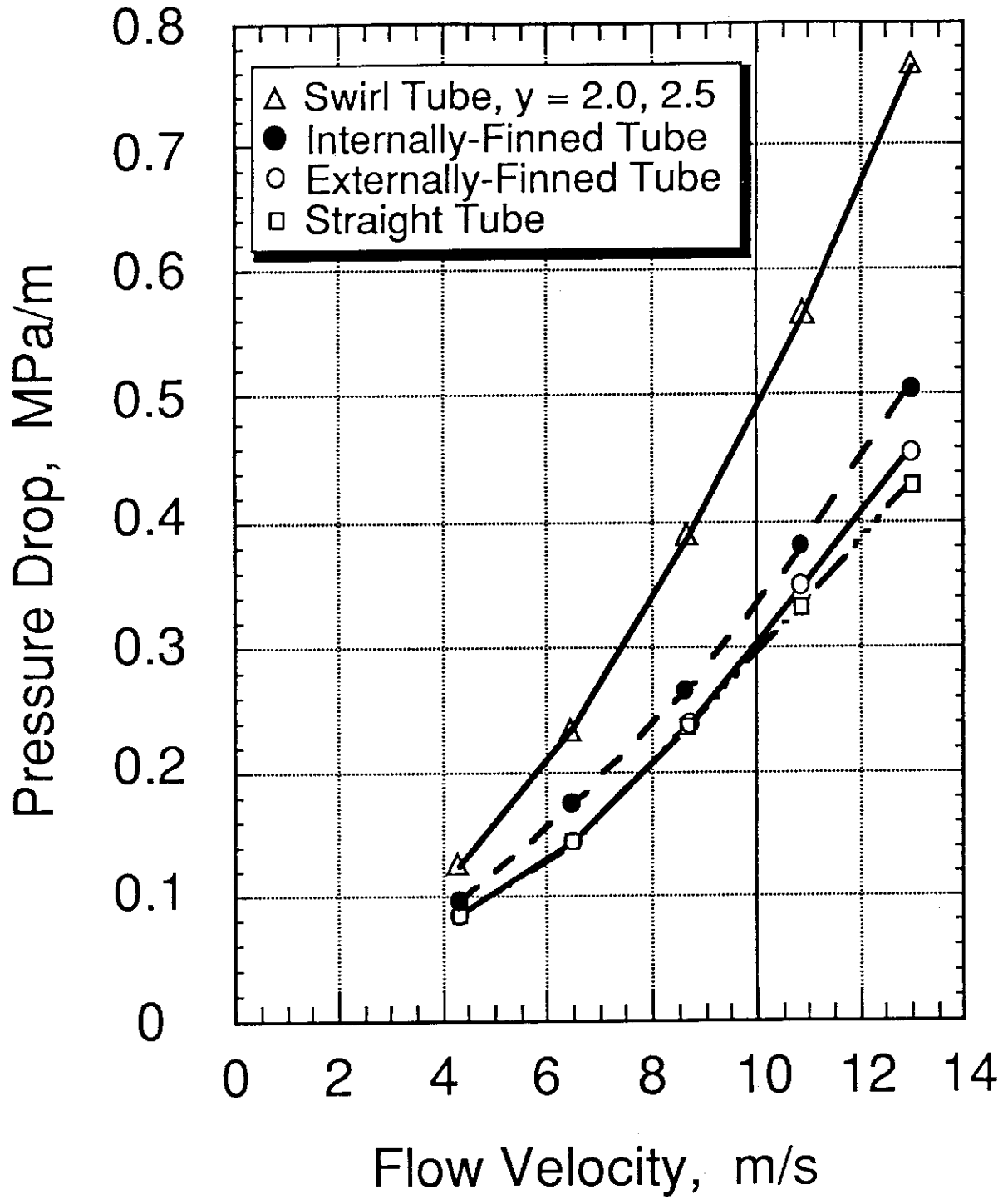

Figure 2-9 Pressure Drop of Test Samples

3. EVALUATION OF CRITICAL HEAT FLUX CORRELATIONS FOR ONE-SIDED HEATING CONDITION

3.1 Introduction

R&Ds of plasma facing components which the surfaces directly face the tokamak plasma such as the ITER have intensively been conducted. The performance requirements for the ITER plasma facing components are summarized in Table 3-1 [1]. Plasma facing components, in particular divertor plates, are subjected to severe one-sided heat loads from the tokamak plasma. Peak of the steady state heat flux on the surface of the divertor plate is estimated to be 15 to 30 MW/m^2 in the ITER conceptual design phase. A tube with a twist tape inserted, namely a swirl tube, or internal fins will be employed to the cooling tube for the divertor plate to enhance heat transfer into the cooling water. Performance tests of divertor mock-ups with the swirl tube or the smooth tube have been performed in several laboratories [20-23].

From the thermal-hydraulic point of view, it is very important to predict a critical heat flux (CHF) value and a safety margin of the cooling tube used in the divertor plate. Although numerous CHF correlations based on the condition for uniform circumferential heating were developed [2-7, 24], none of correlations based on one-sided heating conditions are available in the literature. It is, however, the worth trying a comparison of the experimental data with predictions obtained by the existing CHF correlations and models to evaluate their applicabilities. Since use of CHF data for highly subcooled flow regime in the swirl tube or the internally-finned tube is further complicated, experimental CHF data obtained with smooth walled tubes are evaluated first.

The present study describes the experimental CHF data and the existing CHF correlations in sections 3.2 and 3.3, respectively. In section 3.4, a comparison among them is presented.

3.2 Experimental CHF data

Critical heat flux experiments of various types of tube geometries have been performed under one-sided heating condition in a hydrogen ion beam test facility. [25] Figure 3-1 represents an example of the experimental CHF data as a function of the water flow

velocities of 2.3 to 15.5 m/s for the water inlet pressures of 0.44, 0.7 and 0.96 MPa. In the figure, it is noted that heat fluxes at the tube outer surface (incident heat flux) were measured and employed in the summary because of difficulty of translating incident heat flux into inner wall heat flux due to one-sided heating conditions.

Many experiments and studies on critical heat flux have been carried out under different experimental conditions as shown in Table 3-2 [6, 8-10, 25-27]. Nariai et al. [28] proposed that a formatted experimental data should be presented to ease the comparison. We also propose the publication of similarly formatted experimental data including heating profiles in each direction. Four experimental CHF data obtained under the one-sided heating condition are available in the evaluation for fusion applications. To evaluate the experimental CHF data to the existing CHF correlations, CHF values defined in the tube inner surface are necessary. In the present study, since it is the first step of the analysis, the heat flux at the tube inner surface is numerically predicted from the incident heat flux using a technique proposed by Horiike et al. [8] and Koski et al. [10]. In their analyses, the finite element method was used for the calculations and Thom's correlation [29] was used for predicted the heat transfer coefficient in a highly subcooled flow boiling. With respect to subcooled flow boiling, Shah's correlation [30] can also be used. Figure 3-2 shows a comparison of two correlations for the subcooled flow boiling proposed by Shah and Thom as a function of the wall superheat, $T_{wall} - T_{sat}$. Heat transfer coefficient predicted by Shah seems to strongly depend on the wall superheat compared to that by Thom. Although a deviation of heat transfer coefficient is confirmed between these correlations, a difference of heat flux at the tube inner wall between them is within less than 4 percents. After comparison of the correlations with the experimental data, temperature profiles predicted by Shah's correlation gave better results. Therefore, Shah's correlation was applied in the present analyses.

Figure 3-3 shows an example of numerical heat flux distributions at the tube inner surface for three different cooling tubes, which are normalized by each peak heat flux as a function of an angle from the top of the tube. The heat flux at the tube inner surface are also indicated in the right ordinates. For the straight and the rectangular faced tubes, the profiles deviate from cosine distribution with increasing angle because of thermal conductivity through the tube wall. Comparing with heat flux profiles along the circumference at the tube inner wall between the straight and the rectangular-faced tubes, a small deference are observed. This is a reason that a thickness at a angle of 90 ° from the top for the straight tube is similar to that for the rectangular-faced tube. Therefore, as

discussed in Chapter 2, it may be explained by this reason that CHF values of the straight tube are almost same as those of the rectangular-faced tube. In cases of the straight tube and the rectangular-faced tube, their profiles slightly deviate from cosine distribution with increasing the angle, while the flux profile in the case of the externally-finned tube is completely different compared with other profiles. It is a reason that the externally-finned tube geometry was originally developed to reduce the temperature gradient across the tube due to one-sided heating condition. It also means that this tube geometry is more close to that under uniform circumferential heating condition compared to the straight tube.

3.3 Existing CHF correlations

Many CHF predictable correlations have been developed under a condition for uniform circumferential heating with different experimental configurations by Gunther [2], Knoebel [3], Griffel [4], Tong [5, 24], Inasaka-Nariai [6], Katto [7], and so on. In this study, five CHF correlations as described below are compared with our experimental data to evaluate the applicability of the existing CHF prediction under one-sided heating condition.

Tong (1975) correlation was developed by modifying an original Tong correlation [24] to quantify the effects of local subcooling, vapor generation and condensation, and two-phase friction on CHF. The form of Tong (1975) [5] correlation used to predict the CHF is

$$q_{CHF}=0.23 f_0 G H_{fg}\left(1 + 0.00216Pr^{1.8} Re^{0.5} Ja\right), \quad (1)$$

$$f_0=8Re^{-0.6}\left(D_e/D_0\right)^{0.32} , \quad (2)$$

where q_{CHF}, G, H_{fg}, Pr and Ja are critical heat flux in MW/m^2, the water mass flux in $kg/(m^2 \cdot s)$, the latent heat of evaporation in kJ/kg, the ratio of the exit pressure to the critical pressure of water, and the Jacob number, respectively. This correlation can be used in the ranges for pressure of 7 to 14 MPa, mass fluxes of 5×10^5 to 4.4×10^6 kg/m^2s, and void fraction of up to 0.35.

For the application of the original Tong correlation [24] to a wide range of pressure,

Inasaka and Nariai proposed the following equation;

$$\frac{q_{CHF}}{H_{fg}} = C_{Tong}\frac{G^{0.4}\cdot m^{0.6}}{D^{0.6}}, \quad (3)$$

$$C_{Tong} = 1.76 - 7.433\chi_{eq} + 12.222\chi_{eq}^2, \quad (4)$$

$$\frac{C}{C_{Tong}} = 1 - \frac{52.3 + 80\chi_{eq} - 50\chi_{eq}^2}{60.5 + (10P)^{1.4}}. \quad (5)$$

where m, D, χ_{eq}, and P are the dynamic viscosity of water in Pa•s, the tube inside diameter in meter, the thermal equilibrium quality at the exit, and the pressure at the local point of CHF in Pa, respectively. This correlation can be used in the following ranges; 2 mm ≤ D ≤ 20 mm, 3 mm ≤ L (heated length) ≤ 200 mm, 0.1 MPa ≤ P ≤ 20 MPa, 1.3 Mg/m^{2}s ≤ G ≤ 20 Mg/m^{2}s, -0.001 ≥ χ_{eq} ≥ -0.46.

Katto extended an original Katto model, which is derived on physical model of liquid sublayer dry-out mechanisms, to be applied to a wide pressures (0.1 to 20 MPa) and proposed the extended Katto model for the CHF prediction (see reference [7]).

Other CHF correlations are indicated as follows;

- Gunther:

$$q_{CHF} = 71987\cdot u^{0.5}\cdot\Delta T_{sub,\ outlet} \quad (6)$$

where 0.1 MPa ≤ P ≤ 1.1 MPa, 1.5 m/s ≤ u ≤ 12.2 m/s.

- Knoebel:

$$q_{CHF} = 4.85 \times 10^5\left(1 + 1.71 \times 10^{-4}\cdot G\right)\left(1 + 0.124\Delta T_{sub}\right). \quad (7)$$

where 1.5 MPa ≤ P ≤ 3 MPa, 1 m/s ≤ u ≤ 15 m/s.

Figure 3-4 shows a comparison of each CHF prediction by their correlations as a function of water mass flux when a smooth walled circular tube is applied. Parameters, outer and inner diameters, pressure at the local point of CHF occurred, coolant bulk temperature and heated length, are kept to be constant values of 7 mm, 10 mm, 0.665

MPa, 318 K and 100 mm, respectively. Although some correlations are slightly out of ranges for the simulation condition, these CHF correlations are compared because none of the correlations under one-sided heating conditions. In the figure, it should be noted that the above correlations predict CHF values with a deviation or a discrepancy as large as around ± 40 %, even for the same simulated heating condition is applied for. Although this reason is not clear yet, these correlations obtained from the experimental data may strongly depend on the experimental conditions, such as a vertical or horizontal flow, quality of the coolant, pressure range, wall roughness of the test section, upflowing and downflowing.

3.4 Comparisons

Comparison of experimental data obtained under one-sided heating condition with the existing correlations is shown in Fig. 3-5 for the straight tube. The ordinate indicates the ratio of the experimental CHF value to that predicted with each correlations. The experimental data show relatively good agreement with the correlations proposed by Inasaka-Nariai, Knoebel and Katto (extended Katto) with an accuracy of -20 to +10 %. In particular, Inasaka-Nariai correlation can predict the experimental CHF data within an accuracy of ± 10 %. Tong (1975) correlation systematically underpredicts CHF values for over the range of mass flows investigated in the present experimental conditions, though Koski et al. reported that Tong (1975) correlation has been shown to be reasonable for their experimental results obtained under one-sided heating condition. It might be reason that they, however, didn't apply the original Tong (1975) correlation, e.g., the void fraction correlation used by Tong was not used in the analysis. On the other hand, our results are completely different to the results obtained by Celata et al., which reported that Tong (1975) correlation predicts higher CHF values in comparison with their data under uniform circumferential heating condition.

The ratio of the experimental CHF values to that predicted by each correlation is also plotted in Fig. 3-6 as a function of the mass flux in the externally-finned tube. Although heat flux profile along the circumference at the tube inner wall is more close to a uniform heat flux profile, all the existing correlations underestimate that the CHF values. For example, the experimental CHF data obtained under one-sided heating condition are up to 2 times larger than predicted by Inasaka-Nariai, 2.4 times larger than by Knoebel

and the extended Katto, and up to 3 times larger than by Tong (1975), respectively. Only Gunther correlation can predict the present CHF values except in a lower mass flux region, within an accuracy of around -20 %. Although this tube geometry compares better to uniform circumferential heating than the straight tube, no correlations based on uniform heating condition can be applied. For the externally-finned tube, a new CHF correlation is needed for the prediction of the CHF under one-sided heating condition.

Figure 3-7 also shows comparison of experimental CHF data with the correlations in the rectangular faced tube. 10 mm-Inner diameter of this tube is slightly larger than those of the other tubes. All the existing correlations also systematically underpredict CHF values for over the range of the mass flows investigated in the present experimental conditions, even if heat flux profile at the tube inner surface is similar to that of the straight tube. This is mainly attributable to the high degree of sensitivity of existing CHF correlations to the inner diameter, while in the experiment a small difference for different inner diameter.

Using existing correlations for uniform circumferential heating, therefore, it is difficult to predict the CHF values under one-sided heating condition. It also means that a new CHF correlation will be necessary for predicting CHF of the externally-finned tube and the rectangular faced tube under one-sided heating condition. To predict the CHF values under one-sided heating condition, it is very important to be verified heat transfer mechanisms because of no heat transfer correlations for one-sided heating conditions.

3.5 Conclusions

1. Incident CHF values obtained by the experiment under the one-sided heating condition have been translated to the CHF values at the tube inner surface with applying Shah's correlation for the subcooled flow boiling region.
2. Experimental CHF data of the straight tube under the one-sided heating condition shows relatively good agreement with Inasaka-Nariai, Knoebel, and the extended Katto correlations with an accuracy of -20 to +10 %, but Tong (1975) and Gunther correlations show larger deviations than the other correlations.
3. Large difference between experimental results and the existing CHF correlations are observed, although heat flux profile along the circumference of the externally-finned tube is more close to uniform heating condition compared to that of the straight tube.
4. All the existing correlations systematically underpredict CHF values for over the range of mass flows investigated in the present experimental conditions, even if heat flux profile at the tube inner surface of rectangular faced tube is similar to that of the straight tube. This is mainly attributable to the high degree of sensitivity of existing CHF correlations to the inner diameter, while in the experiment a small difference for different inner diameter.
5. Further experiments under the one-sided heating condition are necessary to derive a new CHF correlation for fusion applications.

Table 3-1 Required Performances of Plasma Facing Components for ITER

Operation Phase		Physics		Technology	
Components		First Wall	Divertor	First Wall	Divertor
- Peak/Aver. Surface Heat Flux	MW/m^2	0.6/0.15	15~30	0.6/0.15	15~30
- Peak Volumetric Heat Load in Structure	MW/m^3	20	5	15	4
- Number of Pulses (Full Load)	10^4	1		2~5	
- Total Burn Time	h	400		10^4~$3x10^4$	
- Peak Neutron Damage (Steel)	dpa	0.7	0.3	12~36	5~15
- Incident DT-Ions:					
• Peak Flux	$10^{20}/m^2s$	1	4000	1	4000
• Energy	eV	10~100	50~100	10~100	60~200

Table 3-2 Experimental Conditions of Critical Heat Flux with Water

P	ΔTsub	G	V	OD/ID	Γ	Φ		Power Source	Ref.
MPa	k	$kg/m^2 s$	m/s	mm	——	r	z		
0.44 ~0.96	106 ~134	4290 ~ 14400	4.2 ~15.0	10/7	y=2, 2.5	FLAT		H^+ beam	Araki, et al [13]
0.4 ~0.9	30~80	——	3~7.5	14/10		FLAT		H^+ beam	Horiike et al [14]
~ 0.9	50°C outlet	~1.24 kg/s	——	(17.5-27) /(10-14)	y=2	FLAT		H^+ beam e beam	Schlosser et al [15]
1.14 ,outlet	29°C outlet	——	5.0 ~12.0	9.5/8	y=2	FLAT	FLAT	e beam	Koski et al [16]
0.1 ~2.2	15.6 ~117.5	2207 ~ 33533	2.2 ~33.5	ID/(2.5-5)		FLAT	FLAT	Heater	Celata et al [17]
0.3 ~1.1	20 ~95	9300 ~ 29900	4.3 ~30.2	ID/3		FLAT	FLAT	Heater	Inasaka et al [11]
0.77 , 1.66	24 ~57	4600 ~ 40600	4.7 ~40.4	ID/3		FLAT	FLAT	Heater	Boyd et al [18]

Four data from the top are under a heating condition on one side of the test tube and other three data are uniform circumferential heating condition, respectively.

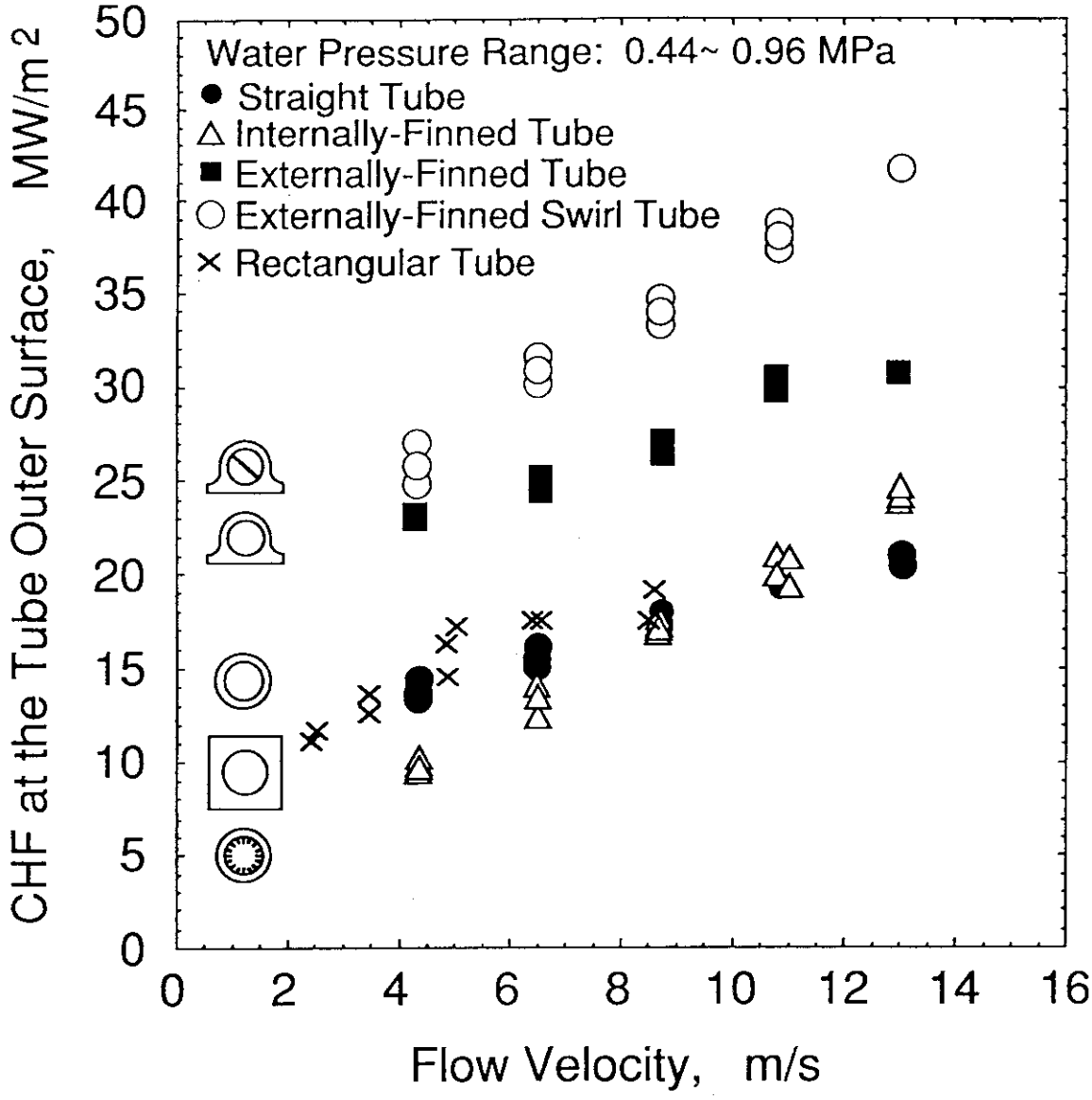

Figure 3-1 Experimental CHF Data as a Function of Flow Velocity

It is noted that the ordinate shows CHF at the tube outer surface, but not that at the tube inner surface.

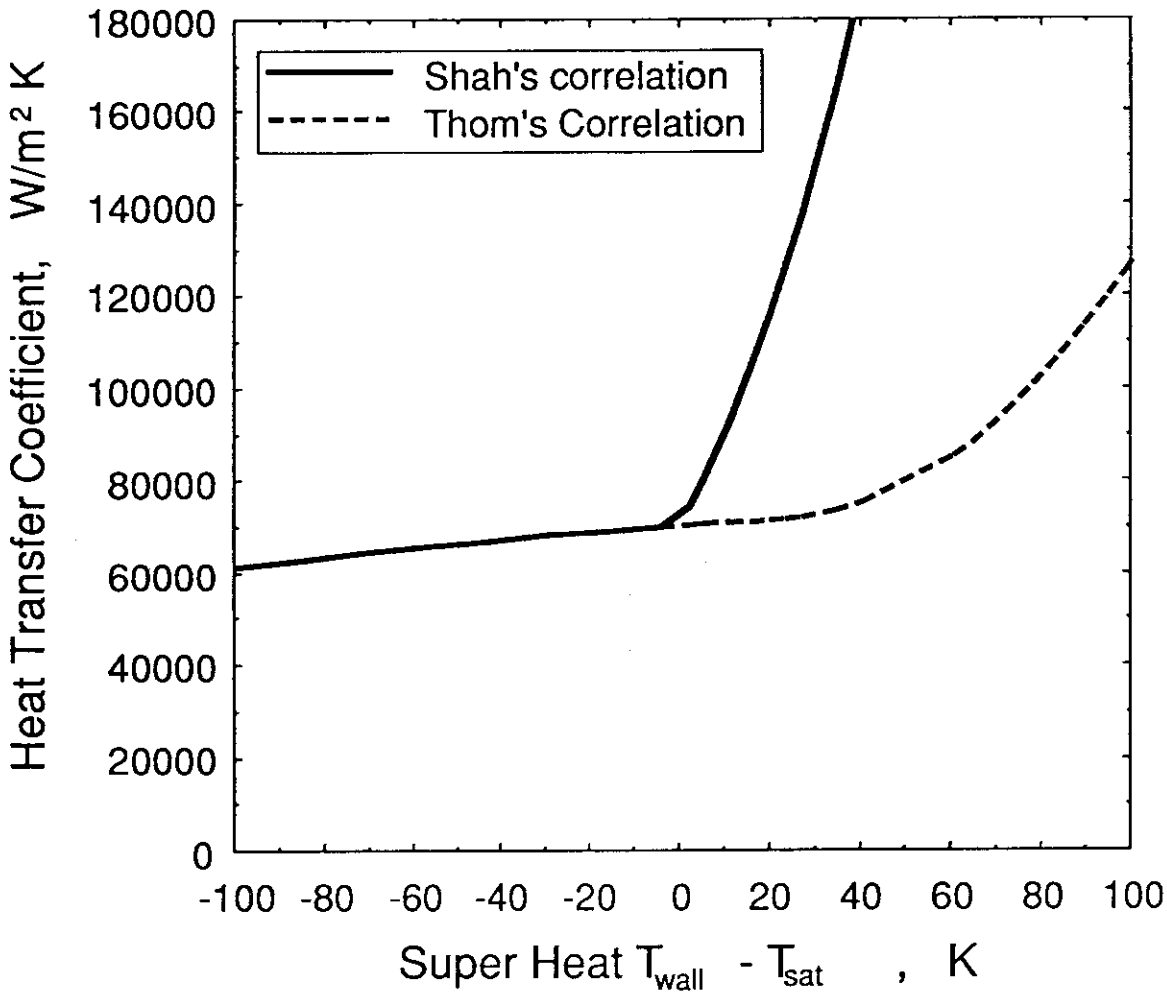

Figure 3-2 A Comparison of Correlations for the Subcooled Water Flow Boiling

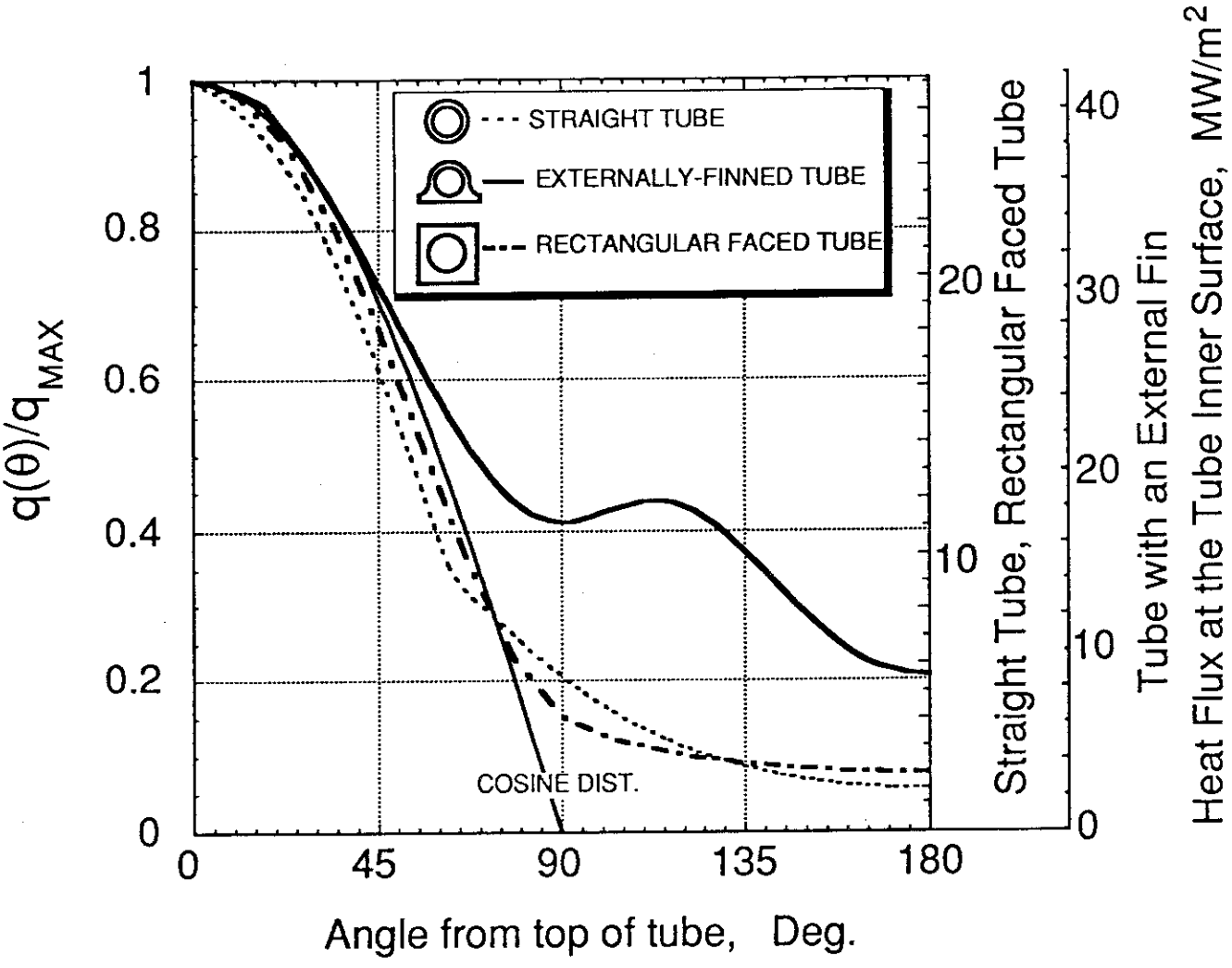

Figure 3-3. Typical Heat Flux Profiles at the Tube Inner Wall Under a Condition for One Side Heating

The ordinate shows normalized heat flux profile at the tube inner surface by the maximum heat flux. The figure also indicates heat flux profiles with right sided ordinates under a condition for local pressure and mass flux to be around 0.7 MPa and 8.58 x10 ^{3} kg/m^{2} s.

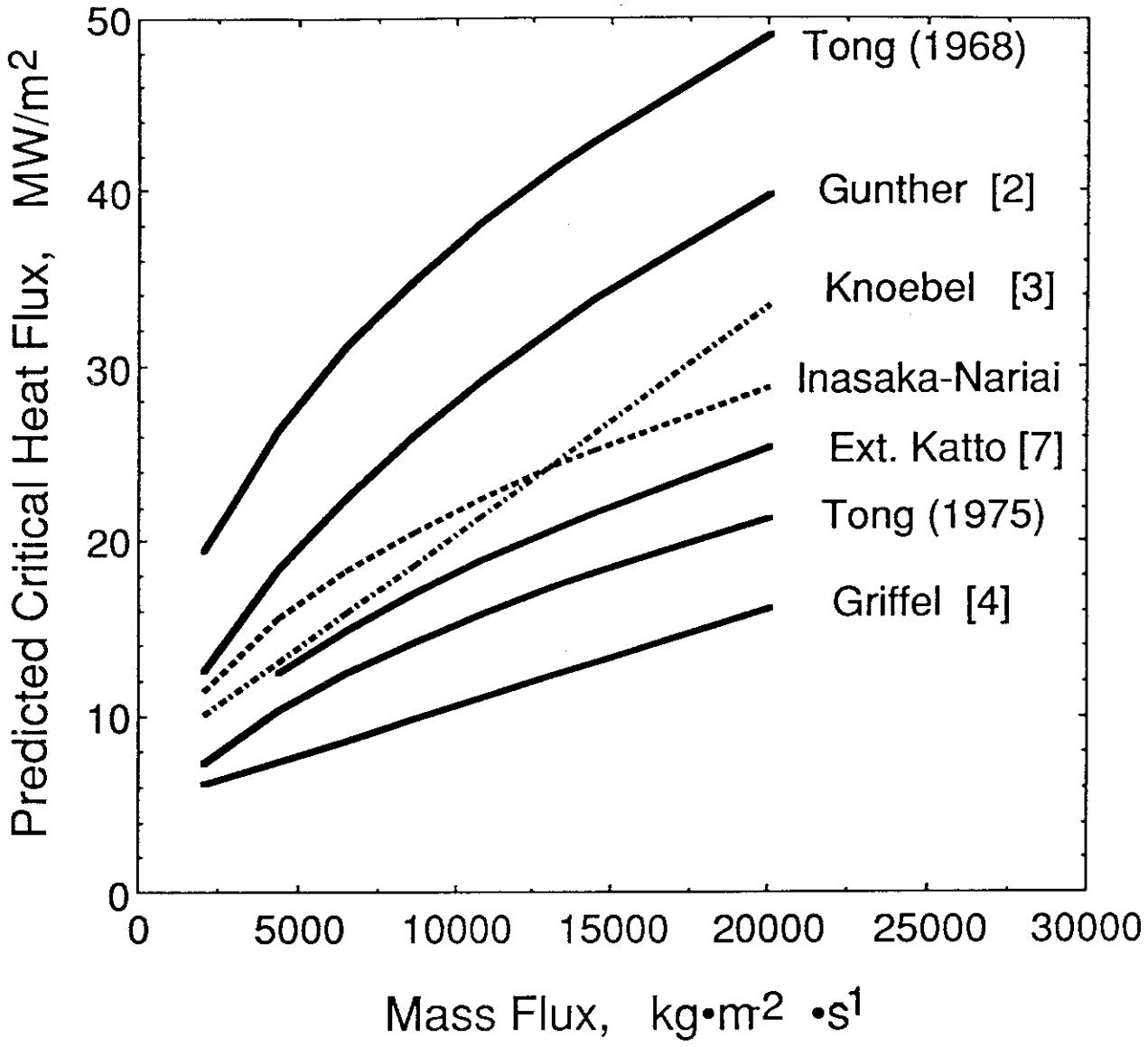

Figure 3-4 A Comparison of the Existing CHF Predictable Correlations

All data were calculated under the following conditions;

Tube Inner Dia. (mm)	: 7
Local Pressure (MPa)	: 0.665
Bulk Temp. (K)	: 318.0
Heated Length (mm)	: 100

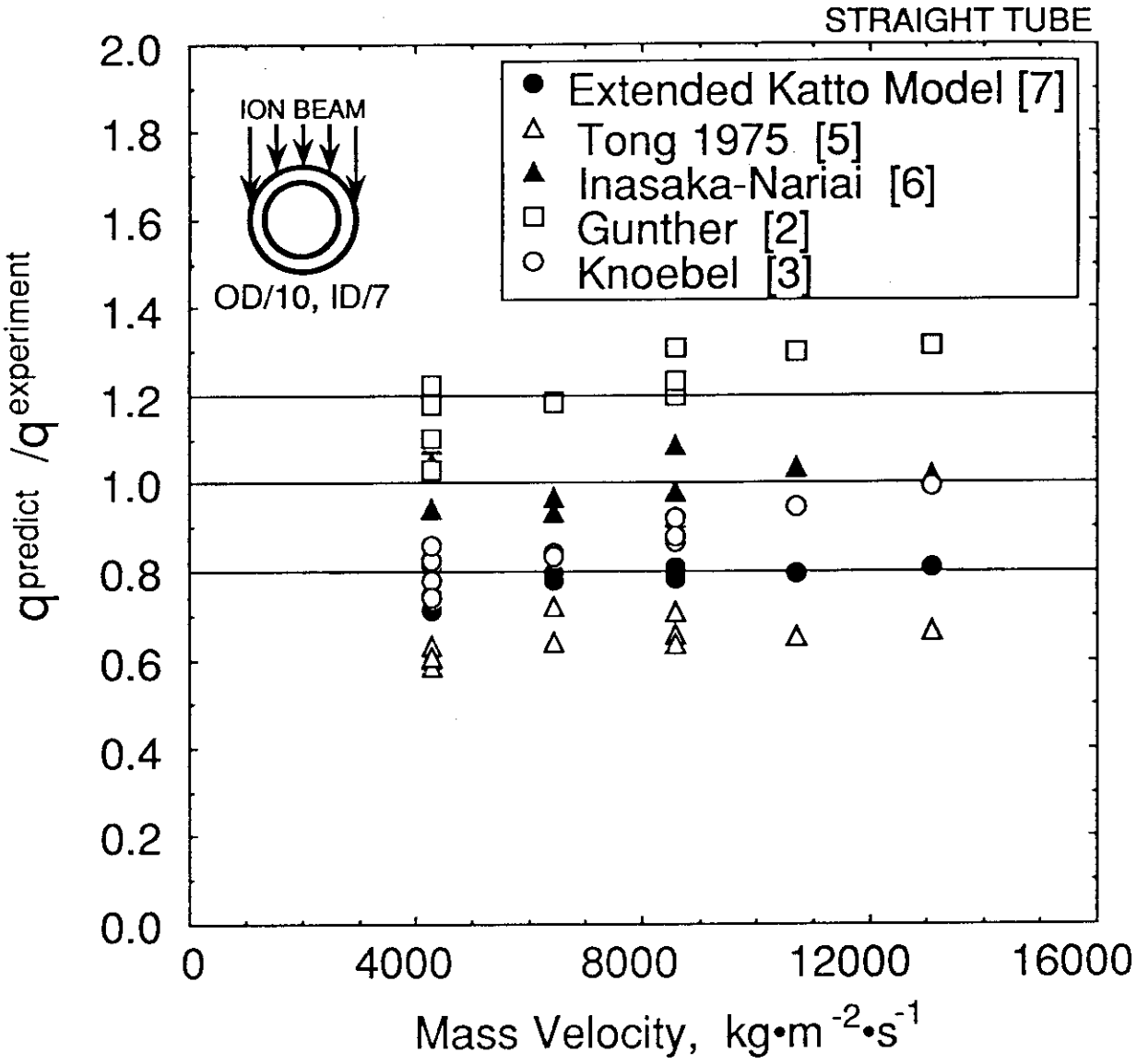

Figure 3-5 A Comparison of Experimental CHF Data with the Existing CHF Predictable Correlations (1)

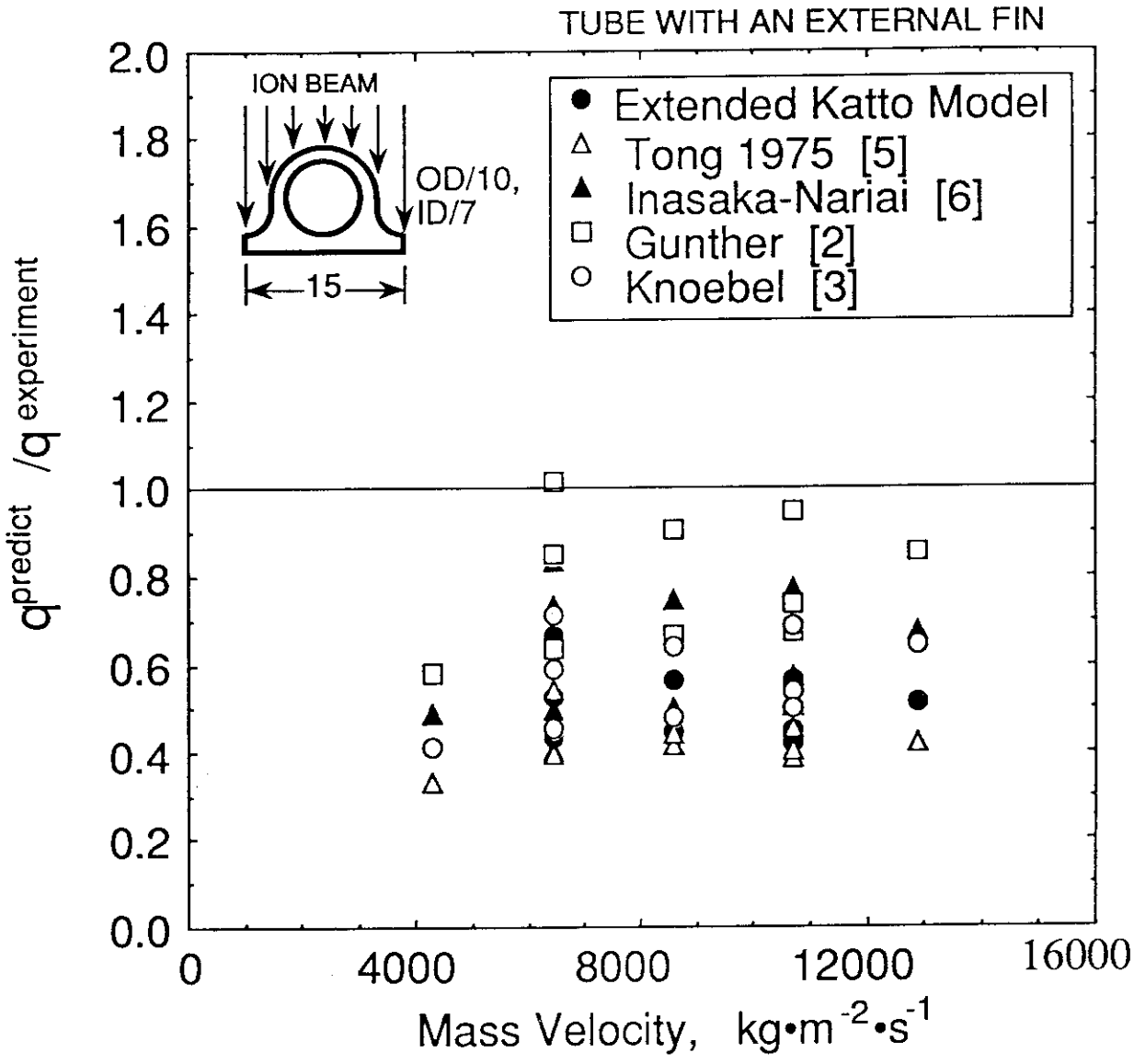

Figure 3-6 A Comparison of Experimental CHF Data with the Existing CHF Predictable Correlations (2)

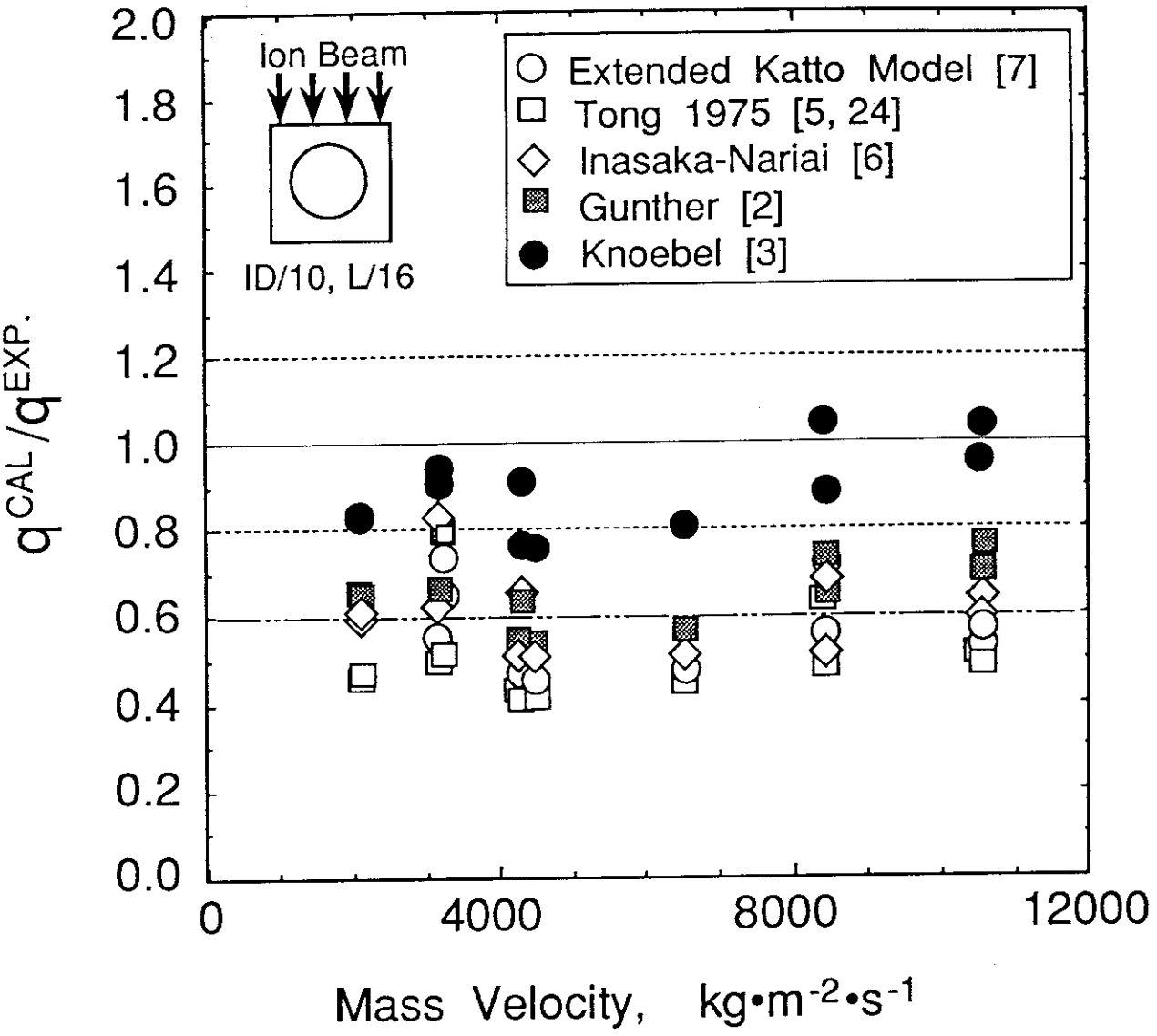

Figure 3-7 A Comparison of Experimental CHF Data with the Existing CHF Predictable Correlations (3)

4. THERMAL CYCLING EXPERIMENT OF BONDED CFC/OFHC-Cu DIVEROTR MOCK-UPS

4.1 Introduction

Research and developments on next generation fusion devices, such as ITER/FER [31, 32], are intensively conducted at JAERI. From the high heat flux viewpoint, plasma-facing components which mainly consist of first walls and divertor plates are required to handle heat loads not only in normal operation but also in plasma disruption. Experimental studies of various materials under thermal shock heat loads have been reported elsewhere [33-36].

In the ITER/FER normal operations, stationary heat fluxes and thermal cycles are estimated to be 0.2 - 0.6 MW/m^2 on the first wall and 10 - 30 MW/m^2 on the divertor and for more than 10^4 cycles, respectively [1]. Therefore, for the heat removal in the divertor, it is necessary to use forced convective cooling structures with high efficiency. Then, a tube with a twisted tape inserted is proposed for the divertor cooling tube from the promising results of burnout experiments. In order to minimize the impurity flux into plasma, low-Z materials will also be preferred as the armor tile of plasma-facing components and therefore high performance carbon based materials, in particular newly developed carbon-fiber-composites, have been selected.

In accordance with the heat flux level, three types of heat removal structures are considered, i.e., a conductively cooled (mechanically attached), a radiatively cooled, and a directly cooled (bonded) structures, respectively. For the first wall, the conductively and the radiatively cooled structures have been proposed and tested because of relatively low heat fluxes deposited, and the results have already been reported [37]. Therefore, this chapter focus on a description about R&Ds of the divertor plate. To obtain the promising heat transfer from the armor tile to coolant, the armor tile material should metallurgically be attached to the metal (cooling tube or cooling structure). In this case, it is very important to evaluate an adhesive property between the armor tile and the metal because of poor compatibility of thermomechanical properties. To investigate the overall performance of the bonds against large number of cyclic heat loads, thermal cycling tests are performed for bonded carbon-fiber-composite/OFHC (CFC/OFHC) divertor mock-ups with and without the molybdenum interface structure.

The test facility and divertor mock-ups including residual stress analysis will be

described in section 4.2 and 4.3, respectively. Experimental results under the large number of cyclic heat load are presented in section 4.4.

4.2 High heat flux test facility

Two test facilities are available for high heat flux experiments at JAERI. One is an electron beam facility, namely JEBIS [33, 38], and the other is a particle beam engineering facility, namely PBEF [4-10]. In the present experiment, the PBEF facility was used in order to derive relatively wide heat flux profile compared to the JEBIS. A schematic and the performances of the facility are shown in Fig. 4-1 and Table 4-1 as shown in section 2.1, respectively. The PBEF facility can deliver a hydrogen ion beam of up to 5 MW for durations from 10 ms to 10 s. Major dimensions of the main vacuum chamber are 1.5 m in diameter and 5.0 m in height. An ion source, which was originally developed for neutral beam injection systems of JT-60 [39], is installed at the top of the main chamber. Two test sections with forced convective cooling lines in the chamber are prepared to obtain different beam profiles on the sample. Each test section has two cooling lines which independently supplies the deionized water of up to 100 l/min for the inlet pressure of up to 2 MPa. Since the similar heated area compared with the ITER is obtained in the lower test section, the divertor mock-up set at this position is connected with the lower cooling line in the chamber.

A commercially developed infrared camera that has a maximum sampling speed of 50 ms/frame is also mounted to investigate surface temperature of the sample during heating. All output signals, such as temperatures from thermocouples, water flow rate, and pressures, are analyzed by a high-speed multi-channel data logger system controlled by a computer NEC/PC9801, whose sampling time and an interval time are 30 ms/channel and 10 ms, respectively.

4.3 CFC/OFHC-Cu divertor mock-ups

4.3-1 Manufacturing procedure

In testing thermomechanical performance of the bonds, seven divertor mock-ups were prepared in which ten pieces of bonded samples per mock-up were brazed in line

with a single cooling tube. Typical dimensions of the bonded samples as shown in figure 4-2 are 25 mm wide, 25 mm long, and 35 mm high including the armor tile (height of 10 mm). An advantage of this configuration is to have a possibility of *in-situ* repair when the armor tile were failed.

Manufacturing process of the divertor mock-ups is shown in figure 4-3. After machined with or without Ti-Ag metallizing on the interface of CFCs, CFCs were degassed in vacuum environment with temperature of around 1000 °C to improve the adhesive property between the CFC armor tile and the copper heat sink before brazing to the metal. Subsequently, the CFC tiles were brazed on the copper heat sink at around 850 °C for several minutes in vacuum environment with different Ti/Cu/Ag content braze materials. In the divertor mock-ups, x-y plane of CFC is oriented perpendicular to the water flow direction because the CFC has high thermal conductivities in the directions. After that, ten bonded samples were brazed to the cooling tube in vacuum environment.

Divertor mock-ups with fine-grained graphite tiles were also prepared in this experiment. For some divertor mock-ups, an intermediate material made of molybdenum was inserted between the armor tile and OFHC-Cu in order to perform further improvement of the adhesion. Thickness of the molybdenum intermediate was 2 mm in these mock-ups.

No heat transfer enhancements such as a twisted tape insertion were applied in all the cooling tubes because main objectives are to investigate the overall performance of the bonds. These mock-ups were manufactured by Hitachi Ltd., Kawasaki Heavy Industries Ltd., Mitsubishi Heavy Industries Ltd., and Toshiba Ltd., with applying newly developed brazing technologies [40, 41].

4.3-2 Residual braze stress analysis

Residual stresses due to brazing (residual braze stress) for different armor tile materials were analyzed using three-dimensional code because of highly anisotropic property of the CFC material. In the analyses, temperature dependence of mechanical properties of the OFHC-Cu were considered [41]. Highly anisotropic properties of various CFCs [42] were also considered in each direction. Figure 4-4 shows an example of peak residual braze stresses of the bonds as a function of the reference temperature corresponding to stress-free temperature in a material combination with CX-2002U and OFHC copper. In Fig. 4-4(a), thermal and shear stresses of each direction in the CFC material close to the

interface are indicated. Also, in 4-4(b) equivalent stresses by Mises and Tresca are indicated. With respect to stress-free temperature of the braze material in the interface, it could be assumed to be much lower, i.e., 600 °C, because the CFC armor tile was brazed on the OFHC-Cu heat sink at a temperature around 850 °C, which is much higher than the softening temperatures of the braze material (600 °C) and OFHC-Cu heat sink (250 °C), respectively. Based on the result shown in Fig. 4-4(a), maximum residual braze stress is estimated to be about -46 MPa in y-direction which appears in the CFC material close to the bonded layer. It is found that this value is close to the ultimate strength of CX-2002U, ; -49.5 MPa.

On the other hand, Mises and Tresca equivalent stresses as shown in Fig. 4-4(b) exceeds the ultimate strength of CX-2002U. Since date of ultimate strength in each direction of CFC material are only available, thermal stress in each direction has been investigated as the first step in this analysis, and therefore other equivalent stress, for example, von Mises equivalent stress is not applied [43].

Figure 4-5 shows a typical residual braze stress profile of cross sectional plane (Y-Z plane) at x=25.0 mm for three directions after cooldown from brazing. In x- and y-directions, compressive stress remains in the CFC armor tile and tensile stress in the OFHC-Cu heat sink close to the bonded layer. In z-direction, only compressive stress appears in the region of the bonded layer. Their analytical results show relatively good agreement with the results of the manufactured test samples in the point that no cracks or detachments were observed in many samples by surface observation before thermal cycling test.

4.4 Experiments and Analysis

4.4-1 Experimental procedure

The experimental conditions were determined on the basis of the transient thermal analyses to rationally turnaround the experiment. The preliminary numerical result shows that the stress inducing fracture at the interface is affected by the interface temperature and less dependent on the temperature distributions in each constituent material [44]. For the FER/ITER operation heat flux of 10 MW/m^2, numerical results show that a steady state temperature in the bonded layer reaches 320 °C in the material of CX-2002U and OFHC copper combination. Since heat transfer coefficient in the cooling tube was expected to be

about 1.98 x 10^4 W/m^{2}K in the present experiments, the heat flux of 16.0 MW/m^2 for pulse duration of 1.5 s was selected as an appropriate combination that raises the interface temperature to be 320 °C, as shown in Fig. 4-6. The cyclic heating condition of 16 MW/m^2 for the pulse duration of 2 s with the interval time of 60 s was also expected to simulate the equivalent temperature of the interface for a steady state heat flux of 12.5 MW/m^2.

Because of an uncertainty for the surface heat flux estimation from results obtained by water calorimetry [21, 43, 45], heat fluxes and their profiles deposited to the surface of the mock-up were directly measured by a multi-channel calorimeter. Heat flux profile as shown in Fig. 4-7 is quasi-Gaussian, in which horizontal axis indicates the position along the flow direction and zero position is corresponding to center of the sample. Temperature responses of the armor surface and the OFHC-Cu heat sink close to the interface were measured by the commercially developed infrared camera and thermocouples to observe the integrity and failure of the bonds, respectively.

4.4-2 Experimental and analytical results

In the experiments, main objectives are to investigate the overall performance of the bonds against thermal cycles under the ITER/FER equivalent heat flux condition. After 1,000 thermal cycles under the heating condition of 16 MW/m^2 for 1.5 s, several specimens with the CFC materials were found to survive without cracks and failures, leading us to conceive of promising prospect for the divertor plates that can withstand a steady state heat flux of 10 MW/m^2. However, all the specimens were damaged to occur cracking near the interface, clearly indicating the further needs for R&Ds on the bonds and on its configuration for steady state heat fluxes higher than 12.5 MW/m^2. As shown in Fig. 4-8, some armor tiles including CFC were detached from the OFHC-Cu heat sink during heating. This reason is mainly attributable to initial lack of the braze material. Although a crack appeared at the outer surface of the CFC close to the bonded layer, some specimens have withstood 12.5 MW/m^2 for 1,000 cycles without increase of the surface temperature. From the SEM observation, the crack stopped at a pore of the CFC and its length was within 1.0 mm as shown in Fig. 4-9.

In the bonded fine-grained graphite/OFHC-Cu divertor mock-ups with molybdenum intermediate (Gr/Mo/OFHC), the integrity of the bonds after 1,000 thermal cycles has

been confirmed under the heating condition of 16 MW/m^2 for 1.0 s which corresponds to the steady state heat flux of 8 MW/m^2. Some Gr/OFHC-Cu samples has withstood cyclic heat loads up to 10 MW/m^2 for 1,000 cycles with small increase of the surface temperature, although many longer cracks appeared at the outer surface of the graphite close to the bonded layer. Their results agree with the other experimental results [21, 43, 46], although configurations and material combinations of the divertor mock-ups are slightly different.

For higher heat fluxes, all the bonded Gr/Mo/OFHC-Cu samples were damaged in large cracking in the graphite armor tile near the interface. After several hundreds of the shots, surface temperature of the graphite armor tile increased to higher than 1000 °C, while temperature of OFHC-Cu close to the bonds decreased due to initiation of cracks at the graphite close to the bonded layer and their growth shot by shot. It is clear that bonded Gr/Mo/OFHC-Cu sample will not withstood any longer for higher heat flux of 8 MW/m^2 and therefore the graphite materials might be unsuitable for the armor tile material of the ITER/FER divertor plate under high heat flux environment due to its lower fracture toughness.

No advantages on insertion of molybdenum as the intermediates were observed in this experiment. This reason might be explained as follows; although a braze material with low thermal expansion is preferred for brazing between the graphite tile and the molybdenum intermediate, a same kind of the braze material was used for brazing between graphite to molybdenum and OFHC copper to reduce a number of thermal cycles during manufacturing process.

The stress amplitude of the sample under the thermal cycles was analyzed using the numerical results of the residual braze stress in the elastic-plastic numerical model. Figure 4-10 shows an example of time histories of thermal stresses in the material composed of CX-2002U and OFHC copper under cyclic heat flux of 16 MW/m^2 for duration of 1.5 s. As results, the maximum stress amplitude at the CFC armor tile close to the interface as shown in the figure (a) is estimated to be around 11.5 MPa in x-direction, 15.2 MPa in y-direction, and 27.8 MPa in z-direction for the simulated steady state heat flux of 10 MW/m^2. Therefore, it is expected that stress amplitude in z-direction mainly induces fracture at the CFC close to the interface.

Figure 4-10(b) also shows time histories of thermal stresses under cyclic heat flux of 16 MW/m^2 for duration of 2.0 s. The maximum stress amplitudes are also expected to be around 14, 20, and 33 MPa in each direction, respectively. Comparing these results with

numerical results obtained under the ITER/FER equivalent heating condition, the stress amplitude of the sample under the simulated pulse heat condition resulted to slightly higher value. The reason might be an influence of different temperature distributions in each constituent material between their conditions.

4.5 Discussions

To predict thermal fatigue lifetime of the bonds against thermal fatigue, analytical results have been compared with the experimental results. Smid et al. [21, 46] summarized formatted data which showed a damage map in heat flux vs. thermal cycles. This map, however, is not enough to evaluate the lifetime of the bonds. Therefore, new damage map as shown in figure 4-11 is proposed through this study. The horizontal and vertical axes indicate number of thermal cycles and surface heat flux on the sample. The vertical axis in the right side also indicates an example of a maximum stress amplitude calculated during thermal cycles in the material of CX-2002U and OFHC copper. In the figure, circular- and triangular symbols show the results obtained for material combinations of CFC (CX-2002U, A05, PCC-1S, MFC-1, MCI-felt, and JCC) with OFHC copper, and of graphite (IG-430U and PD-330S) with the copper, respectively. In judging the durability of the bonds from the limited present data, it can be summarized that the bonded CX-2002U/OFHC-Cu and PCC-1-2S/OFHC-Cu samples have relatively good performances compared to the other material combination bonds. In particular the CX-2002U/OFHC-Cu sample withstands the thermal stress amplitude up to 33 MPa for 1,000 cycles. From the experimental data, however it was not confirmed that small crack appearing at the corner of the CFC close to the bonded layer induces further fracture propagation. This reason might be attributable to their higher porosity (~ 20 %) compared to those of the fine-grained graphites (several percents). Since limited data are available for the lifetime evaluation, it is difficult to predict the lifetime of the bonds and further experiments are necessary.

4.6 Conclusions

1. The durability of the divertor mock-ups with CFC armor tiles was confirmed after 1,000 thermal cycles under the condition at which the thermal stress on the interface is expected to be equivalent to the value for a steady state heat flux of 10 MW/m^2.

2. In the bonded fine-grained graphite/OFHC-Cu divertor mock-ups with molybdenum intermediate (Gr/Mo/OFHC), the integrity of the bonds was confirmed through the experiment under the heating condition of 16 MW/m^2 with 1.0 s for 1,000 cycles corresponding to the steady state heat flux of 8 MW/m^2. Some Gr/OFHC-Cu samples have resisted to up to 10 MW/m^2 for one thousand cycles without increase of the surface temperature, although many longer cracks appeared at the outer surface of the graphite close to the bonded layer.
3. Some CFC/OFHC-Cu samples have resisted to 12.5 MW/m^2 for one thousand cycles without increase of the surface temperature, although cracks appeared at the outer surface of the CFC close to the bonded layer.
4. Analytical results of residual braze stress of the bonds show relatively good agreement with the manufactured test samples and no cracks or detachments in many samples were observed by surface observation.
5. A new damage map in terms of the number of thermal cycles and surface heat flux is proposed. A maximum stress amplitude calculated during thermal cycles, which is very important for the lifetime evaluation of the bonds, is also taken into account in the map.

Table 4-1 Performances of the Test Facility

	PBEF
Acceleration Voltage, kV	30 - 100
Acceleration Current, A	up to 50
Pulse Duration, s	0.01 - 10
Working Gas	H_2
Beam Species	Hydrogen
Type of Ion/Electron Source	Magnetic Multi-pole Ion Source
Maximum Heat Flux, MW/m^2	> 260
Maximum Heating Area, cm	10 x 20
Water Cooling System	$60m^3/hr$ with 2 MPa
Pressure in the Test Bed, Pa	<0.053

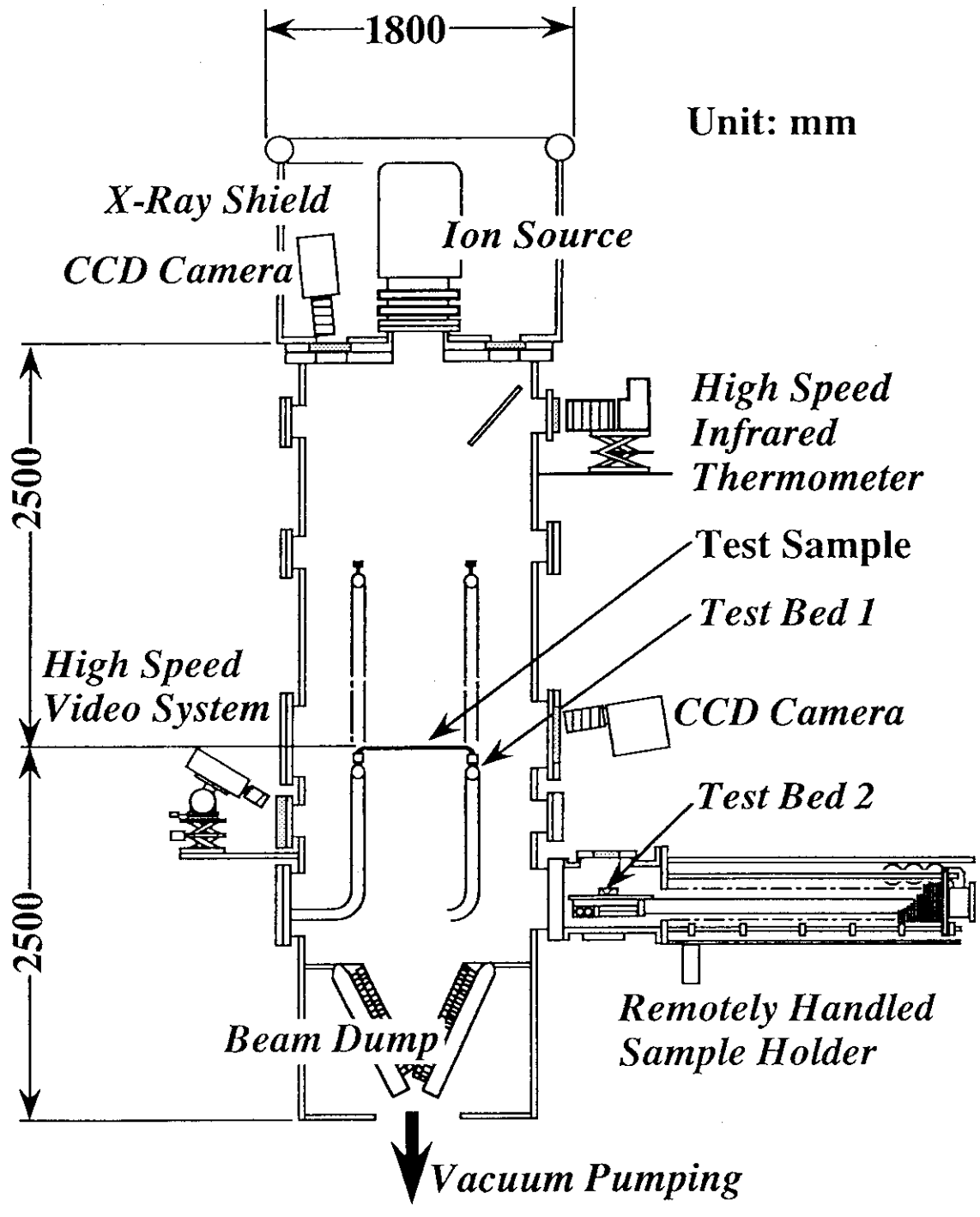

Figure 4-1. Schematic of Particle Beam Engineering Facility (PBEF).

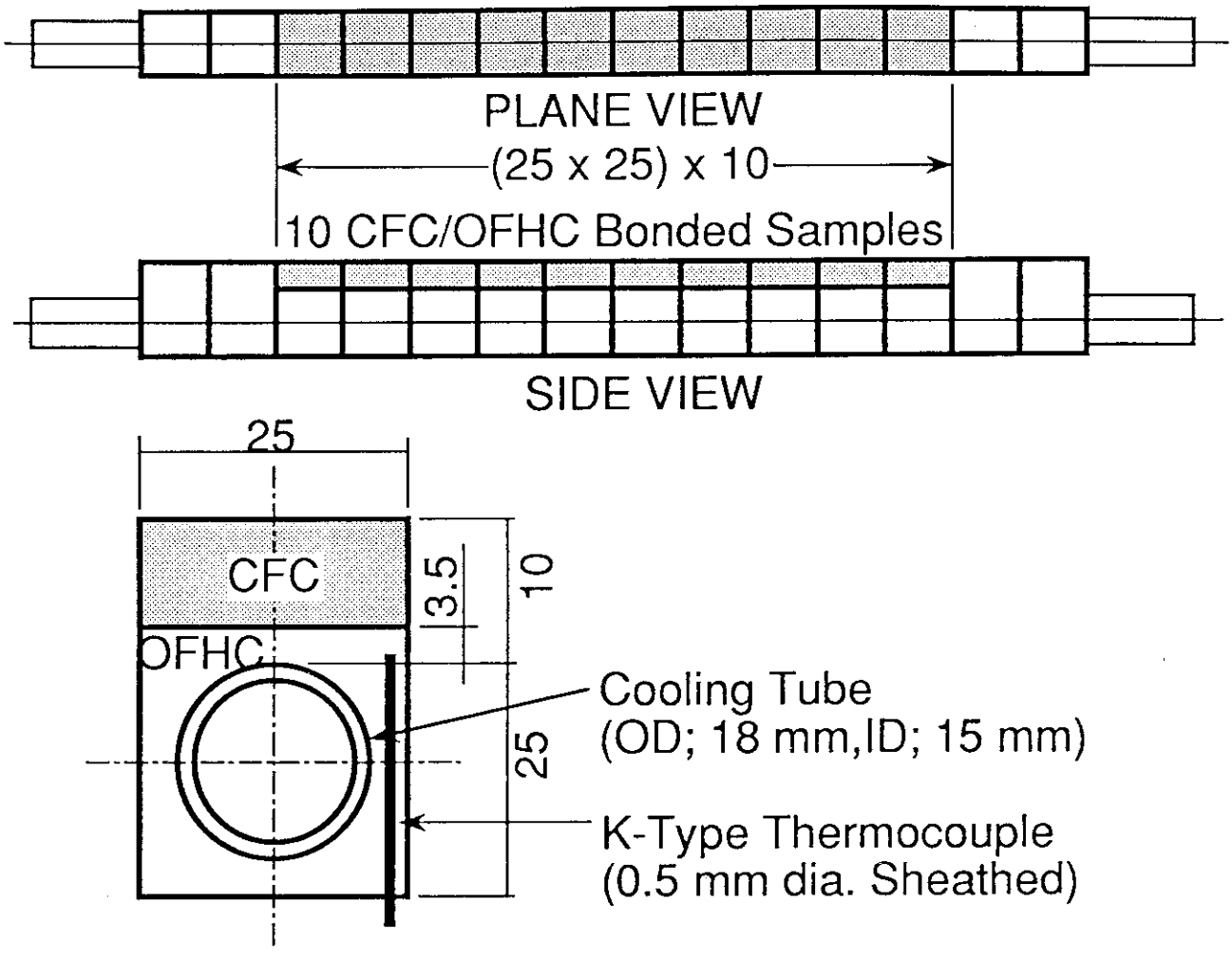

Figure 4-2. CFC/OFHC Bonded Divertor Mock-up

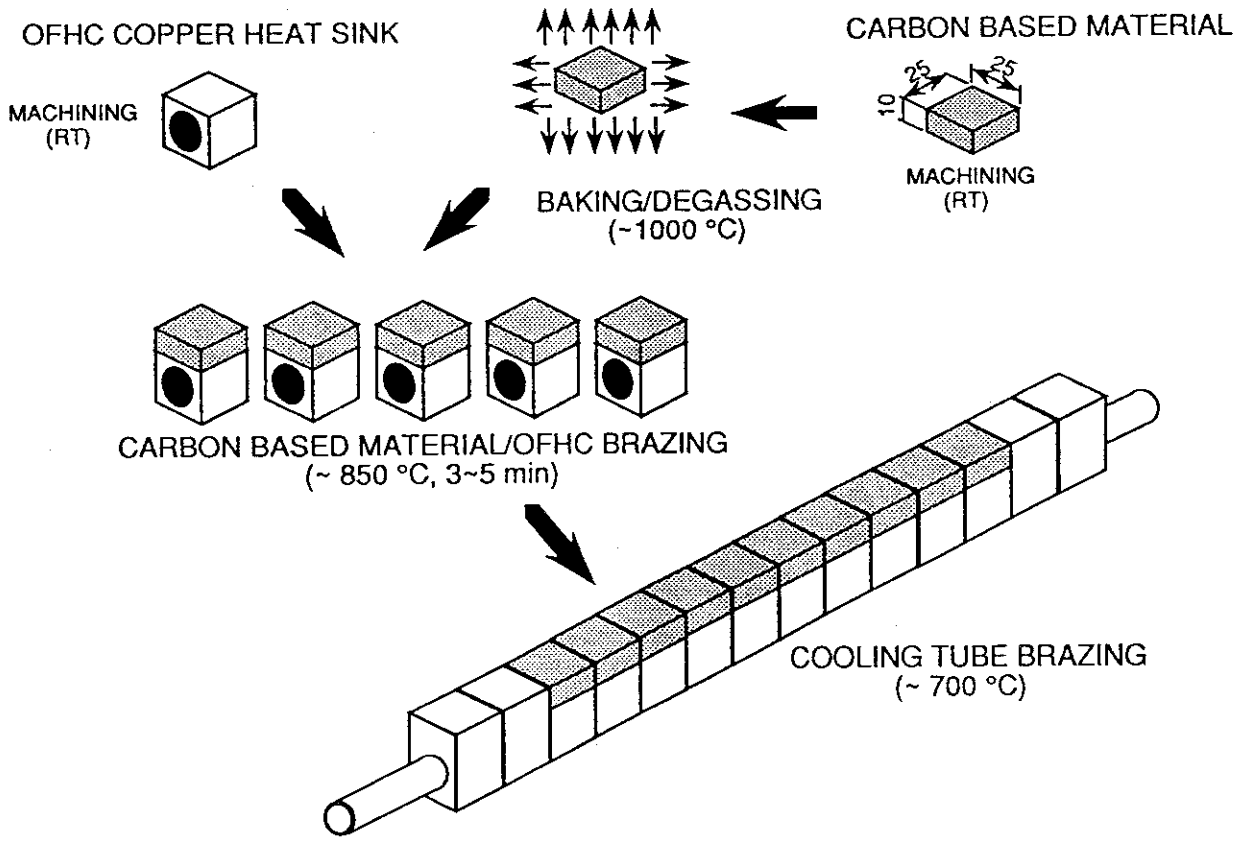

Figure 4-3. Manufacturing Process of CFC/OFHC Divertor Mock-up

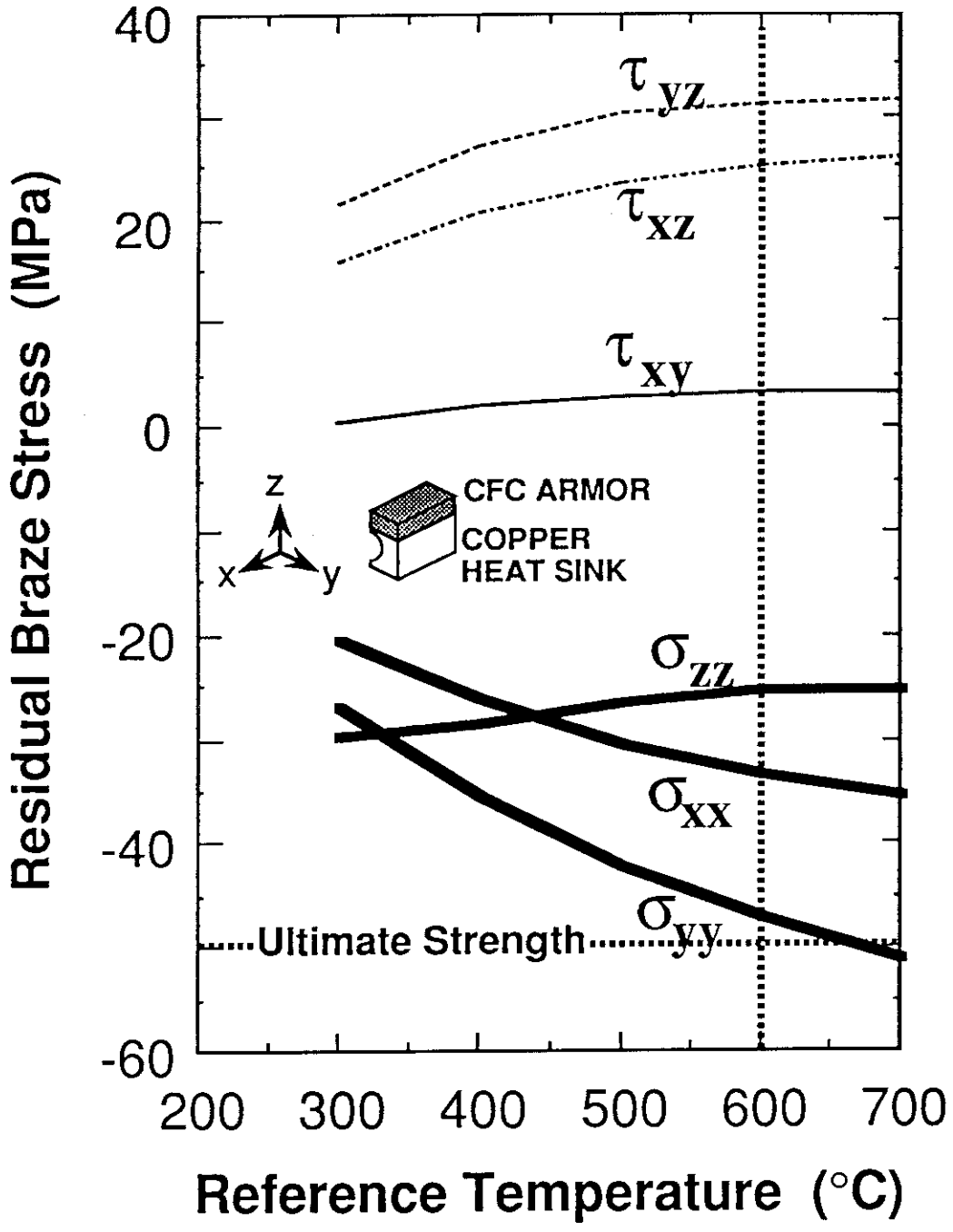

Figure 4-4(a). Maximum Residual Stress from Brazing as a Function of Stress-Free Temperature.

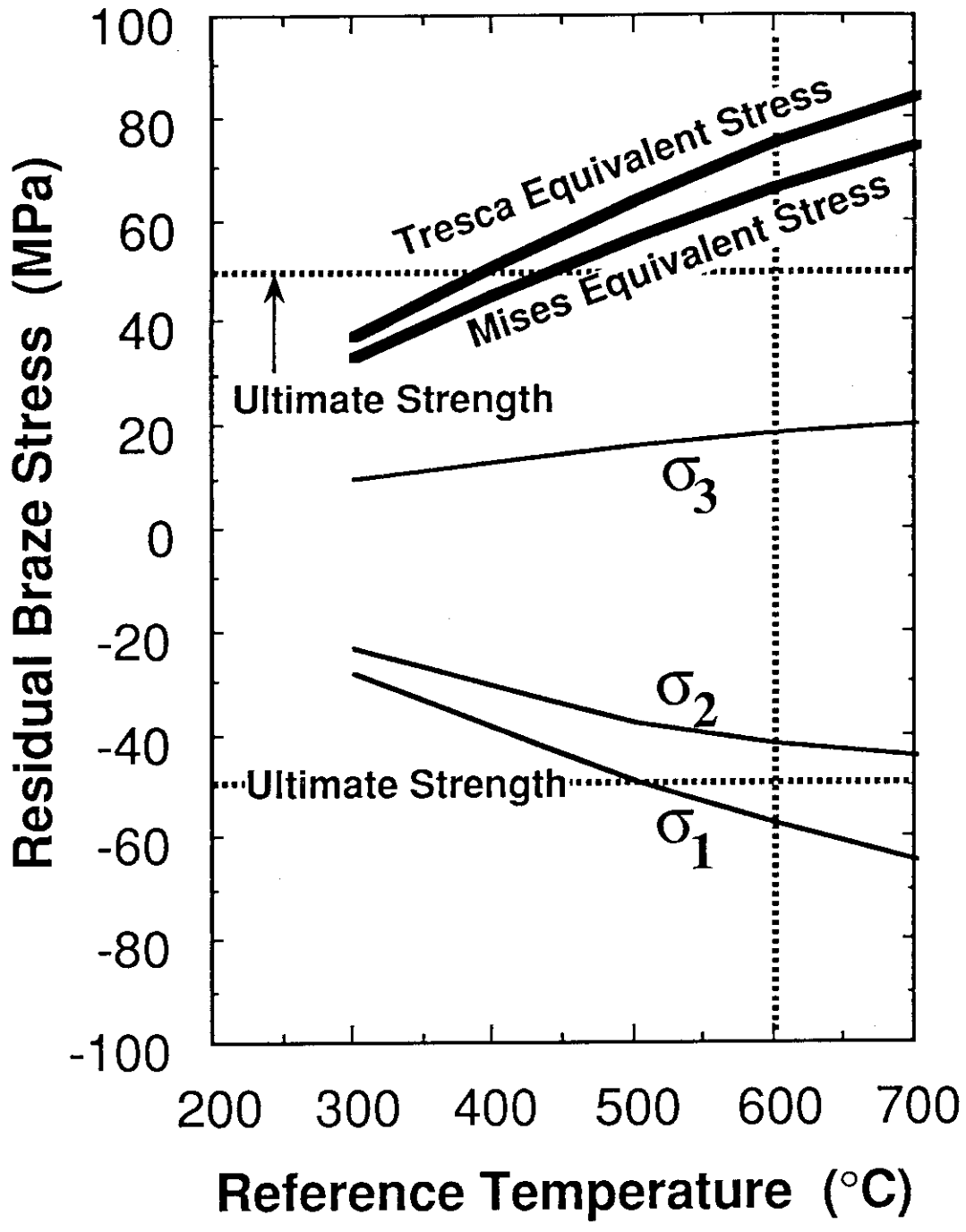

Figure 4-4(b). Mises and Tresca Equivalent Stresses from Brazing as a Function of Stress-Free Temperature.

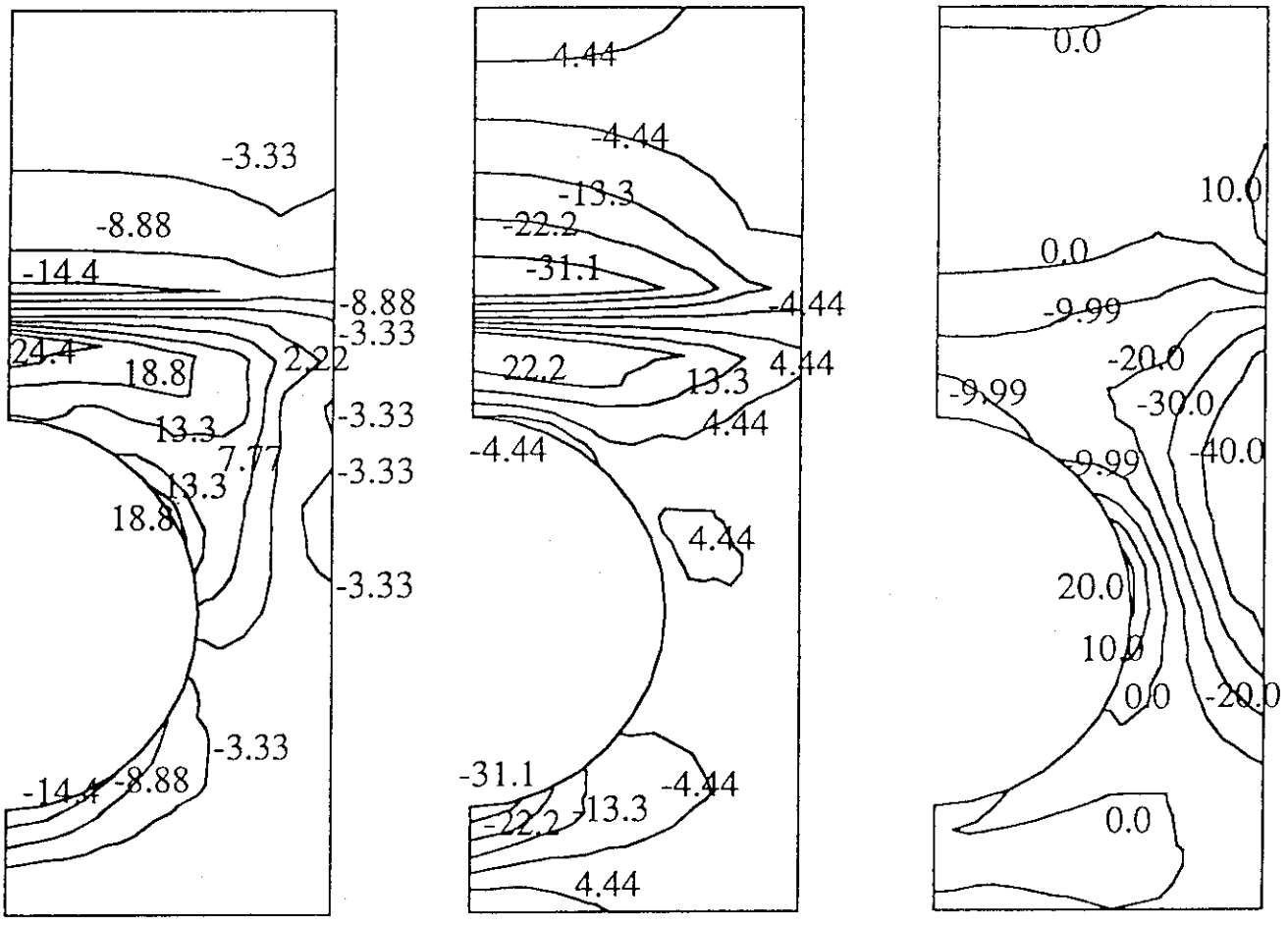

(a) X-Direction (b) Y-Direction (c) Z-Direction

(UNIT;MPa)

Figure 4-5 Residual Stress Profiles of Cross Sectional Plane for Three Directions

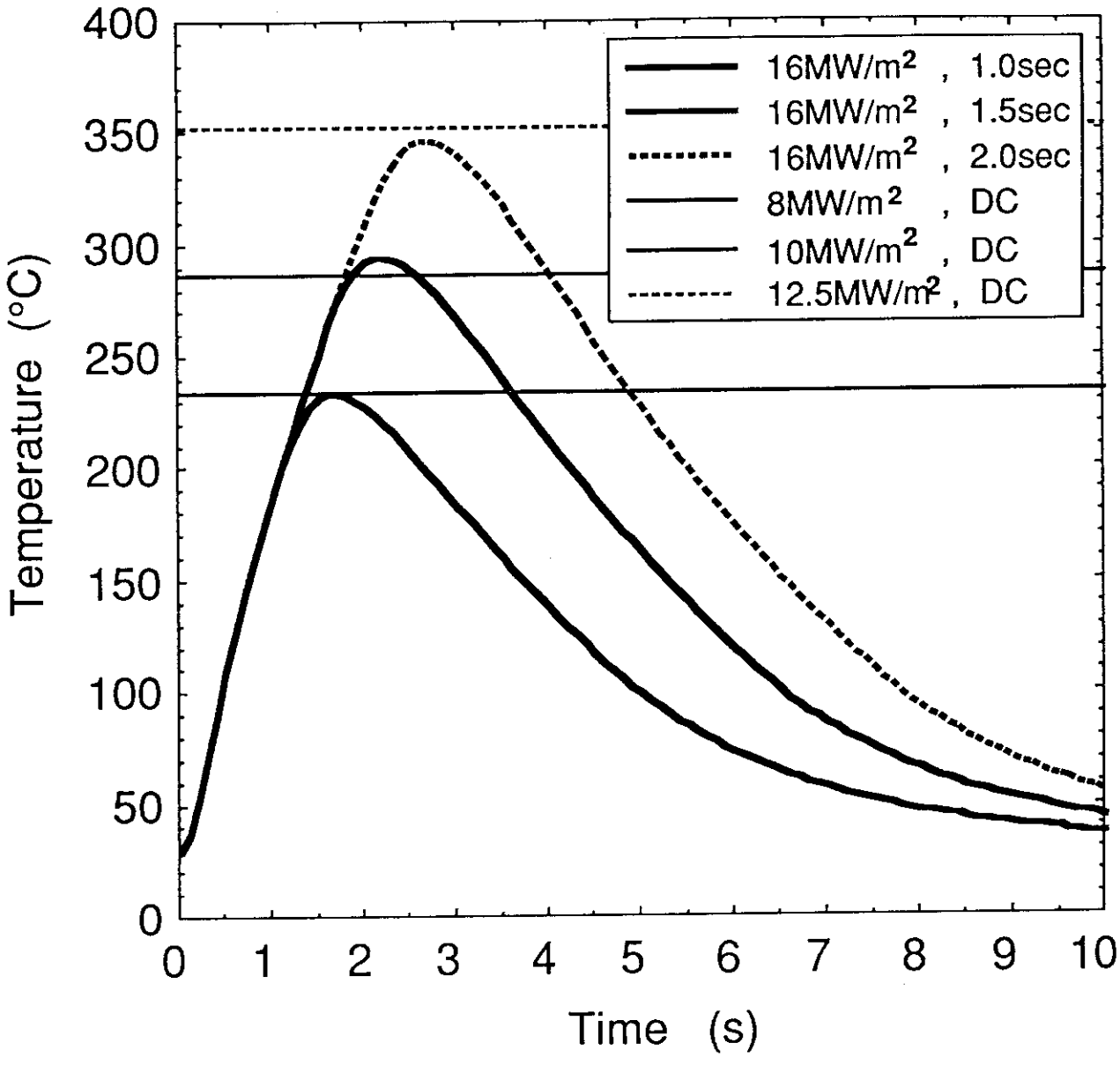

Figure 4-6. Temperature Response of the Interface for Different Beam Durations.

Peak heat flux deposited to the surface of the mock-up is kept at 16 MW/m^2 .

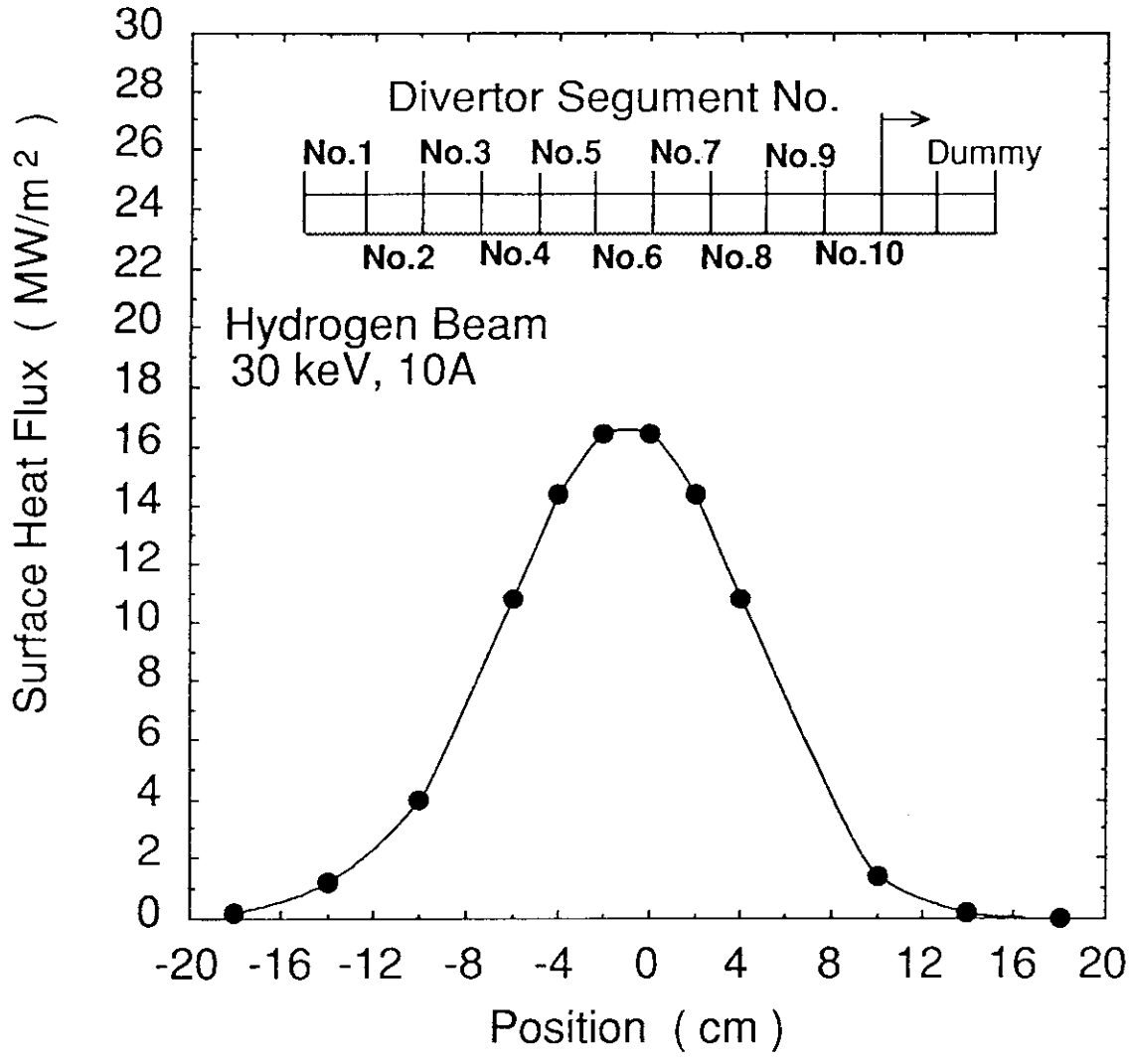

Figure 4-7. Measured Surface Heat Flux Profile

Each copper tip which has 2 cm^2 in heated area and 1 cm^3 in volume was used for surface heat flux measurements.

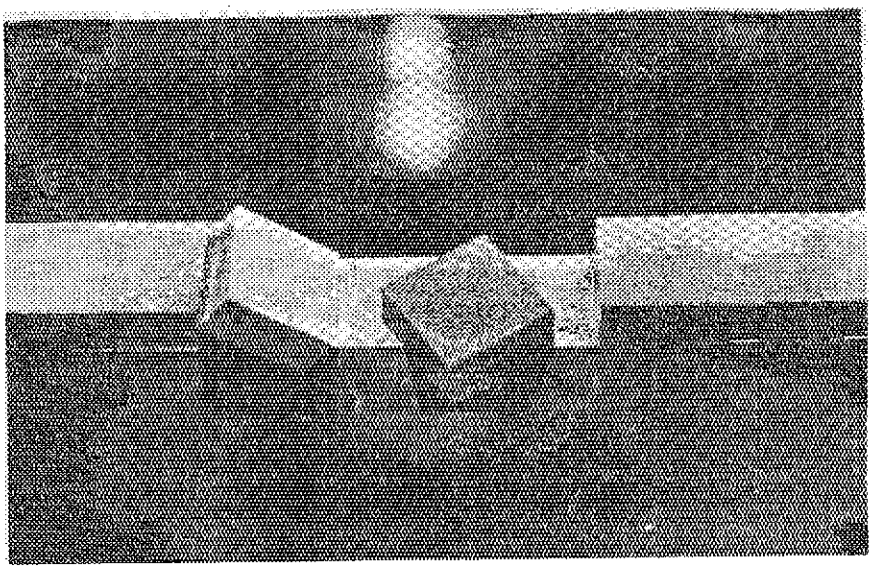

Figure 4-8 An Example of Damaged CFC/OFHC-Cu Divertor Mock-Up after Cyclic High Heat Loads

After 117 cyclic high heat loads under the surface equivalent heat flux of 12.5 MW/m^2, three CFC armor tiles, i.e., A05, JCC, and CX-2002U, were detached from the OFHC-Cu heat sink due mainly to lack for brazing materials.

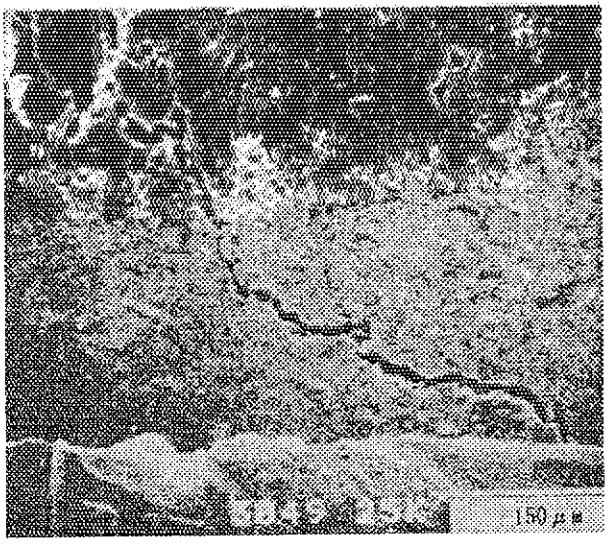

Figure 4-9 SEM Observations - Crack Formation -

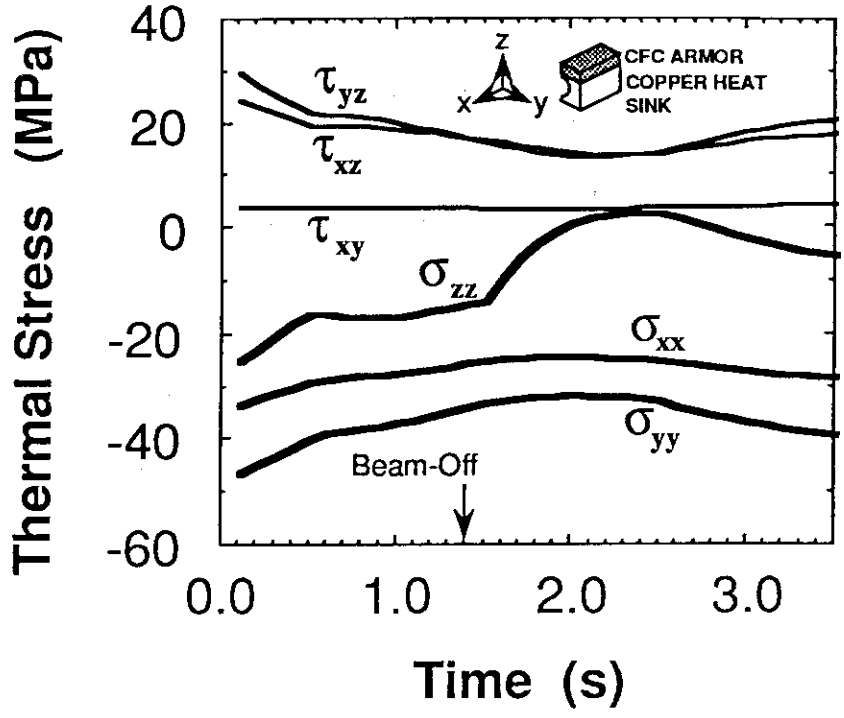

(a) Heating Condition; 16MW/m^2 , 1.5s

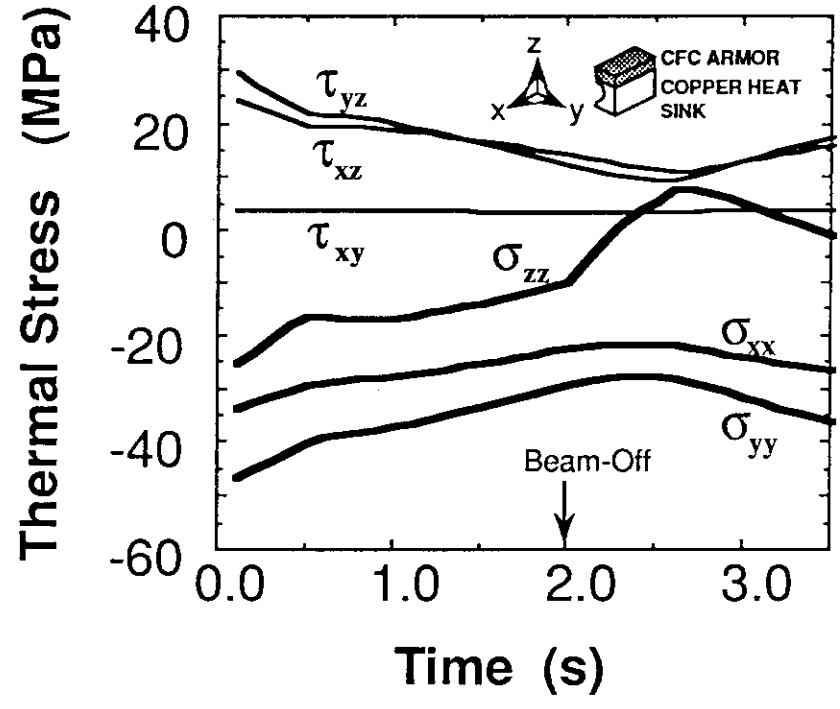

(b) Heating Condition; 16MW/m^2 , 2.0s

Figure 4-10 Time Histories of Three-Directional Stresses

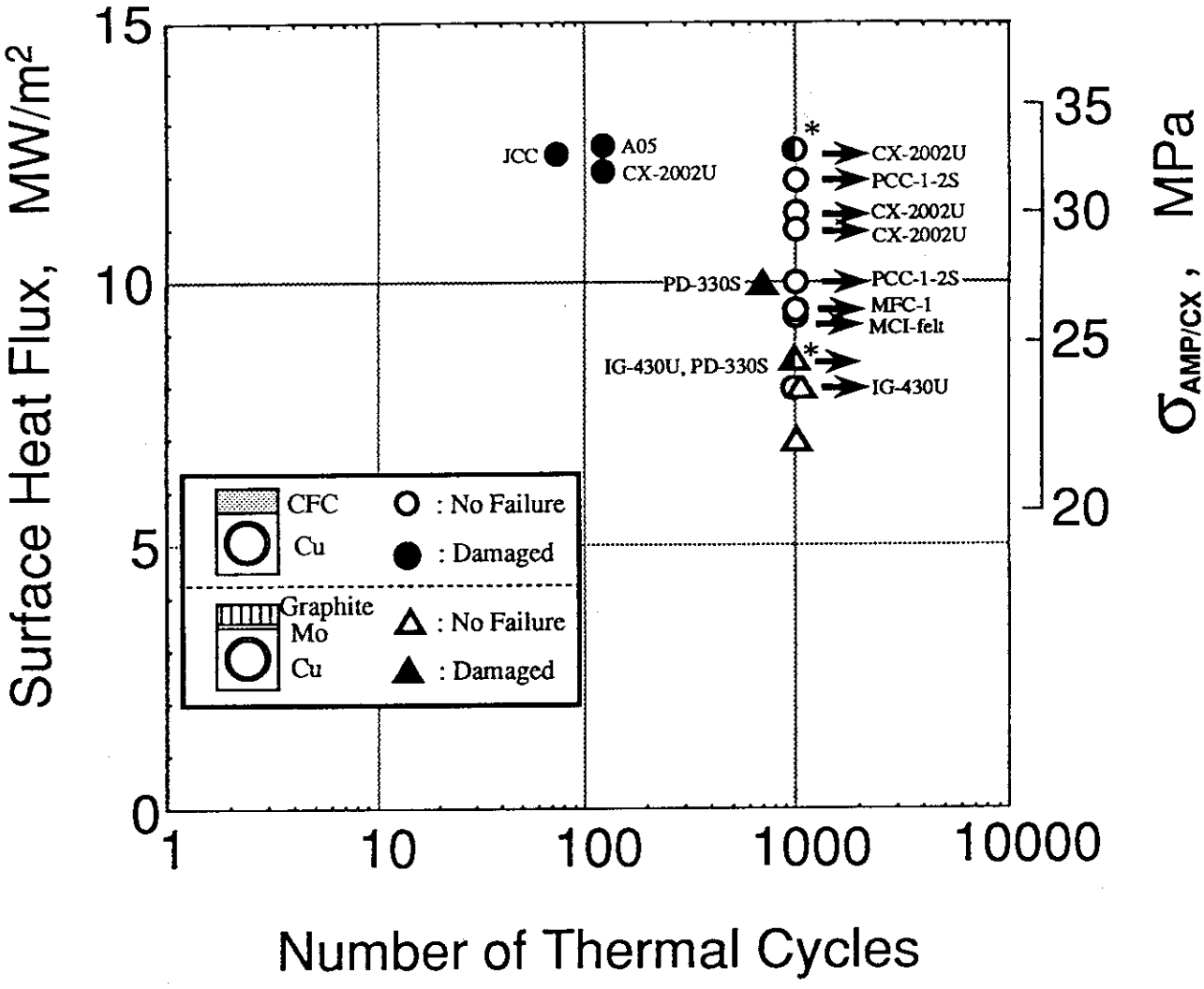

Figure 4-11. Thermal Cycling Resistivity of Bonded Diverotr Mock-ups

* ; although a small crack was found at a corner of the armor tile close to the bonded layer, increase of the surface temperature was not observed during thermal cycles.

5. EVALUATION ON SWEEPING EFFECTS OF THE DIVERTOR SEPARATRIX FOR HIGH HEAT FLUX COMPONENTS

5.1 Analytical Study

5.1.1 Introduction

Plasma facing components (PFCs) which the surfaces directly face the tokamak plasma are subjected to severe heat loads not only in normal operation but also in off-normal operation as described above. Figure 5-1 shows a schematic of ITER [1]. Since the ITER has a double null configuration, the divertor plates are installed at an upper and lower positions of the plasma. The divertor plate is subjected to thermal radiation from plasma, high plasma particle fluxes, and high energy neutrons. Especially, charged particles moving along magnetic field lines inject to the divertor plate and produce a peaked heat flux.

A detailed configuration of the lower divertor plate is shown in Fig. 5-2. Main plasma is detached from the divertor plate by magnetic field. A intersecting point of the magnetic lines, which is shown as "X-point" in the figure, is called a separatrix or a null-point because a magnetic field strength becomes zero at this point. Since the magnetic field lines intersect the divertor plate at two points, which are called striking points, high heat fluxes are subjected around these points as shown in Fig. 5-2.

Figure 5-3 shows a closs sectional view of the outboard striking point. To obtain a good compatibility with plasma, the surface of the divertor plate is covered with armor tiles made of low-Z materials, e.g., carbon-based materials or beryllium. In particular, carbon-fiber-reinforced carbon composites (CFCs) are recommended in the ITER design, because CFCs have high thermal conductivity and an excellent characteristics against thermal shock heat loads [36]. The armor tiles are brazed on the cooling tube to reduce thermal resistance between the armor and the tube, as shown in Fig. 5-3. A schematic of the ITER heat flux profile on the divertor plate is also shown in the figure. A full width at half maximum (FWHM) of the profile depends on the peak heat flux. For a peak heat flux of 30 MW/m^2, FWHM is estimated about 3 cm.

Table 5-1 summarizes a required performances for the divertor plate. In the ITER normal operating condition, a peak heat flux of the divertor plate is estimated to become 10 to 30 MW/m^2. Durability of the divertor plate mock-ups with large numbers (>

1,000) of cyclic heat loads has been confirmed under a condition for the surface heat flux up to 15 MW/m^2 [47, 48]. However, still higher heat fluxes will be deposited on the surface of the divertor plate of ITER. From the engineering point of view, it will be difficult to remove a stationary heat flux of over 15 MW/m^2 without applying some methods to effectively reduce the surface heat flux. For this objection, several possibilities to reduce divertor peak heat load have been proposed and examined. Examples are (i) a bias divertor concept like a beam energy recovery system, (ii) a separatrix sweeping concept, (iii) broadening power width in SOL by effectively increasing perpendicular transport by application of ergotic magnetic field [49, 50], (iv) a remote radiation cooling in a divertor region by impurity injection, and (v) an enlarged or expanded divertor concept [51]. These methods have their own attractive features as well as concerns in actual application. In the case of (i), only energetic ion beams are decelerated and collected to a collector electrode at a voltage close to that of the beams after separating from electrons. An effective performance has experimentally and analytically been confirmed in the beam energy recovery system [52, 53]. The application of this concept to the divertor plate, however, will be slightly difficult because a tokamak plasma can not be separated into ions and electrons. In the case of (iii), physics mechanism is straightforward, while the compatibility with the enhanced confinement of a main plasma will be concerned, since the confinement of a plasma edge region is somewhat degraded. Case (iv) is expected to be one of the promising methods for the heat flux reduction in future reactor, and, in the experiments, a fairly effective reduction of heat load was demonstrated [54]. However, a certain control method to prevent the backflow of impurity into a main plasma must be established. In the case of (v), expansion of flux surface can directly reduce the heat load, while the large coil current (order of MA) near the plasma and large spatial area for installation of the divertor plate in the vacuum vessel will be needed to expand the flux surface. On the other hand, the separatrix sweeping concept which is based on averaging the peak heat flux deposited to the divertor plate by sweeping the edge plasma will be useful. As considering with the surface heat flux pattern of the ITER divertor plate, the high heat flux region is localized within a few centimeters. A separatrix sweeping technique which has already developed in the present tokamak devices has been proposed in the ITER design as one of the most promising techniques to reduce the heat flux.

Numerical studies on the separatrix sweeping for ITER have been reported [1, 55, 56]. However, the ITER design document [1] and Wesley [55] presented no systematic

results. Hassanein [56] also made one-dimensional analyses and concluded that higher sweeping frequencies and longer sweeping distances substantially reduced the substrate surface temperature and might increase the divertor lifetime. However, the one-dimensional analyses can not consider the aeolotropy of thermal conductivity of CFCs. In general, the thermal conductivity parallel to the CFC fibers is 2 to 5 times larger than that of perpendicular to the fiber. To take into account the aeolotropy of thermal conductivity, three-dimensional analysis is quite necessary in thermal analyses of CFCs.

Therefore, in the present study three-dimensional thermal response analyses have been performed for the ITER divertor plate. The present analyses give consideration to the aeolotropy of the thermal conductivities in three directions. Analytical conditions and results are described in section 5.1.2 and 3, respectively. In section 5.1.4 discussions are made, and conclusions are given in section 5.1.5.

5.1.2 Analytical conditions and procedure

The ITER divertor plate has two high heat load regions as shown in Fig. 5-2, i.e., inboard side and outboard side of the divertor plate. Since the heat flux of the outboard side is higher than that of the inboard side, the thermal analyses of the outboard side are performed in the present study.

A schematic of the separatrix sweeping concept is shown in figure 5-4. Time-averaged heat flux distributions are also shown in the figure, which can be produced by the separatrix sweeping. The separatrix sweeping can be performed by a modulation of the magnetic field around the intersecting point. Two kinds of modulations have been proposed in the ITER design. One is a sawtooth modulation and the other is a sinusoidal modulation. In the case of sawtooth modulation, the heat flux profile on the divertor plate moves at a constant speed. On the other hand, moving speed changes with time in the case of the sinusoidal modulation. It means that the sweeping becomes slow at around both of turning points, which causes higher heat loads around both ends of the sweeping area as shown in figure 5-4. In the present study, the thermal analyses have been performed for the case of the sawtooth modulation, because the sweeping effect is much effective than that of the sinusoidal modulation.

From the analytical result on acceptable AC loss of SC coil systems [57], sweeping frequency f and sweeping distance ΔL in ITER would be estimated to be up to 2 Hz and

± 15 cm at the operational plasma current of 22 MA, respectively, when normal conducting in-vessel coils are installed for fast sweeping. For the plasma current substantially below 22 MA (~ 11 MA), still faster sweeping condition of $f \approx$ 5 - 6 Hz with ΔL of ± 10 cm will be acceptable. In the present study, the thermal analyses have been carried out with a sweeping frequency of 1 to 5 Hz, and with a sweeping distance of ± 5 to ± 15 cm.

With respect to the surface heat flux profile on the divertor plate for ITER, figure 5-5 shows an expected heat flux profile on the divertor plate [58]. Since slightly uncertain factors such as a peaking and safety factors are included in predicting the heat flux profile, total heat load on the divertor plate has been kept to a constant value in this analysis. From the previous investigation [1], peak heat flux (q_{peak}) times full width at a half maximum (FWHM) on the divertor surface has been determined to be a constant value of around 90 MW•m^{-2}•cm normalized by 15 MW/m^2 x 6 cm. In the present analysis, q_{peak} of 30 MW/m^2 with FWHM of 3 cm has intensively been considered.

Three-dimensional analyses with different sweeping conditions have been performed for a monoblock type of the ITER divertor plate as shown in Fig. 5-6 for promising material combination of CX-2002U as the armor and dispersion strengthen copper (DS-Cu) with a twisted tape as the cooling tube. Material data for their thermal properties are taken from Ref. [42, 59]. In the analyses, temperature dependence of thermal properties are considered. At temperatures above 900 K, thermal properties such as thermal conductivity and specific heat of the materials are linearly extrapolated since no available data exist.

In general, the swirl tube is applied as a cooling tube for the divertor plate since it has a high performance in heat transfer compared to the straight tube [25]. With respect to heat transfer between the tube wall and coolant for the swirl tube, Kim et al. [60] and Milola et al. [61] tried to evaluate nonuniform heat transfer of swirl tube in both nonboiling and subcooled boiling regions. Their studies, however, were made by two-dimensional analysis based on an assumption that the heat transfer coefficient is independent of inner wall flux variation. Because of creating the swirl flow in the tube, it will be difficult to determine the heat transfer coefficient along the circumference and the flow direction of the swirl tube. Unfortunately, very little study was made on this type of heat transfer phenomenon, and therefore the heat transfer coefficient in the present analysis is assumed a constant value of 9.0 x 10^4 W/m^{2}K predicted by Gambill et al. [19] as following equation;

$$\frac{h_s}{h_a} = \frac{2.18}{y^{0.09}}, \quad (1)$$

where h_s and h_a are heat transfer coefficients in cases of swirl flow and axial flow, respectively, y is the twist ratio defined by the ratio of inner diameter of the tube to 180-deg. twist length. Axial flow velocity of 10 m/s was selected. Since the cooling water at the inlet pressure of 3.5 MPa is supplied to the divertor plates, the water saturation temperature is expected to be around 250 °C. Although a constant heat transfer coefficient will be applicable in nonboiling region, it should be noted that these analyses will include an error in subcooled boiling region. Inlet water temperature is also kept to a constant value of 50 °C.

During the sweeping, the surface of the divertor plate as shown in Fig. 5-4 experiences periodic heat flux variation with different time evaluations, depending on the target location. In the present analyses, thermal response on the divertor plate near edge location has been evaluated. At this location, maximum temperature is expected to occur and the maximum heat load passes twice this location in a very short time since it reverses at the edge.

5.1.3 Analytical results

5.1.3-1 Sweeping frequency dependence

Figure 5-7 shows an example of temperature responses at typical points of the divertor plate near edge location as indicated in Fig. 5-4 under the following sweeping condition; sweeping frequency of 2.0 Hz, sweeping distance of ±10 cm, and peak heat flux of 30 MW/m^2 with FWHM of 3 cm. At this time, some special definitions such as minor-temperature change and major-temperature variation, namely ΔT_{minor} and ΔT_{major} as shown in the figure, should be necessary for the evaluation of the sweeping effect from thermal-hydraulic point of view. In the present study, ΔT_{major} is defined a maximum temperature rise, and ΔT_{minor} is also defined a temperature change from the minimum temperature to the maximum temperature after steady state heating condition is achieved. These definitions are applied for the surface of the armor, interface between the armor and the cooling tube, and the cooling tube inner wall.

Figures 5-8(a), 8(b) and 8(c) show maximum temperatures at the typical points of the divertor plate near edge location described above as a function of the sweeping frequency for different sweeping distances. Peak heat flux of 30 MW/m^2 with full width at a half maximum of 3 cm on the divertor plate is applied in the analyses. In general, surface temperature decreases with increasing the sweeping frequency. Especially, an increase of the sweeping frequency up to 3.0 Hz is very effective for the reduction of surface temperature on the divertor plate. For still higher sweeping frequencies, however the temperature reductions as shown in Fig. 5-8(a) are expected to be small due to large thermal capacity of the armor material. With respect to temperature responses of the interface and the cooling tube wall, small temperature reductions are also expected. In particular, temperature of the cooling tube wall is expected to be below 250 °C corresponding to the saturation temperature of water at a pressure of 3.5 MPa in all the present sweeping conditions. These results reveal that 1.0 Hz sweeping frequency is enough high in averaging the heat flux in the interface and the cooling tube wall due to large thermal capacity of the armor material. To keep surface temperature below 1,000 °C, which is allowable limit due to the sublimation of the armor material, sweeping frequency of higher than 2.0 Hz with the distance of ± 8 cm will be necessary. For shorter sweeping distance of ± 7 cm, any solutions that reduce the surface temperature below 1,000 °C during the operation can not be found at the sweeping frequencies in the range of 1.0 to 5.0 Hz because averaged surface heat fluxes under those sweeping conditions are higher than 15 MW/m^2.

Since an additional minor-temperature change on the divertor plate occurs with applying the sweeping, it is also important to investigate ΔT_{minor} for the evaluation of the overall effectiveness of the sweeping. Figure 5-9 shows ΔT_{minor} on the surface for different sweeping distances. Table 5-2 also summarizes minor-temperature changes at the typical points for different sweeping conditions. With increasing the sweeping frequency, ΔT_{minor} on the armor surface effectively decreases from around 300 K for 1 Hz to 90 K for 5 Hz. On the other hand, small minor-temperature changes on the interface and the cooling tube wall are expected for the reason described above.

5.1.3-2 Sweeping distance dependence

Figures 5-10(a), 10(b), and 10(c) show maximum temperatures at the armor surface,

the interface and the cooling tube wall, as a function of the sweeping distance for different sweeping frequencies, respectively. Each maximum temperature drastically decreases with increasing the sweeping distance. An increase of the sweeping distance is very effective in reducing the maximum temperatures.

Figure 5-11 also shows the minor temperature changes at the typical points. In general, larger differences between the minor-temperature changes for different sweeping frequencies are expected when the sweeping distance becomes longer. Although differences of ΔT_{minor} on the armor surface will be observed during the sweeping, they are relatively small, i.e., within 30 K for 1 Hz and 10 K for higher sweeping frequencies and will be acceptable levels for the lifetime evaluation of cyclic heat loads. On the other hand, differences of ΔT_{minor} in the interface and cooling tube wall also increase with the sweeping distance. Especially, at relatively low sweeping frequencies below 2 Hz, it should be noted that longer sweeping distance results in lower temperature, but in higher ΔT_{minor}. Therefore, for longer sweeping distance, higher sweeping frequency is required to reduce the temperature and ΔT_{minor} on the divertor plate.

5.1.4 Discussions

It is sure that an additional periodic minor-temperature change on the divertor plate occurs by applying the sweeping technique, although the maximum surface temperature effectively decreases. From the lifetime evaluation point of view, thermal fatigues of the divertor plate not only in the major-temperature variations but also in additional periodic minor-temperature change should be evaluated. Unfortunately, there is very little study in the literature. It is, however, the worth trying an evaluation of their influences from the experimental results, which were obtained in other experiments such as thermal cycling test of the divertor plate mock-ups.

It is already confirmed in the experiments that various types of the divertor mock-up configurations have endured for large numbers (> 1,000) of cyclic heat loads with the surface heat flux up to 15 MW/m^2 [47, 48]. In the experiment [48], surface temperature and ΔT_{major} of the armor tile were reached to around 1,200 °C and 1,180 K at the inlet water temperature of 20 °C during thermal cycles. On the other hand, the maximum temperature and ΔT_{major} of the armor tile are expected to be around 1,000 °C and 950 K in the case of applying the separatrix sweeping heat load in ITER. Thus, it will be predicted that the divertor plate can endure under cyclic heat loads for the major-temperature

variation of around 950 K, which corresponds to the surface heat flux of 30 MW/m^2 with the sweeping in ITER.

For the evaluation of additional periodic minor-temperature changes during the sweeping, it may be slightly difficult to investigate their additional influences on the lifetime evaluation of the divertor plate by the numerical analyses because no lifetime or thermal fatigue evaluation codes under cyclic heat loads on the bonds are available in the literature. To evaluate the influence of the periodic minor-temperature changes, a thermal response experiment of the divertor plate mock-up has been performed by simulating the sweeping condition of 30 MW/m^2, 1.0 Hz, ± 10 cm, 30 s for 1,000 major thermal cycles [62]. The divertor mock-up has successfully endured for >1,000 cycles of the major-temperature variations without increase of the surface temperature and failures on the bonds. Measured ΔT_{major} and ΔT_{minor} were around 500 K and 200 K, respectively. Although heat load pattern, ΔT_{major}, and ΔT_{minor} obtained in the experiment were slightly different compared with those in ITER, it is confirmed that the divertor plate mock-up has resisted to the sweeping heat loads for large numbers of the periodic moinor-temperature change of 200 K at ΔT_{major} around 500 K. ΔT_{minor} of 200 K corresponds to that in case of 30 MW/m^2, 2.0 Hz, ± 10 cm sweeping in ITER.

Therefore, it will reasonably be expected that the divertor plate can resist to the ITER sweeping heat load condition as follows; peak heat flux on the divertor plate, the sweeping frequency and the sweeping distance are 30 MW/m^2 with FWHM of 3 cm, 2.0 to 3.0 Hz, and ± 10 cm, respectively. However further experiments are needed for the definite evaluation of the influence of additional periodic minor-temperature changes during the sweeping on the lifetime of the divertor plate.

5.1.5 Conclusions

Three-dimensional thermal response analyses of the divertor plate have been performed under applying the separatrix sweeping technique with different sweeping frequencies for different sweeping distances. The following conclusions are drawn;

1. It is clearly expected that the application of the sweeping technique is very effective for the reduction of expected surface temperature on the divertor plate.
2. For longer sweeping distance, higher sweeping frequency is required to reduce the temperature and the additional minor temperature change on the divertor plate.
3. For shorter sweeping distance of ± 7 cm, no solutions to reduce the surface temperature below 1000 °C during the operation can be found at the sweeping frequencies in the range of 1.0 to 5.0 Hz because average surface heat flux under that sweeping condition is higher than 15 MW/m^2.
4. Since an increase of the sweeping frequency up to 3.0 Hz is very effective for the reduction of surface temperature on the divertor plate, linear separatrix sweeping with the sweeping frequency of higher than 3.0 Hz for the sweeping distance of ± 10 cm is proposed to achieve effective sweeping for ITER from thermal hydraulic point of view.

Table 5-1 Required Performances for ITER PFCs.

Operation Phase	Physics		Technology	
Components	First Wall	Divertor	First Wall	Divertor
- Peak/Aver. Surface Heat Flux MW/m^2	0.6/0.15	15~30	0.6/0.15	15~30
- Peak Volumetric Heat Load in Structure MW/m^3	20	5	15	4
- Number of Pulses (Full Load) 10^4	1		2~5	
- Total Burn Time h	400		10^4 ~3x10^4	
- Peak Neutron Damage (Steel) dpa	0.7	0.3	12~36	5~15
- Incident DT-Ions:				
• Peak Flux $10^{20}/m^2s$	1	4000	1	4000
• Energy eV	10~100	50~100	10~100	60~200

Table 5-2 Minor-Temperature Changes at the Typical Points for Different Sweeping Conditions.

ΔT_{MINOR} / f_{SWP}	Armor Surface	Interface	Cooling Tube Wall
	K	K	K
1.0 Hz	286 ~ 312	15 ~ 30	9.5 ~ 20
2.0 Hz	180 ~ 190	3 ~ 10	2 ~ 6.6
3.0 Hz	127 ~ 137	1 ~ 4	< 2.5
4.0 Hz	99 ~ 108	< 2.0	< 1.5
5.0 Hz	81 ~ 90	< 1.0	< 1.0

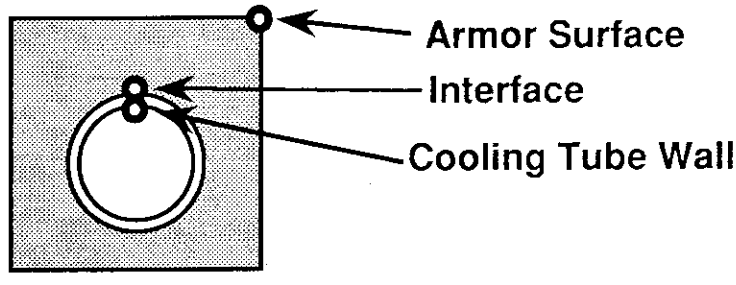

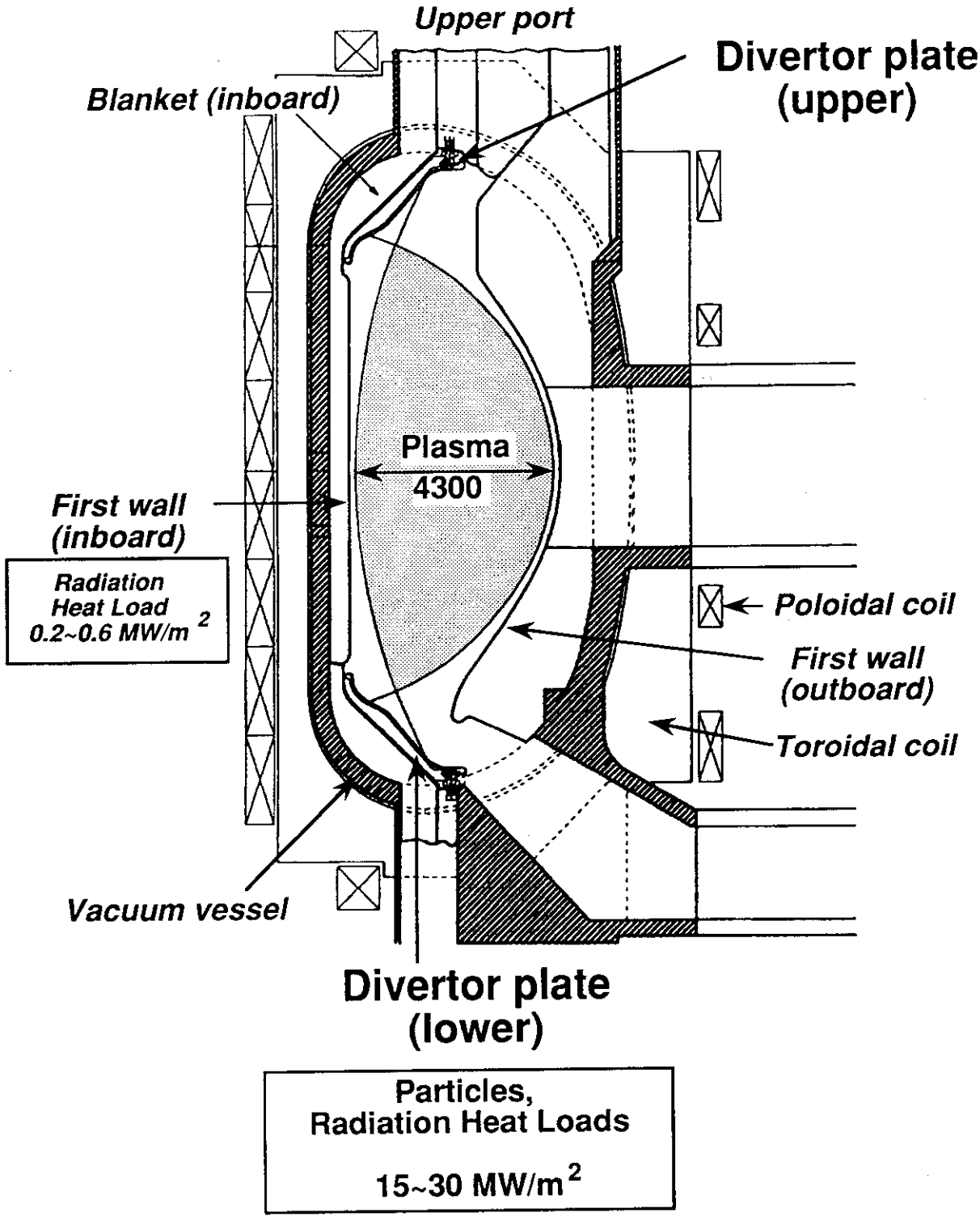

Figure 5-1 Cross Sectional View of ITER

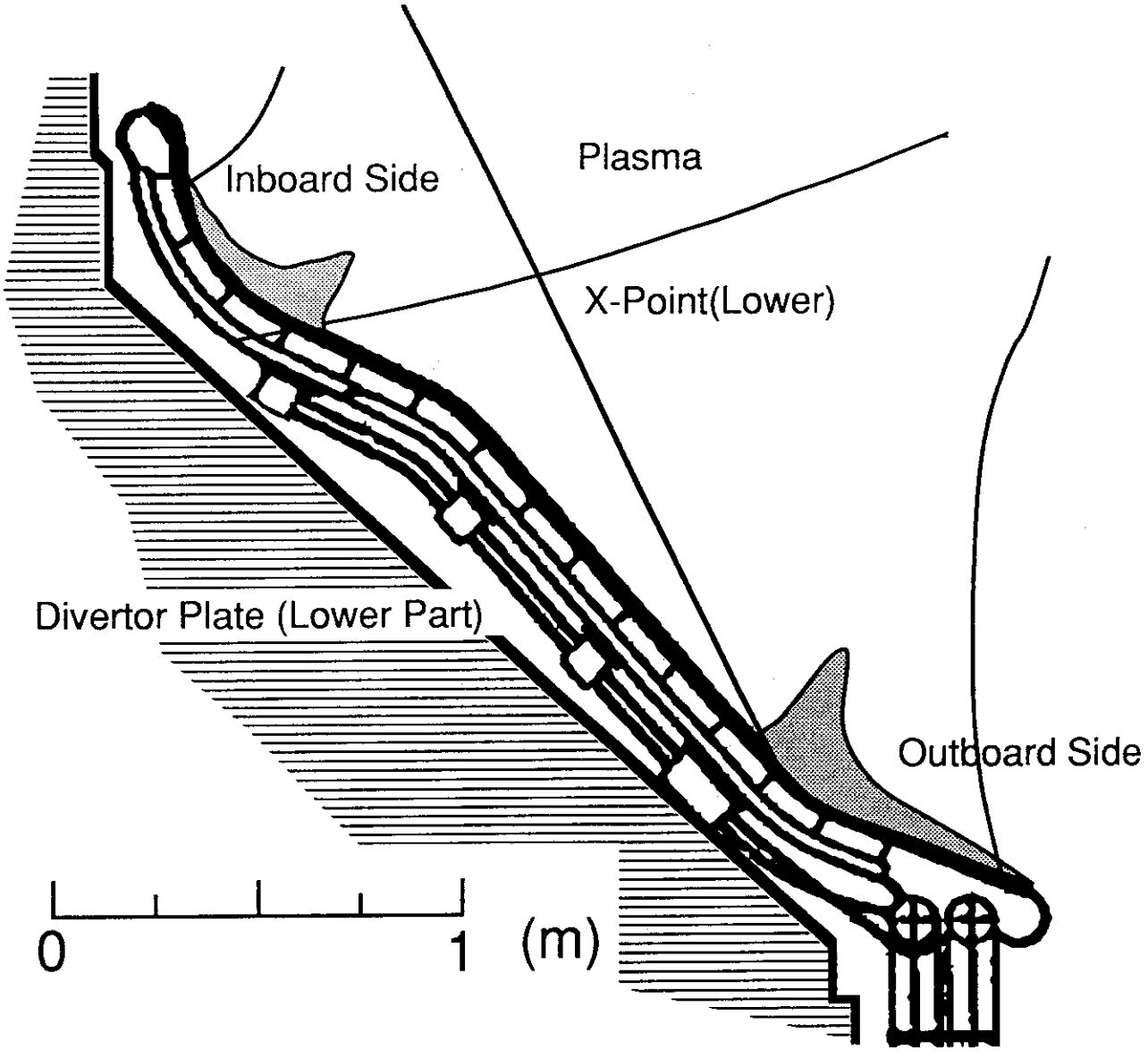

Figure 5-2. Detailed Divertor Plate Configuration.

Each divertor plate is exposed to severe heat loads from the ITER plasma at two parts on it, i.e., inboard and outboard sides. Heat flux on the outboard side of the divertor plate is estimated to be more severe than that on the inboard side.

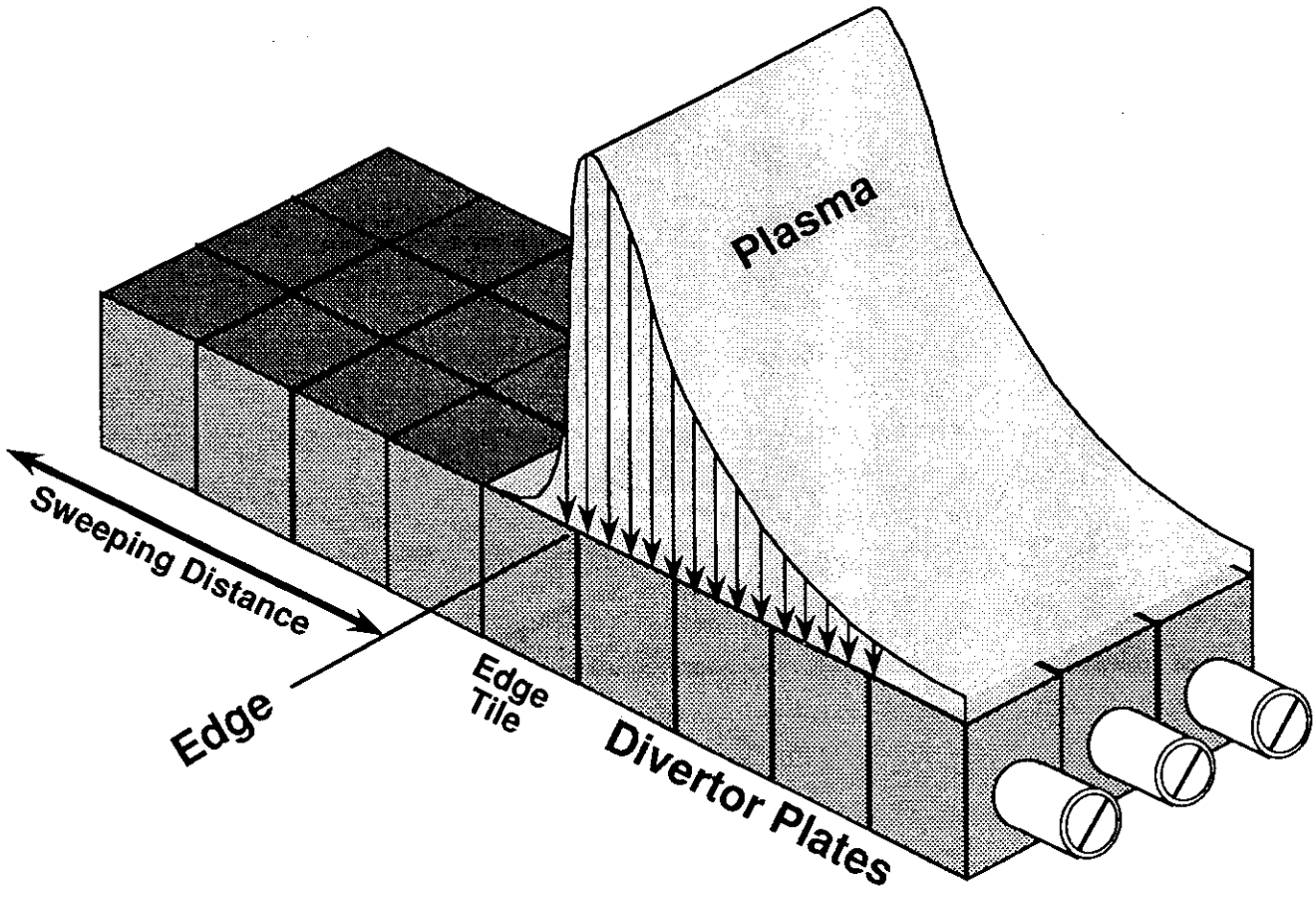

Figure 5-3 An Illustration of the Outboard Side of the Divertor Plate.

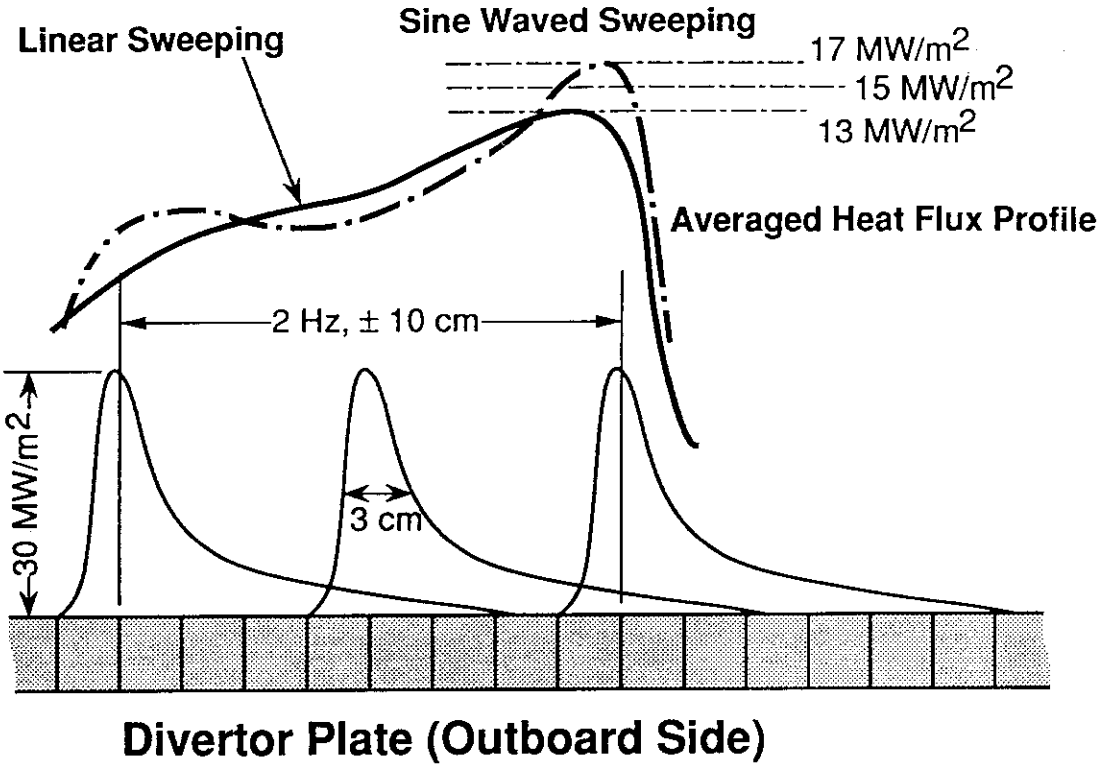

Figure 5-4 Conceptual View of Separatrix Sweeping on the Divertor Plate.

Heat load on the divertor plate is swept within a distance along the moderate center. Averaged heat flux with a sine waved sweeping is estimated to be higher than that with a linear wave.

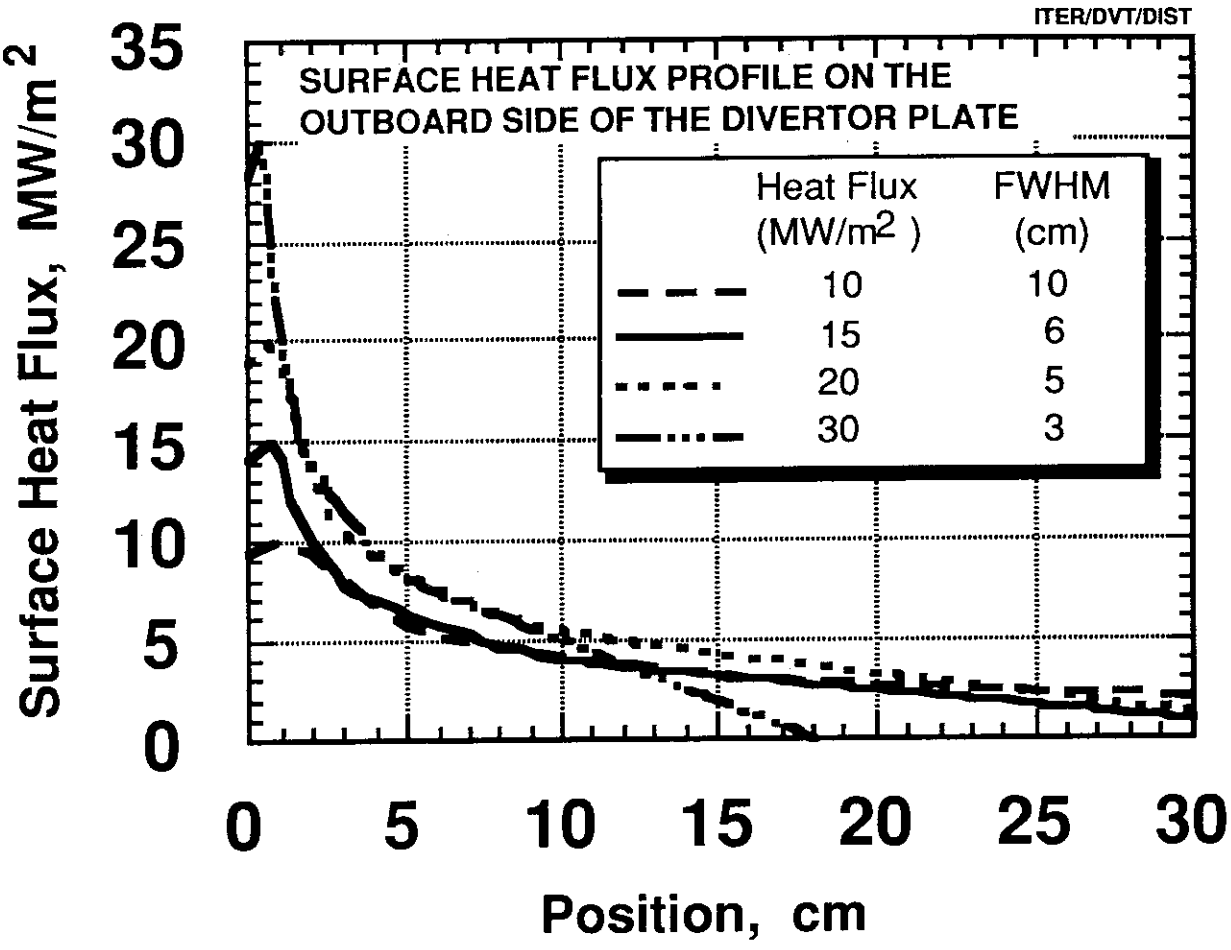

Figure 5-5 Heat Flux Profiles on the Outboard Side of the Divertor Plate.

Total heat loads on the divertor plate is kept to a constant value of 90 $MW \cdot m^{-2} \cdot cm$ normalized by 15 MW/m^2 times FWHM of 6 cm.

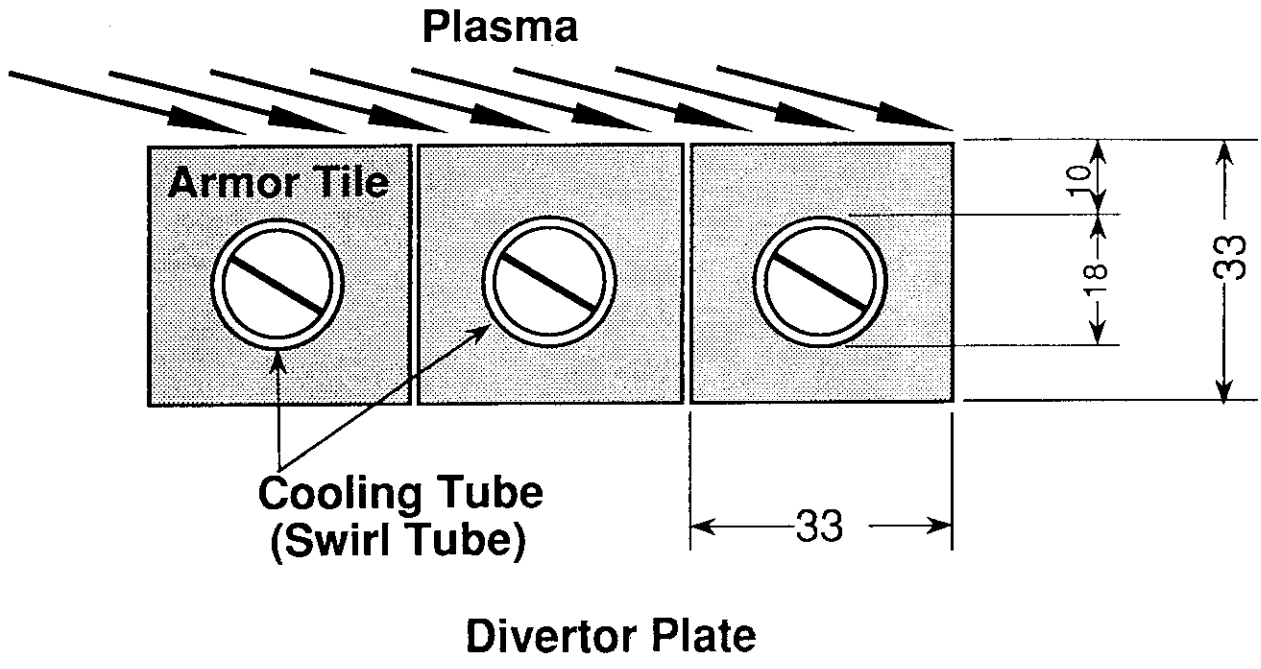

Figure 5-6 Cross-sectional View of the Divertor Plate

Major dimensions of the divertor plate are 33 mm wide, 33 mm high, and 25 mm deep, respectively. In the analysis, high carbon based material, CX-2002U that is felt type of 2-D carbon fiber reinforced carbon composite, is selected as the armor and OFHC-Cu as the cooling tube.

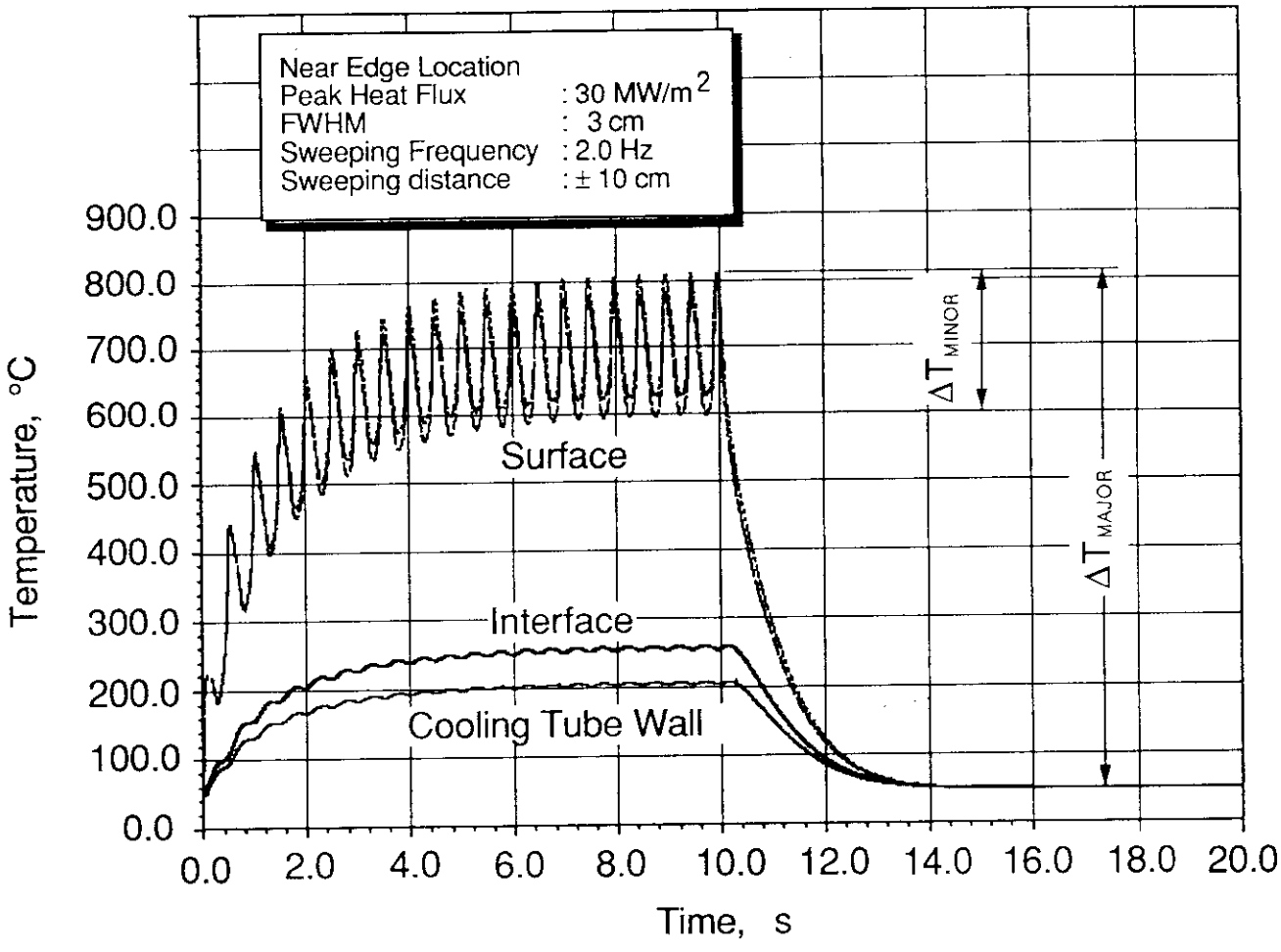

Figure 5-7 An example of Temperature Responses at Typical Points of the Divertor Plate.

Minor-temperature change and major-temperature variation, namely ΔT_{minor} and ΔT_{major}, are defined as show in here.

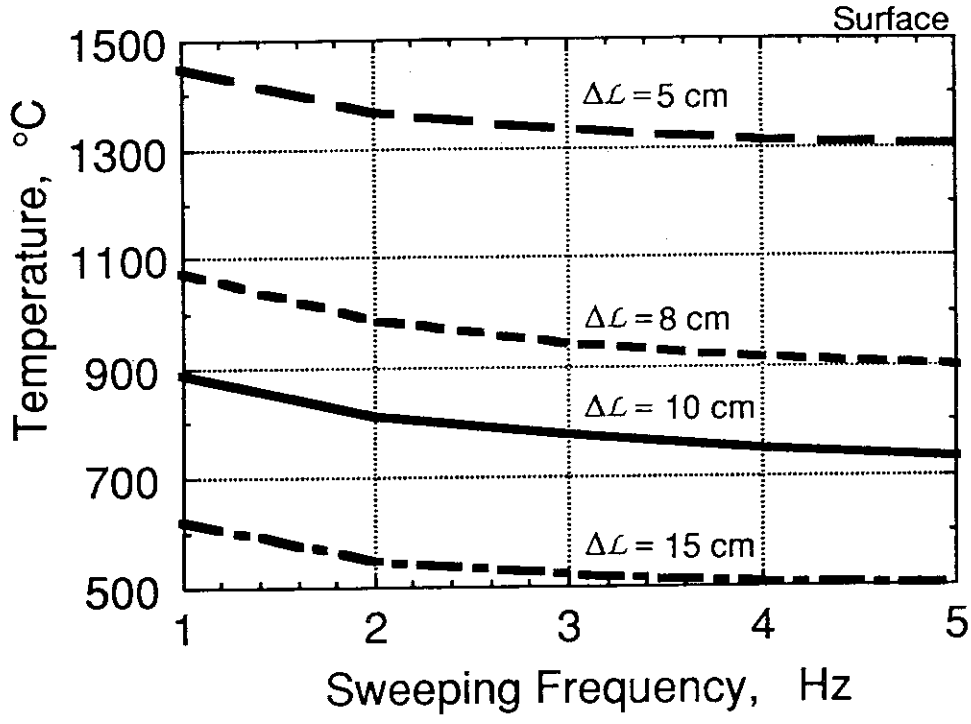

(a) Armor Surface

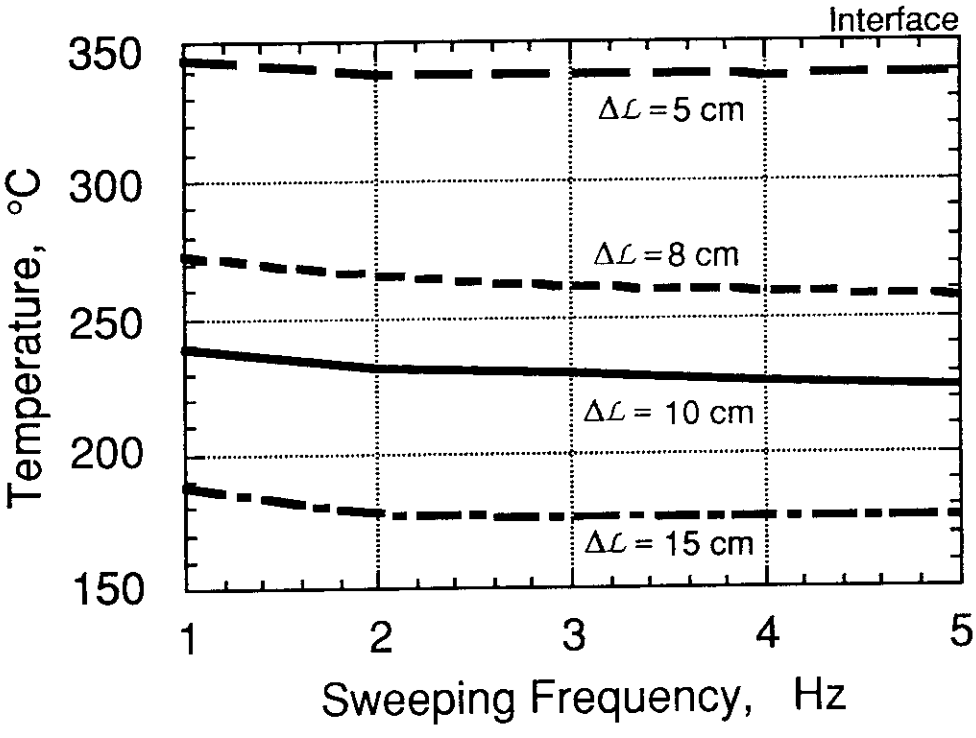

(b) Interface Between the Armor and the Cooling Tube Wall

Figure 5-8 Maximum Temperatures on the Divertor Plate Near Edge Location as a Function of the Sweeping Frequency.

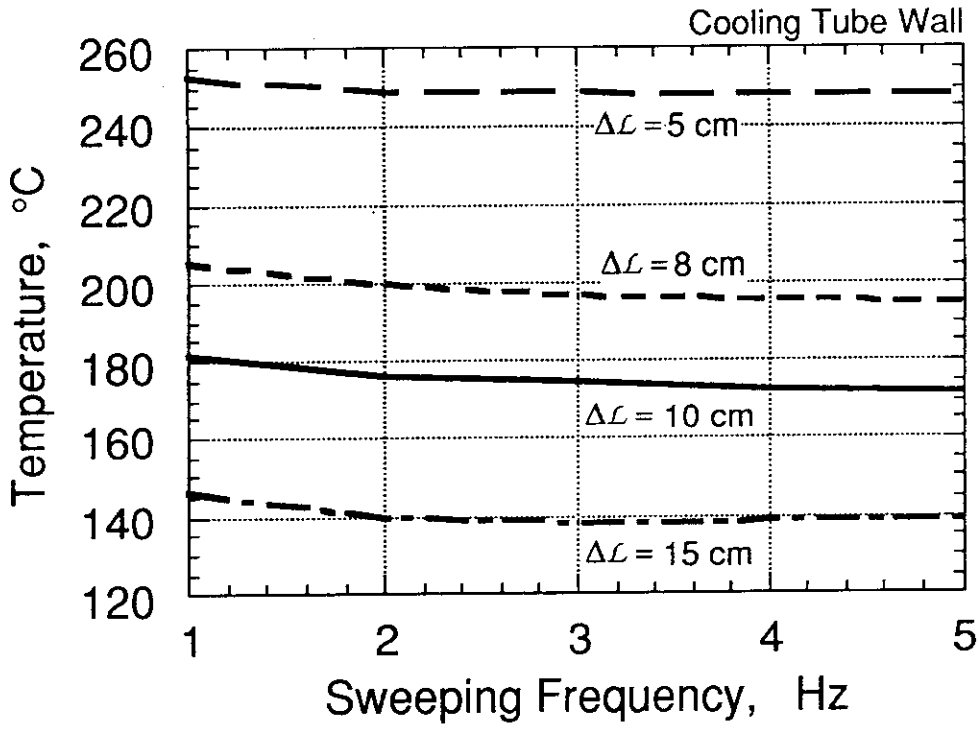

(c) Cooling Tube Inner Wall

Figure 5-8 Maximum Temperatures on the Divertor Plate Near Edge Location as a Function of the Sweeping Frequency.

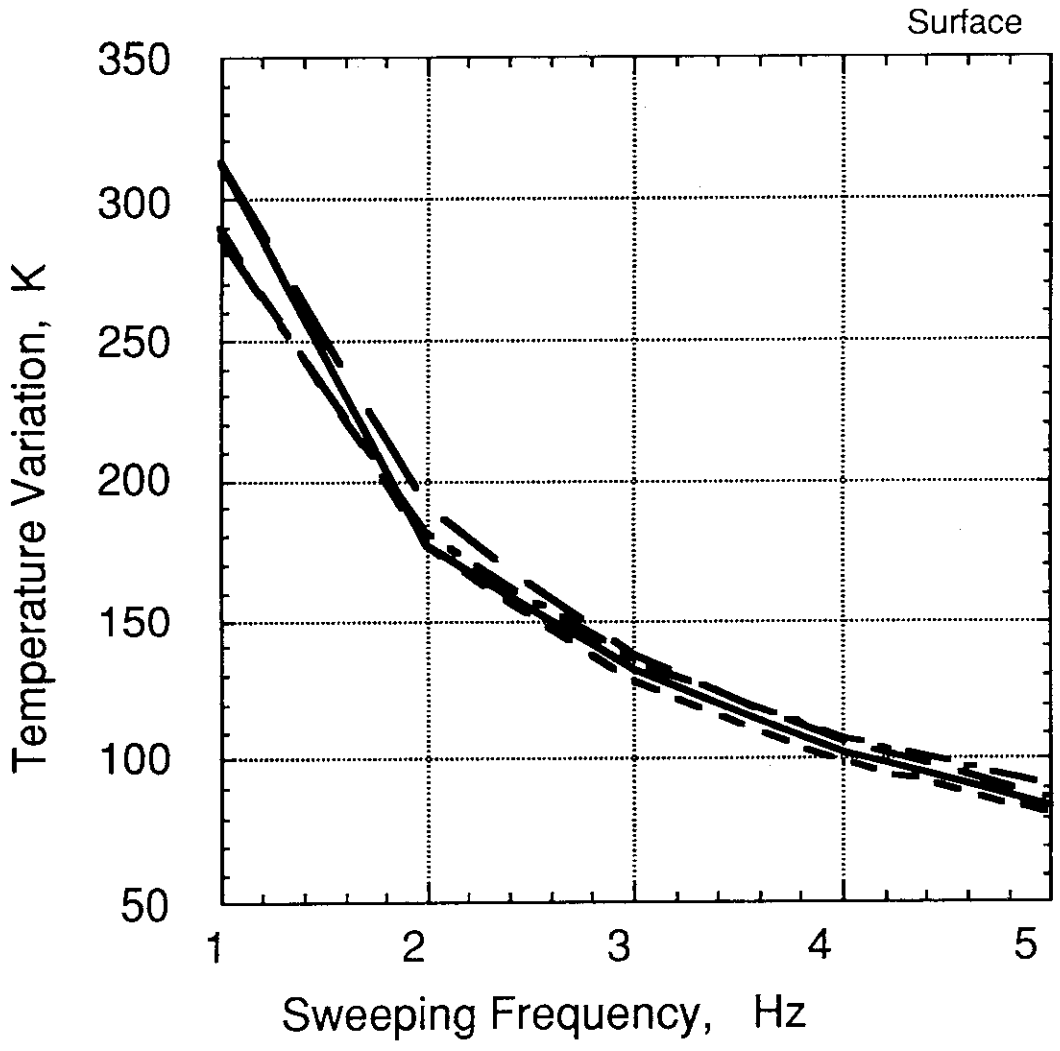

Figure 5-9 Minor-Temperature Change on the Surface of the Divertor Plate for Different Sweeping Distance.

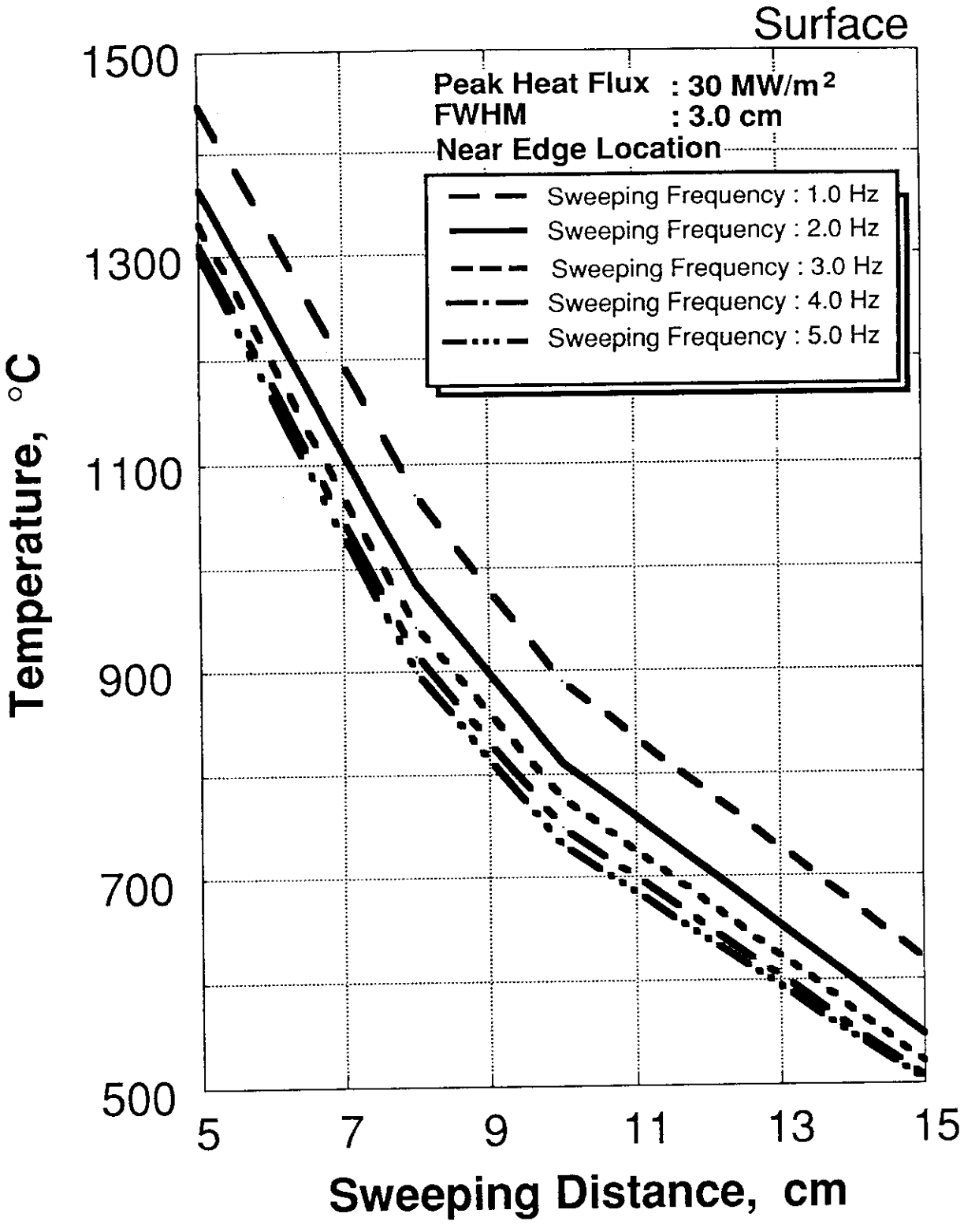

Figure 5-10 (a) Maximum Temperatures on the Surface of the Divertor Plate Near Edge Location as a Function of the Sweeping Distance.

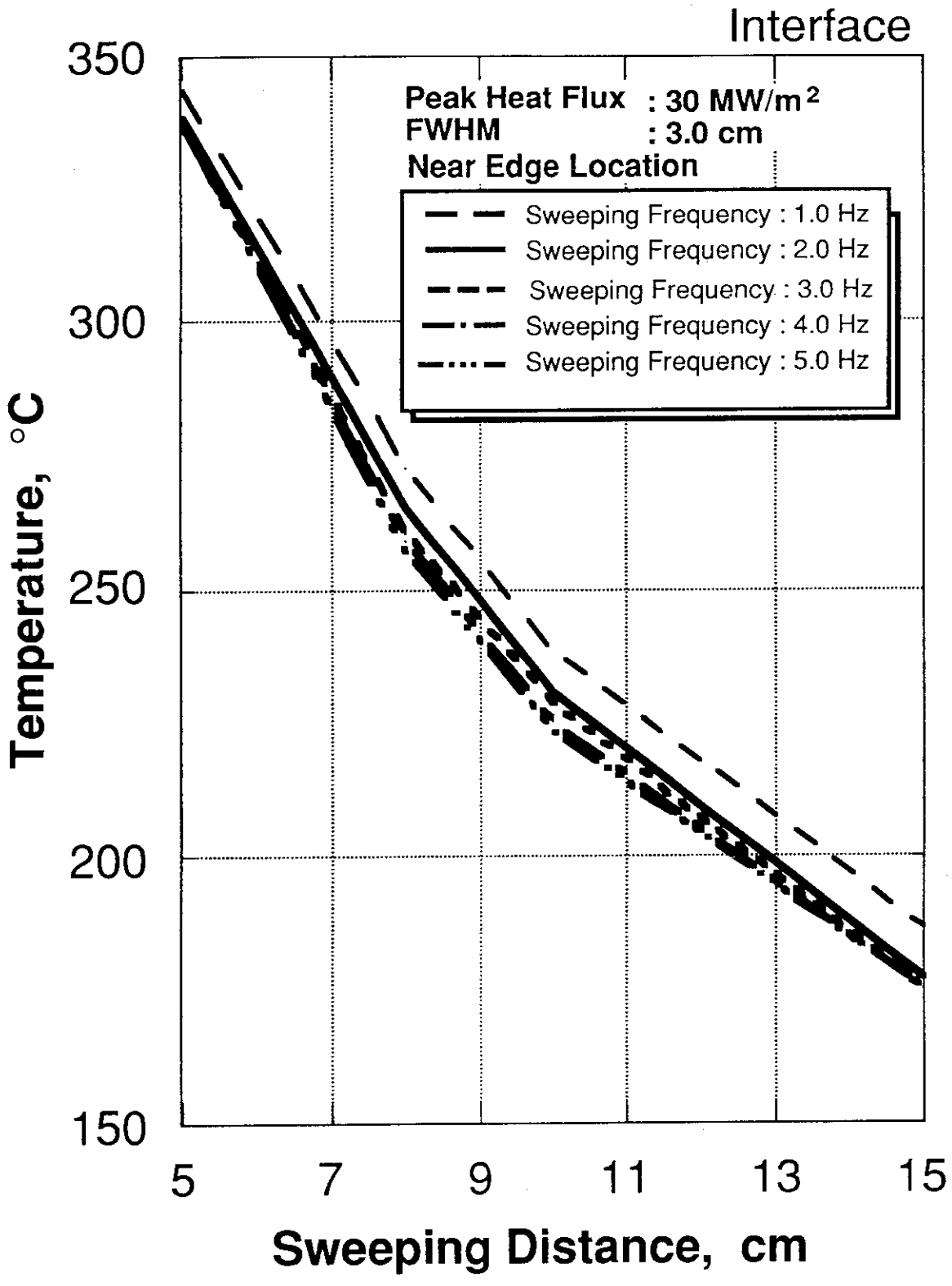

Figure 5-10 (b) Maximum Temperatures in the Interface of the Divertor Plate Near Edge Location as a Function of the Sweeping Distance.

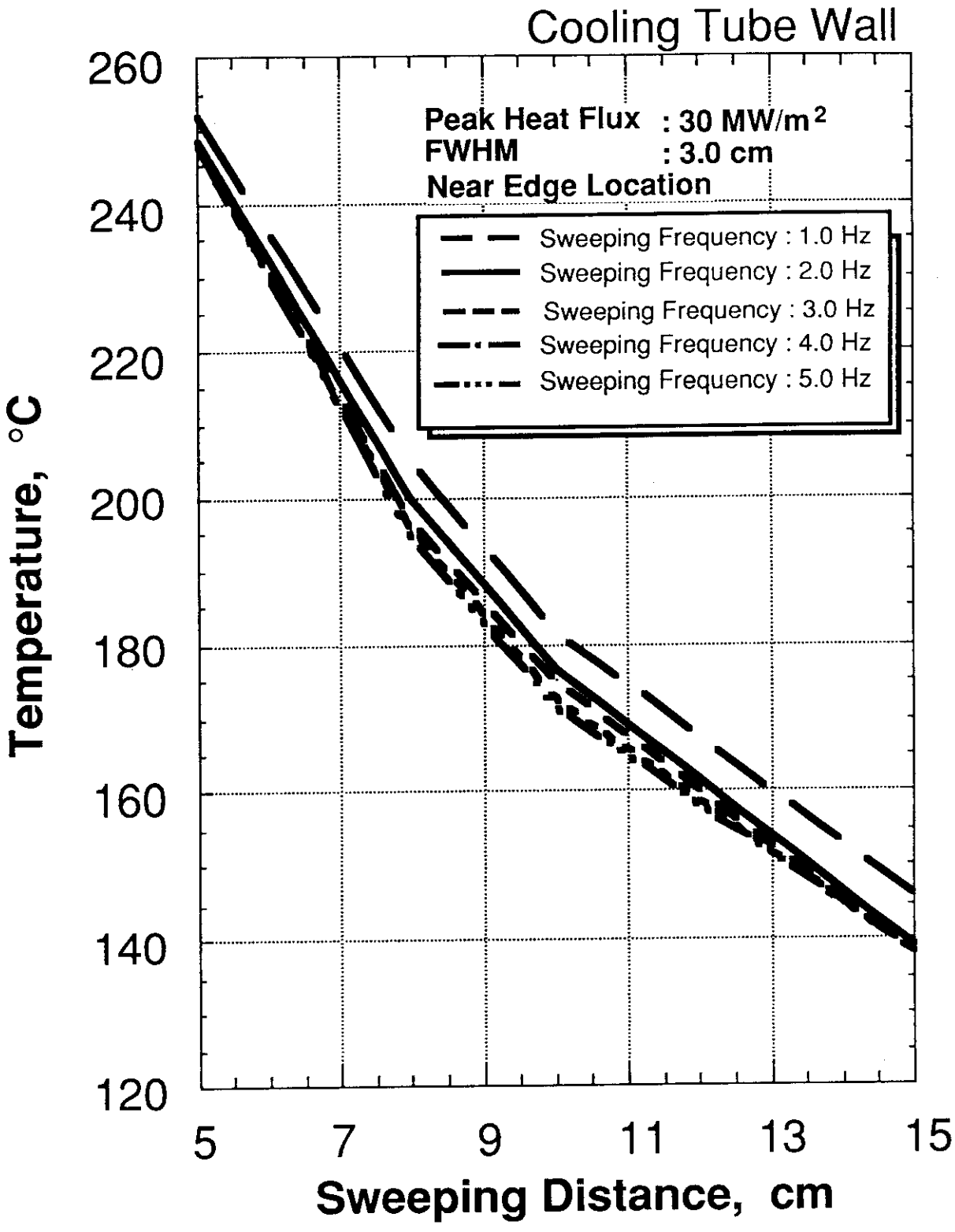

Figure 5-10 (c) Maximum Temperatures in the Cooling Tube Wall of the Divertor Plate Near Edge Location as a Function of the Sweeping Distance.

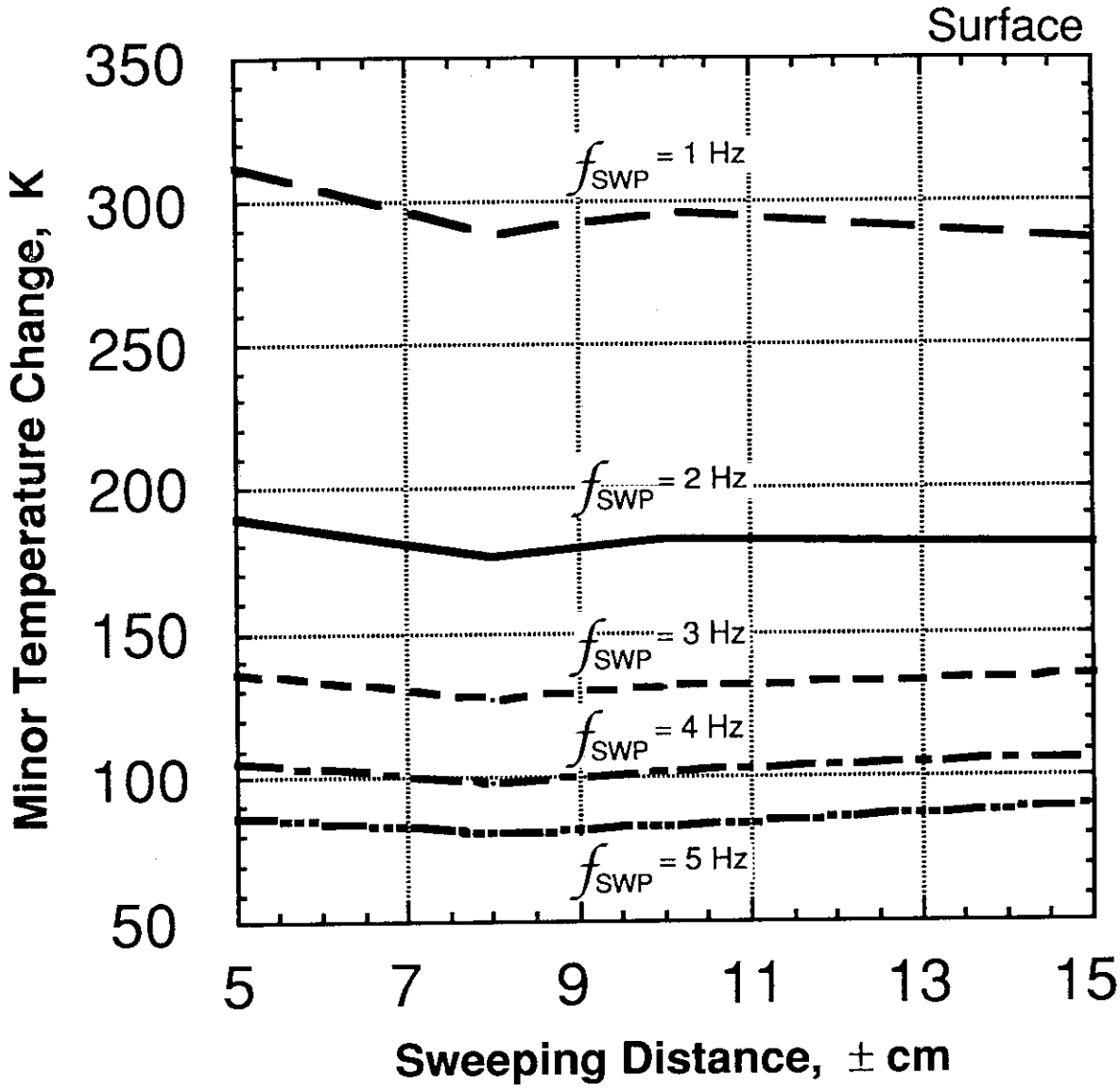

Figure 5-11(a) Minor-Temperature Changes on the Surface of the Divertor Plate as a Function of the Sweeping Distance.

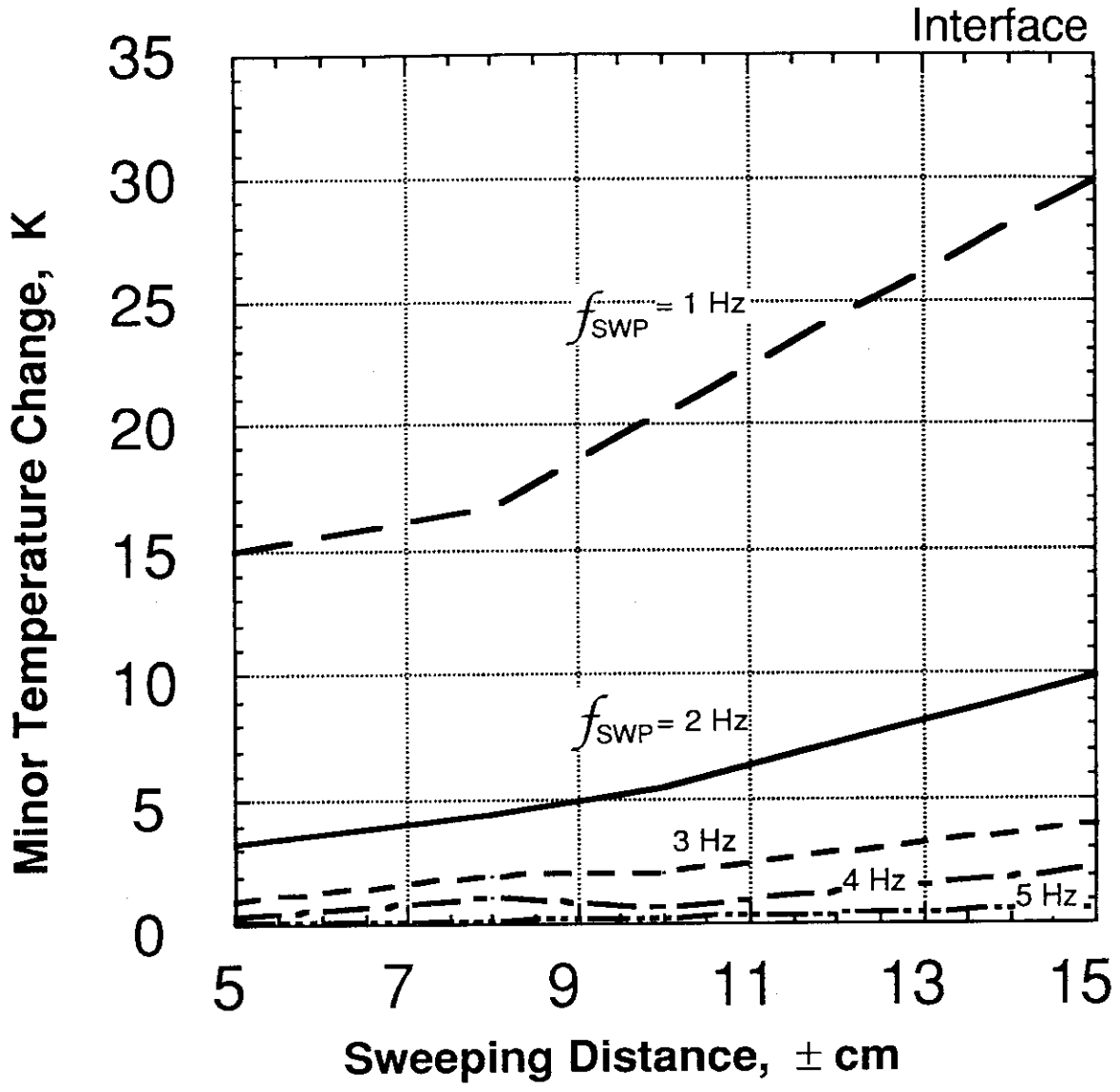

Figure 5-11(b) Minor-Temperature Changes in the Interface of the Divertor Plate as a Function of the Sweeping Distance.

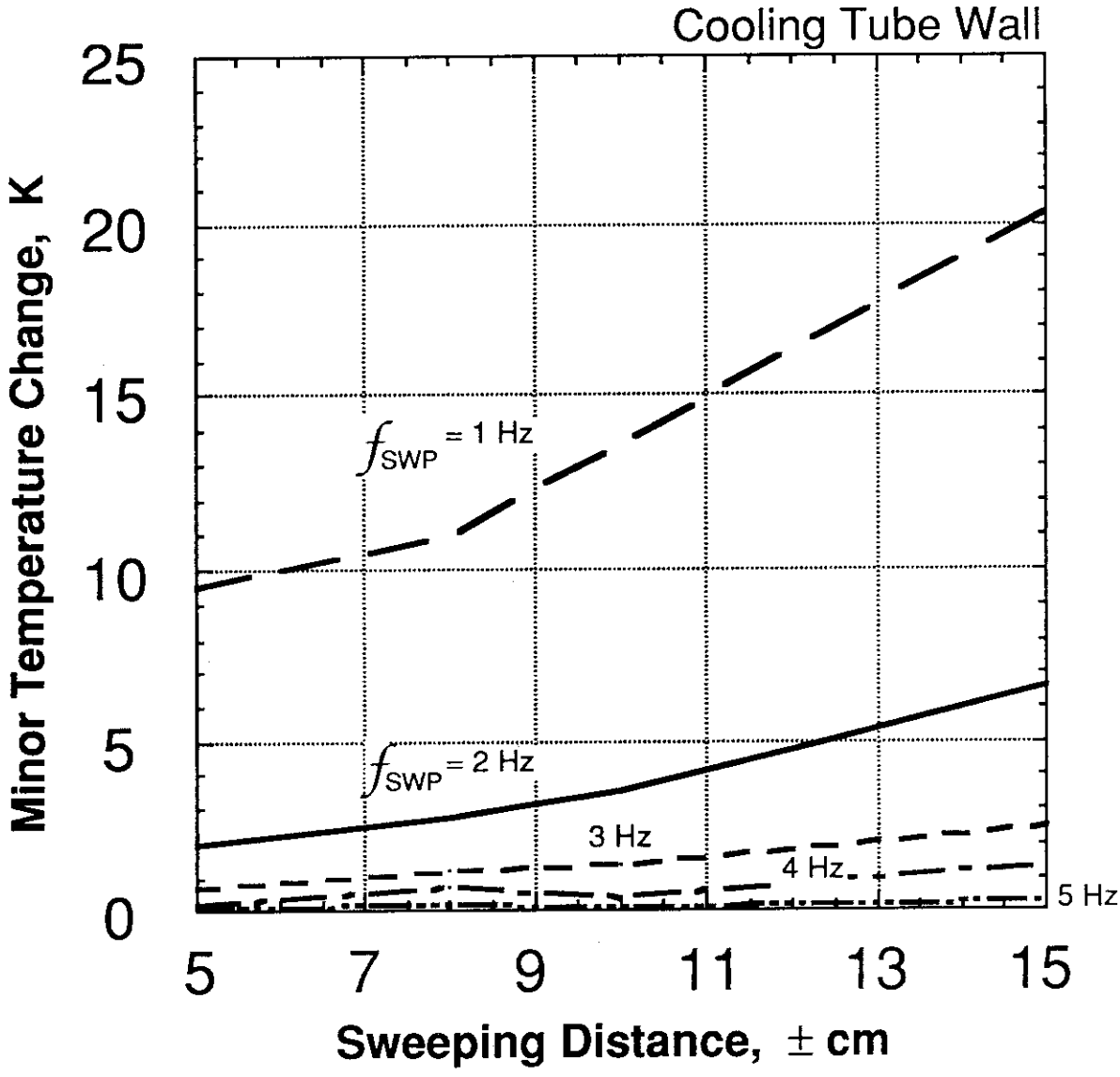

Figure 5-11(c) Minor-Temperature Changes in the Interface of the Divertor Plate as a Function of the Sweeping Distance.

5.2 Experimental Study

5.2.1 Experimental set-up and conditions

JAERI Electron Beam Irradiation System, namely JEBIS as shown in Fig. 5-12, was used in the experiment. In Table 5-3, major performances of JEBIS are also summarized. JEBIS can provide intense electron beams of up to 400 kW for durations from 0.001 s to continuous wave. An electron gun which has originally been developed for JEBIS is installed at the top port of the chamber. The electron gun consists of two parts, i.e., plasma generator and accelerator grid system. After hydrogen arc discharging in the plasma generator, only the electrons are extracted and accelerated at the set energy value by the grid system provided. Subsequently, moderate energetic electron beams enter into a pair of coils, namely bending and sweeping coil system, to sweep them on the target. By changing of magnetic field between the coils, the energetic electron beams can be swept on the target. In this experiment, a sweeping frequency with a linear wave caused by the magnetic field change is selected to 1.0 Hz. A sweeping distance defined by a length from the beam center is also selected to ± 10 cm. These values, 1.0 Hz and ± 10 cm, are within the acceptable parametric values for ITER.

With respect to a heat flux, a uniformly profiled heat flux will be necessary in the cross-sectional direction of the target, but the profile in the water flow direction is also required to simulate the ITER relevant profile as shown in Fig. 5-5. In the experiment, heat flux profile deposited to the target surface by the electron beam has been measured with a calorimeter made of graphite material because of strong dependence on the sample material.

Figure 5-13 shows the electron beam profile used in this experiment. Peak heat flux and full width at a half maximum, namely q_{peak} and FWHM, are 32 MW/m^2 and 1.9 cm, respectively. This figure also shows the expected heat flux profile on the divertor plate for ITER which has peak heat flux of 30 MW/m^2. In perpendicular to the water flow direction, almost uniform profile in the JEBIS experiment is observed. On the other hand, the measured heat flux profile in the flow direction, however, is slightly different from the expected ITER condition of 30 MW/m^2 with FWHM of 3 cm. For the complete simulation experiment, several divertor mock-ups will be needed to prevent components inside the chamber from leaked unusable electron beams. Since main objective of this experiment is to evaluate sweeping effect on reducing peak heat flux, it is very important

to keep the value of peak heat flux deposited to the surface of the divertor mock-up around the value expected in the ITER.

5.2.2 Divertor mock-up

Figure 5-14 shows a divertor mock-up used in the experiment. The divertor mock-up consists of four armor blocks made of CX-2002U, which is a two-dimensional carbon fiber reinforced carbon composite (CFC) and has relatively high thermal conductivities in the directions. Thermal and mechanical properties of CX-2002U given in Ref. [59] are used. Typical dimensions of each block are 25 mm width, 25 mm length, and 35 mm height.

Before fabricating the divertor mock-up, all the CFC material were degassed at temperature of around 1000 °C in vacuum environment to improve the adhesive property between the CFC and the cooling tube. And then all the CFC materials were brazed to a single cooling tube made of oxygen free high conductivity copper (OFHC-Cu) at temperature of around 850 °C for several minutes in vacuum environment. In the divertor mock-up, the direction in high thermal conductivity plane of CX-2002U was oriented in perpendicular to the cooling tube as shown in Fig. 5-14.

A K-type of thermocouple which was 0. 5 mm sheath diameter was brazed on the tube close to the interface between the armor tile and swirl tube in order to evaluate thermal response of the the divertor mock-up.

To enhance heat transfer into the coolant, a twisted tape made of stainless steel (AISI-304) with a twist ratio of 2 was inserted in the cooling tube. This type of the tube, namely swirl tube, is expected to having heat transfer coefficient of factor 1.5 to 2 higher compared to the tube without a twist tape [19]. In the experiment, deionized and high pressurized water is supplied to the divertor mock-up under the condition that water flow velocity, inlet pressure, and inlet temperature are 10 m/s, 3.5 MPa, and around 20 °C, respectively. At this water flow condition, heat transfer coefficient between the tube wall and the water is estimated to be around 9×10^4 W/m^{2}K.

Thermal response of the divertor mock-up has been analyzed in three-dimensional model due to the following reasons; first, the armor material has anisotropic thermal properties in each direction, and second, heat flux profile deposited to the divertor mock-up depends on both parameters of sweeping time and their positions. In the analysis,

constant value of the heat transfer coefficient is employed since no predictable correlations along the circumference of the swirl tube exist.

5.2.3 Experimental results

In the experiment, the divertor mock-up has been installed at the center region of the heated area. Figure 5-15 shows thermal response of the interface of the divertor mock-up measured by the thermocouple. In the figure, electron beam current, and outlet coolant temperature are also indicated. During heating, the acceleration current indicates almost flat profile. It means that constant heat flux profile which has a peak heat flux of 32 MW/m^2 is expected on the surface of the divertor mock-up. Within several seconds (4~5 s) after beam-on, interface temperature reaches to constant value of around 130 °C with temperature change of ±10 K. Two different minor-temprature changes of the interface are found in the experiment. This is a reason that a No. 2 block of the divertor mock-up was slightly deviated from the center point since center of the divertor mock-up, a gap between Blocks No. 2 and No. 3, was located at the heated center. Surface temperature of the armor tile which was measured with infrared camera was also expected to around 300 to 500 °C (not indicated). Without damages and temperature changes at the surface and the interface during heating, this monoblock type of CFC/OFHC-Cu divertor mock-up has resisted to a peak heat flux of 32 MW/m^2 for more than 1,000 major cycles under sweeping conditions for 1 Hz, ± 10 cm and 30 s. (It corresponds to the amount of over 30,000 for the periodic number of the minor-temperature change.)

Figure 5-16 shows numerical results of temperature responses at the typical points of the divertor mock-up. Temperature of the interface is expected to reach averaged value of around 120 °C with minor-temperature change of ± 10 K. The surface temperature is also expected to become averaged value of around 400 °C with ΔT_{minor} of 120 K.

Comparing analytical results with experimental data, analytical results show good agreement with the experimental data. This agreement indicates that numerical analysis can predict the experimental results. Therefore, it has been experimentally demonstrated that application of sweeping technique is very effective for improvement in the power handling capability of the divertor plate.

5.2.4 Conclusions

1. Under simulating the sweeping condition of 30 MW/m^2, 1.0 Hz, ± 10 cm, 30 s, experimental results show that the divertor mock-up has successfully endured for >1,000 major thermal cycles without increase of the surface temperature.
2. It has been experimentally demonstrated that application of the sweeping technique is very effective for improvement in the power handling capability of the divertor plate.

Table 5-3 Performances of the Test Facilities

	JEBIS
Acceleration Voltage, kV	20 - 100
Acceleration Current, A	up to 4
Pulse Duration, s	0.001 - CW
Working Gas	H_2
Beam Species	Electron
Type of Ion/Electron Source	Magnetic Multi-pole Plasma Source
Bending and Sweeping Coil	
Frequency, Hz	1 - 1000 in one dim.
Bending Angle, ± °	16
Maximum Heat Flux, MW/m^2	> 2000
Maximum Heating Area, cm	30 x 60
Water Cooling System	$40m^3/hr$ with 4 MPa
Pressure in the Test Bed, Pa	0.05

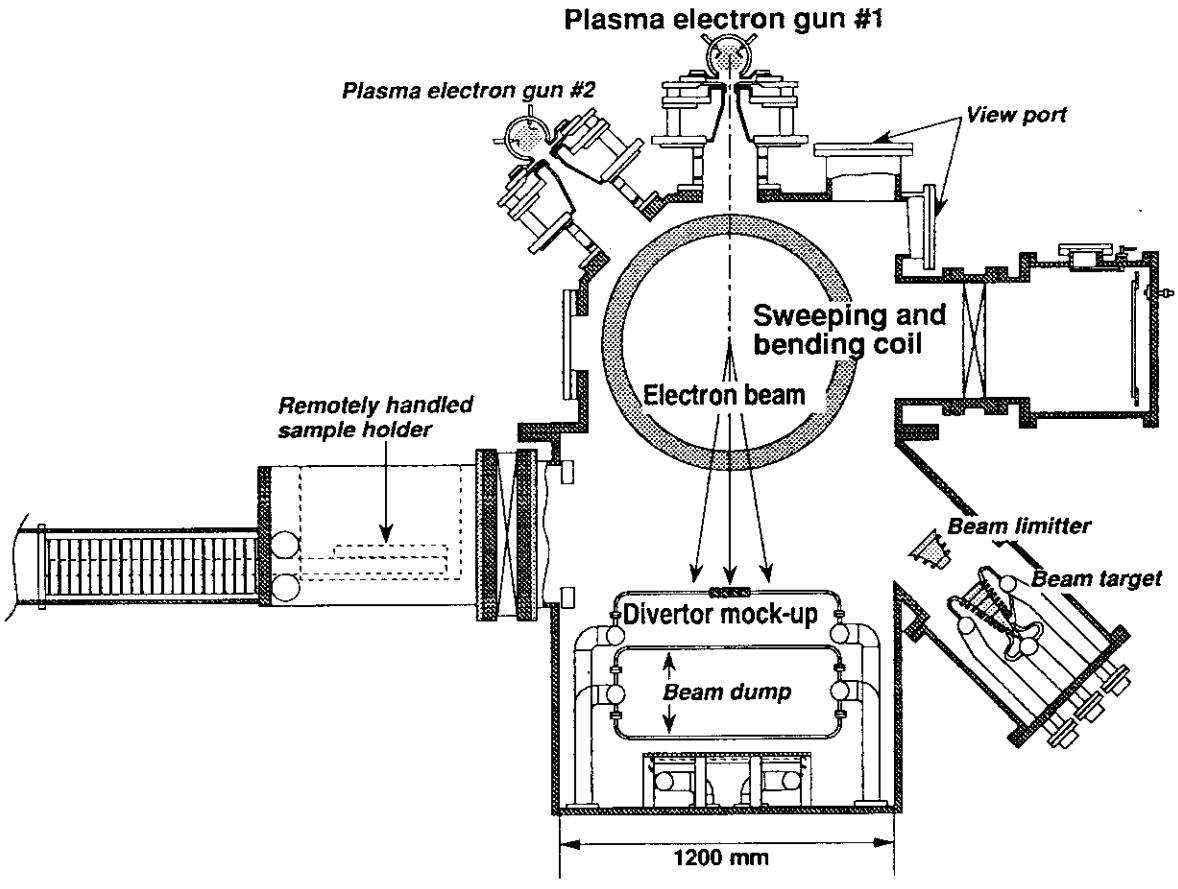

Figure 5-12. Schematic of JEBIS.
(JAERI Electron Beam Irradiation System)

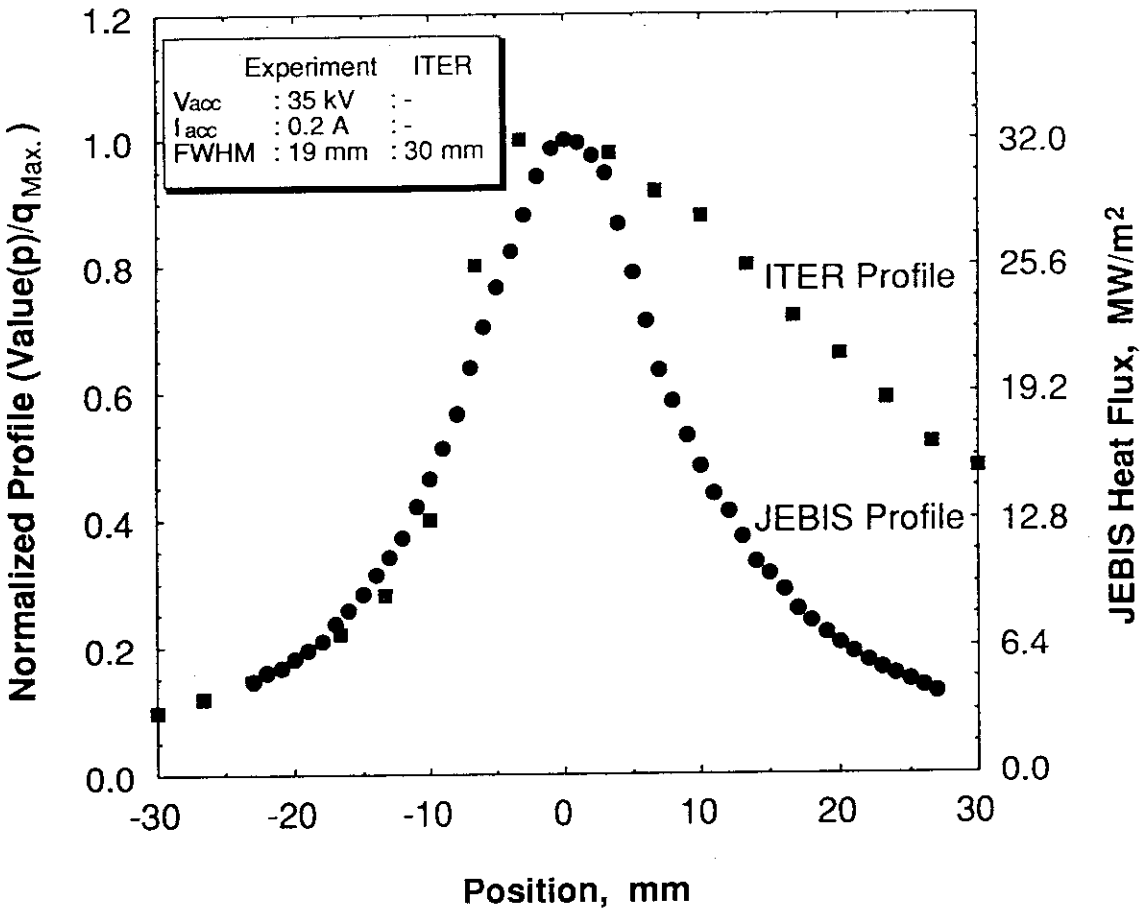

Figure 5-13. Heat Flux Profiles on the Surface of the Divertor Plate in Both Experiment and the ITER

In the figure, V_{acc}, I_{acc}, and FWHM mean the accleration voltage in kV, the acceleration current in A, and a full width at half maximum, respectively.

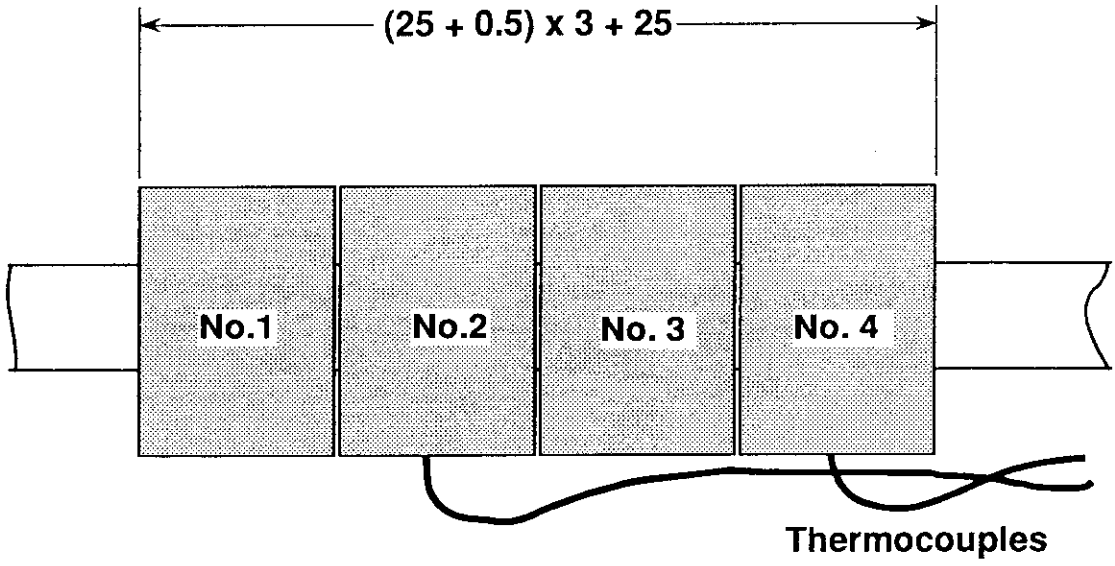

(b) Side View

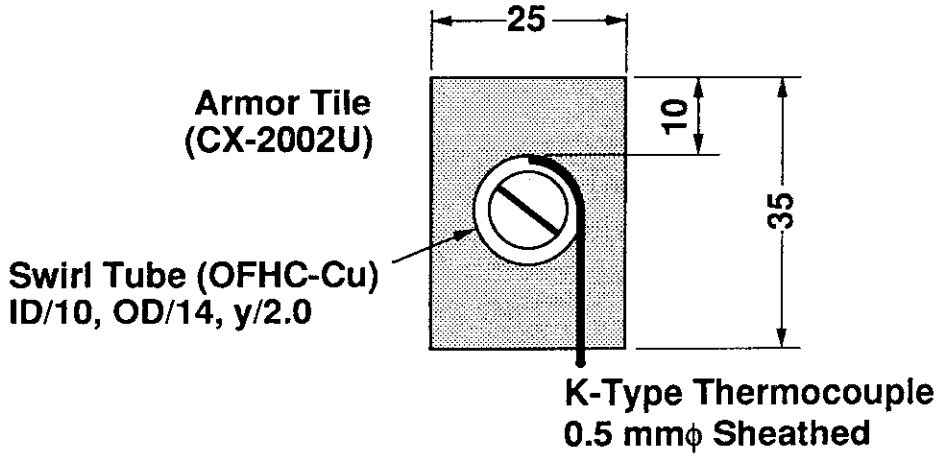

(a) Cross-sectional View

Figure 5-14 Schematic of Divertor Mock-up

Divertor mock-up consists of four blocks with gaps of less than 0.5 mm between blocks.

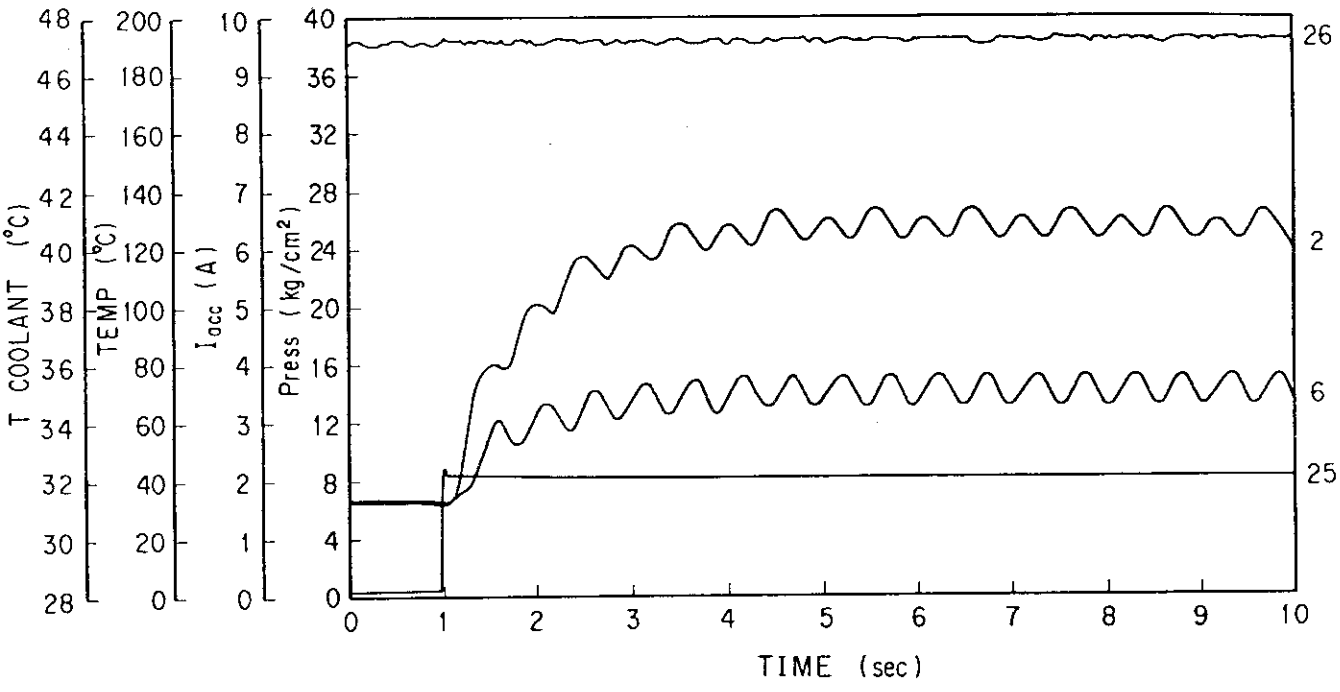

Figure 5-15 Thermal Response of the Interface of the Divertor Mock-up

In the figure, labeled 2, 6, 25, and 26 correspond to interface temperature, water outlet temperature, an electron beam current, and water inlet pressure, respectively.

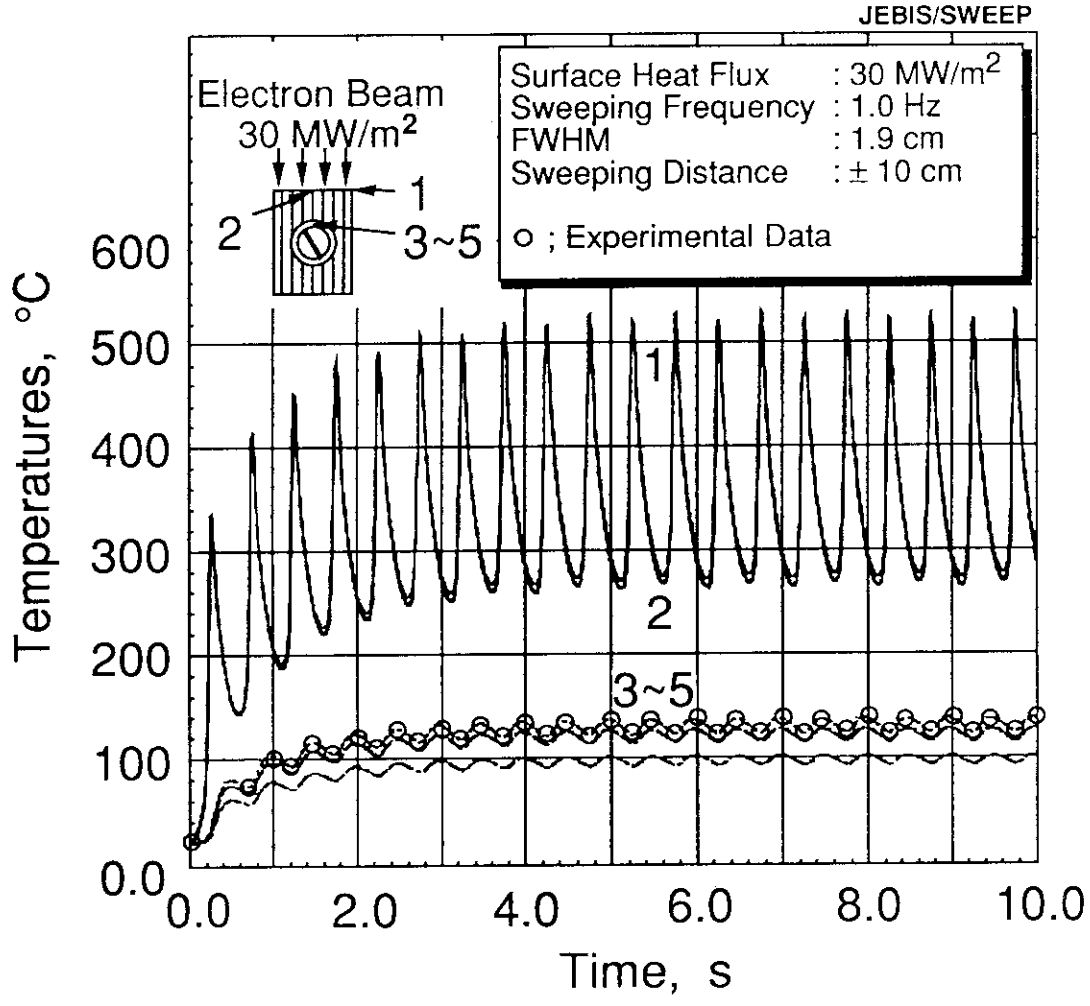

Figure 5-16 Temperature Responses at Typical Points of the Divertor Mock-Up

6. CONCLUSIONS

Through this study, the following conclusions were obtained;

1. Because of one-sided heating conditions for high heat flux components of fusion experimental reactor such as ITER, it is very important to develop cooling tube which can handle high heat flux and debase thermal deformation. For this objective, a swirl tube with an external fin, namely externally-finned swirl tube, was developed for the cooling tube element of high heat flux components for ITER. Major dimension of the tube is 10 mm in outer diameter, 1.5 mm in thickness, 15 mm in an external fin width, and tape twist ratio of 2.5, respectively.

   It was found that the externally-finned swirl tube will induce not only reducing the thermal stress across the tube, but also improving the characteristics of boiling heat transfer along the circumference.

2. An incident critical heat flux of 41 ± 1 MW/m^2 was obtained in the externally-finned swirl tube under the conditions that the flow rate and the inlet pressure were 30 l/min and 0.9 MPa (gauge), respectively.

3 It was found that the critical heat flux of the tube with an external fin is a factor of 1.5 higher than that of the smooth tube at the same conditions. However, similar CHF values were obtained in the smooth tube and the rectangular faced tube.

4. Incident CHF values obtained by the experiment under the one-sided heating condition have been translated to the CHF values at the tube inner surface with applying Shah's correlation for the subcooled flow boiling region. Experimental CHF data of the straight tube under the one-sided heating condition shows relatively good agreement with some correlations with an accuracy of ± 20 %.

   However all the existing correlations systematically underpredict CHF values for over the range of mass flows investigated in the present experimental conditions, even if heat flux profile at the tube inner surface of rectangular faced tube is similar to that of the straight tube. This is mainly attributable to the high degree of sensitivity of existing CHF correlations to the inner diameter, while in the experiment a small difference for different inner diameter. Further experiments are needed for the evaluation of applicability of existing CHF correlations under uniform heating conditions.

5. With respect to development of bonded divertor structure, promising bonds were developed even for poor compatibility of thermomechanical properties between CFC

and metal. Numerical results of residual braze stress in the bonds evaluated by thermal stresses in each direction show relatively good agreement with the results of the manufactured test samples and no cracks or detachments in many samples were observed by surface observation. In the thermal response experiment, the durability of the divertor mock-ups with CFC armor tiles was confirmed under the condition at which the thermal stress on the interface is expected to be equivalent to the value for a steady state heat flux of 10 MW/m^2. Furthermore, some CFC/OFHC-Cu samples have resisted to 12.5 MW/m^2 for 1,000 cycles without increase of the surface temperature, although cracks appeared at the outer surface of the CFC close to the bonded layer.

In order to evaluate lifetime of the bonds under large numbers of cyclic heat load, a new damage map in terms of the number of the thermal cycles and surface heat flux was proposed. A maximum stress amplitude calculated during thermal cycles, which is very important for the lifetime evaluation of the bonds, is also taken into account in the map.

6. In the bonded fine-grained graphite/OFHC-Cu divertor mock-ups with molybdenum intermediate (Gr/Mo/OFHC), the integrity of the bonds was confirmed under the heating condition of 16 MW/m^2 for 1.0 s which corresponds to the steady state heat flux of 8 MW/m^2. Some Gr/OFHC-Cu samples have resisted to up to 10 MW/m^2 for 1,000 cycles without increase of the surface temperature, although many longer cracks appeared at the outer surface of the graphite close to the bonded layer.

7. For the reduction of expected surface temperature on the divertor plate, It is expected by the numerical results that the application of the sweeping technique is very effective even for increase of periodic number of additional minor temperature change during sweeping. From the analytical result which an increase of the sweeping frequency up to 3.0 Hz is very effective for the reduction of surface temperature on the divertor plate, linear separatrix sweeping with the sweeping frequency of higher than 3.0 Hz for the sweeping distance of $\pm$ 10 cm is proposed to achieve effective sweeping results for ITER from thermal hydraulic point of view.

8. It is noted that for longer sweeping distance, higher sweeping frequency is required to reduce the temperature and the additional minor temperature change on the divertor plate.

9. It has been experimentally demonstrated that application of the sweeping technique is very effective for improvement in the power handling capability of the divertor

plate. In the experiment which simulates the ITER relevant sweeping condition in order to evaluate the durability of the bonds against large number of additional minor temperature change during sweeping, experimental results show that the divertor mock-up has successfully endured for >1,000 major and > 30,000 minor thermal cycles without increase of the surface temperature. Numerical results simulated thermal response of the mock-up during sweeping also show good agreement with the experimental result.

ACKNOWLEDGMENT

The author would like to express his sincere appreciation to Professor Saburo Toda of Tohoku University for his precise guidance, useful advice and continuous encouragements on this study. The author would also like to express his sincere thanks to Associate Professor Hidetoshi Hashizume of Tohoku University for his useful comments and discussions.

It is a great pleasure to acknowledge the help Dr. Masahiro Seki of Japan Atomic Energy Research Institute for precise guidance and continuous encouragements on this study. The author wishes to express his sincere gratitude to Dr. John Haines of Prinston Plasma Physics Laboratory in Prinston University for valuable comments and advice on this study.

The author would deeply like to thank Dr. Yoshihiro Ohara and Dr. Masato Akiba of Japan Atomic Energy Research Institute for useful advice, discussions, and continuous helps on this study.

The author would like to thank Dr. Susumu Shimamoto and Dr. Naomoto Shikazono of Japan Atomic Energy Research Institute for their support and encouragement.

REFERENCES

[1] T. Kuroda, G. Vieder, M. Akiba, A.B. Antipenkov, M.Araki, *et al.*, "ITER Plasma Facing Components," *ITER Documentation Series*, No. **30**, IAEA (1991).

[2] F. C. Gunther, "Photographic Study of Surface-Boiling Heat Transfer to Water with Forced Convection", *Trans, ASME*, 73-2, (1951) 115-123.

[3] D. H. Knoebel, *et al.*, "Forced-Convection Subcooled Critical Heat Flux D_2O and H_2O Coolant with Aluminum and Stainless Steel Heaters", USAEC DP-1306, E. I. Dupont de Nemours & Company (Feb. 1973).

[4] J. Griffel, *et al.*, "Forced-Convection Boiling Burnout for Water in Uniformly Heated Tubular Test Sections", NYO-187-7 (Thesis), Columbia University (May 1965).

[5] L. S. Tong, "A Phenomenological Study of Critical Heat Flux", 75HT68, *ASME* (1975).

[6] F. Inasaka, and H. Nariai, "Critical Heat Flux and Flow Characteristics of Subcooled Flow Boiling in Narrow Tubes", *JSME Int. J.* Vol. **30**, (1987) 1595-1600.

[7] Y. Katto, "Prediction of Subcooled Water Flow Boiling CHF over a Wide Range of Pressure", *Japanese Heat Mass Transfer* Vol. **28** (in Japanese), B-144, (May 1991); see also Y. Katto, "A Prediction Model of Subcooled Water Flow Boiling CHF for Pressure in the Range 0.1-20 MPa", in print to *Int. J. Heat Mass Transfer.*

[8] H. Horiike, M. Kuriyama, and H. Morita, "Burnout Experiment in Subcooled Forced-Convection Boiling of Water for Beam Dumps of a High Power Neutral Beam Injector", *Nuclear Tech./Fusion* Vol. **2**, (1982) 637-647.

[9] J. Schlosser, A. Cardella, P. Massmann, P. Chappuis, H. D. Falter, P. Deschamps, and G. H. Deschamps, " Thermal-Hydraulic Tests on NET Divertor Targets Using Swirl Tubes", in *Proc. Seventh of Nuclear Thermal Hydraulics (1991 Winter Meeting)*, San Francisco, (Nov. 1991) 26-31.

[10] J. Koski, A. G. Beattie, J. B. Whitley, and C. D. Croessmann, "Experimental Verification of Subcooled Flow Boiling for Tokamak Pump Limiter Designs", *ASME* 87-HT-45, (1987).

[11] K. Nakashima, S. Yamamoto, T. Uede, *et al.*, "Conceptual Design Study of Fusion Experimental Reactor," JAERI-M 87-145, Japan Atomic Energy Research

Institute (1987)(in Japanese).

[12] R. Haange, "Design of Calorimeter and Beam Dump for JET Neutral Beam Injection Beam Line," in *Proc. of 9th Symp. on Engineering Problems of Fusion Research*, Chicago, (1981) 1356.

[13] J.A. Paterson, G. Koehler, and R.P. Wells, "The Design of Multi-Megawatt Actively Cooled Beam Dumps for the Neutral Beam Engineering Test Facility," in *Proc. of 9th Symp. on Engineering Problems of Fusion Research*, Chicago, (1981) 1666.

[14] F. Dahlgren, "Steady-State Beam Dump for TFTR," in *Proc. of 10th Symp. on Fusion Engineering*, Philadelphia, (1983) 583.

[15] S.L. Milora, S.K. Combs, and C.A. Foster, "A Numerical Model for Swirl Flow Cooling in High Heat Flux Particle Beam Targets and the Design of the Design of a Swirl Flow Based Plasma Limiter," **ORNL-TM-9183**, Oak Ridge National Laboratory (1986).

[16] D.J. McFarlin, A.E. Betz, C.C. Tompson, and A. Golgner, "Active Cooling System for the LLNL MFSTF," in *Proc. of 10th Symp. on Fusion Engineering*, Philadelphia, (1983) 526.

[17] T. Itoh, **JAERI-M 86-114**, Japan Atomic Energy Research Institute (1986)(in Japanese).

[18] C.C. Tompson, D.H. Polk, D.J. McFarlin, and R.R. Stone, "Heat Exchanger Concepts for Neutral Beam Calorimeters," in *Proc. of 9th Symp. on Engineering Problems of Fusion Research*, Chicago, (1981) 1658.

[19] W.R. Gambill, R.D. Bundy, and R.W. Wansbrough, "Heat Transfer, Burnout and Pressure Drop for Water in Swirl Flow Trough Tubes with Internal Twisted Tapes," **ORNL-2911**, Oak Ridge National Laboratory (1960).

[20] M. Araki, M. Akiba, S. Suzuki, M. Dairaku, K. Yokoyama, H. Ise, M. Seki, and S. Tanaka, "Thermal Cycling Tests of Plasma Facing Components for Fusion Experimental Reactors at JAERI", in *Proc. the 14th Symp. on Fusion Engineering*, San Diego (Sept. 1991) 357-360.

[21] I. Smid, C. D. Croessmann, R. D. Watson, J. Linke, A. Cardella, H. Bolt, N. Reheis, and E. Kny, "Performance of Brazed Graphite, Carbon-Fiber Composite, and TZM Materials for Actively Cooled Structures: Qualification Tests", *Fusion Tech.* Vol. **19**, (July 1991) 2035-2040.

[22] R. D. Watson, F. M. Hosking, M. F. Smith, and C. D. Croessmann, "Development

and Testing of the ITER Divertor Monoblock Braze Design", *Fusion Tech.* Vol. **19**, (May 1991).

[23] S. Deschka, A. Cardella, J. Linke, M. Lochter, and H. Nickel, "High Heat Flux Performance of Actively Cooled Divertor Mock-ups", in presented at *the 5th Int. Conf. on Fusion Reactor Materials*, Clearwater, Florida, (Nov. 1991).

[24] L. S. Tong, "Boundary-Layer Analysis of the Flow Boiling Crisis", *Int. J. Heat Mass Transfer*, Vol. **11**, (1968) 1208-1211.

[25] M. Araki, M. Dairaku, T. Inoue, M. Komata, M. Kuriyama, S. Matsuda, M. Ogawa, Y. Ohara, M. Seki, and K. Yokoyama, "Burnout Experiments on the Externally-Finned Swirl Tube for Steady-State and High Heat Flux Beam Stops", *Fusion Engineering & Design* Vol. **9**, (1989) 231-235.

[26] G. P. Celata, M. Cumo, and A. Mariani, "Preliminary Remarks on High Heat Flux CHF in Subcooled Water Flow Boiling", *Int. J. Heat and Tech.* Vol. **8**, (1990) 20-42.

[27] R. D. Boyd, "Subcooled Water Flow Boiling Experiments under High Heat Flux Conditions", *Fusion Tech.* Vol. **13**, (1988) 131-142.

[28] H. Nariai, F. Inasaka, W. Fujisaki, and H. Ishiguro, "Critical Heat Flux of Subcooled Flow Boiling in Tubes with Internal Twisted Tapes", in *Proc. Seventh of Nuclear Thermal Hydraulics (1991 Winter Meeting)*, San Francisco, (Nov. 1991) 38.

[29] J. R. S. Thom, in *proc. Int. Mech. Engng. Pt. C*, **180**, (1966) 3226.

[30] M. M. Shah, "A general Correlation for Heat Transfer During Subcooled Boiling in Pipes and Annuli", *ASHRAE Trans.* Vol. **83**, (1977) 202-217, and also see M. M. Shah, "Generalized Prediction of Heat Transfer During Subcooled Boiling in Annuli," *Heat Transfer Engineering*, **4** (1983) 24-31.

[31] S. Yamamoto, *et al.*, "Tokamak Reactor Operation Scenario Based on Plasma Heating and Current Drive by Negative-Ion-Based Neutral Beam Injector," in *Proc. of 11th Int. Conf. on Plasma Physics and Controlled Nuclear Fusion Research*, **IAEA-CN-47/H-I-3**, Kyoto, (1986).

[32] K. Tomabechi, *et al.*, "ITER: Conceptual Design," in *Proc. of the 13th Int. Conf. on Plasma Physics and Controlled Nuclear Fusion Research, Washington*, **IAEA-CN-53/F-1-1**, (1990).

[33] M. Akiba, *et al.*, "High Heat Flux Experiments at JAERI", in *Proc. of 13th Symp. on Fusion Engineering*, Knoxville, **vol. 1**, (1989) 529-532.

[34] J. G. van der Laan, *et al.*, "Simulation and Analysis of the Response of Carbon-Fiber Composites and Pyrolytic Graphites to Off-Normal High Heat Loads," *Fusion Technol.*, **19**, July, (1991) 2070-2075.

[35] M. Seki, M. Akiba, M. Araki, *et al.*, "Thermal Shock Tests on Various Materials of Plasma Facing Components for FER/ITER," *Fusion Engineering and Design*, **15**, (1991) 59-74.

[36] M. Araki, M. Akiba, M. Seki, M. Dairaku, H. Ise, *et al.*, "Experimental and Analytical Results of Carbon Based Materials under Thermal Shock Heat Loads for Fusion Application," *Fusion Engineering and Design* , **19**, (1992) 101-109.

[37] M. Araki, S. Suzuki, M. Akiba, *et al.*, "Thermal Cycling Tests of Plasma Facing Components for Fusion Experimental Reactors at JAERI," in *Proc. of the 14th Symp. on Fusion Engineering*, San Diego, (1991) 357-360, and also see S. Suzuki, *et al.*, "Electron Beam Irradiation Experiments of First Wall Mock-ups for Fusion Experimental Reactors (I)," *Japan Atomic Energy Research Institute Report*, **JAERI-M 91-085**, 1991 (in Japanese).

[38] S. Tanaka, Y. Yokoyama, M. Akiba, M. Araki, *et al.*, "Design and Experimental Results of a New Electron Gun Using a Magnetic Multipole Plasma Generator," *Rev. Sci. Instrum.*, **62 (3)**, March, (1991) 761-771.

[39] Y. Okumura, *et al.*, "High Magnetic Field, Large-Volume Magnetic Multipole Ion Source Producing Hydrogen Ion Beams with High Proton Ratio," *Rev. Sci. Instrum.*, **55 (1)**, January, (1984) 1-7.

[40] Y. Gotoh, M. Akiba, M. Araki, *et al.*, "Felt-Carbon-Carbon Composite/ Copper Brazed Structures for Active Cooling Plasma Facing Components," in *Proc. of 16th Symp. on Fusion Technol.*, London, (1990) 312-316.

[41] K. Kitamura, M. Akiba, M. Araki, *et al.*, "Experimental and Analytical Studies on Residual Stress in Tungsten-Copper Duplex Structure for a Divertor Application," *Fusion Engineering and Design*, **18**, (1991) 173-178.

[42] M. Yamamoto, *et al.*, "Evaluation Tests on First Wall and Divertor Plate Materials for JT-60 Upgrade," *Japan Atomic Energy Research Institute Report*, **JAERI-M 90-119**, 1990 (in Japanese).

[43] R. D. Watson, F. M. Hosking, M. F. Smith, C. D. Croessmann, "Development and Testing of the ITER Divertor Monoblock Braze Design," *Fusion Technol.*, **19**, (1991) 1794-1798.

[44] M. Araki, M. Akiba, M. Seki, S. Suzuki, *et al.*, "Recent Results of Developmental

Study on Plasma Facing Components at JAERI," in *Proc. of 16th Symp. on Fusion Technol.*, London, (1990) 307-311.

[45] I. Smid, *et al.*, "Response to High Heat Fluxes and Metallurgical Examination of a Brazed Carbon-Fiber-Composite/Refractory-Metal Divertor Mock-up," *Fusion Engineering and Design*, **18**, (1991) 125-133.

[46] S. Deschka, Untersuchung Gefugter Verbund werkstoffe für Fusion-sanwendungen, KfA-Report, (1991) (in Germany).

[47] M. Araki, M. Akiba, M. Dairaku, K. Iida, H. Ise, et al., "Thermal Response of Bonded CFC/OFHC-Cu Divertor Mock-ups for Fusion Experimental Reactors Under Large Numbers of Cyclic High Heat Loads," *J. of Nucl. Sci. Technol.*, **29[9]**, (1992) 901-908.

[48] S. Suzuki, M. Akiba, M. Araki, and K. Yokoyama, "Thermal Cycling Experiments of Monoblock Divertor Modules for Fusion Experimental Reactors," *Fusion Technol.*, **21** (1992) 1858-1862.

[49] M. Azumi, T. Takizuka, M. Sugihara, M. Shimada, and Y. Shimomura, ITER-IL-Ph-13-0-J-5 (1990).

[50] S. Sakurai, S. Takamura, Kakuyugo Kenkyu, vol. 68/No. 1 (1992) 34 (in Japanese).

[51] T. Hino and T. Yamashina, "Evaluation for Metal-Mixed Graphite and High-Z Metal as Plasma Facing Material," in Proc. of 10th Plasma Surface Interaction, (1992) and also be published to J. of Nucl. Mat..

[52] J. Pamela, M. Araki, M. Fumelli, F. Jequier, S. Laffite, et al., "Energy Recovery Experiments with a Powerful Neutral Beam Injector Equipped with a High Atomic Ion Yield Plasma Generator," Nuclear Instru. and Methods in Physics Research, A294 (1990) 299-312.

[53] M. Araki, Y. Ohara, and Y. Okumura, "Design Study of a Beam Energy Recovery System for a Negative-Ion-Based Neutral Beam Injector," Fusion Technol., 17 (1990) 555- 565.

[54] M. Shimada and JT-60 Team, 14th Int. Conf. on Plasma Physics and Cont. Nucl. Fusion Res., Wurzburg, (1992) IAEA-CN-56/A-1-3.

[55] J.C. Wesley, "Thermal Effects of Divertor Sweeping in ITER," in *Proc. of the 14th Symp. on Fusion Engineering*, San Diego, (1991) 933-936.

[56] A. Hassanein, "Analysis of Sweeping Heat Loads on Divertor Plate Materials," in *Proc. the Fifth Int. Conf. on Fusion Reactor Materials*, Clearwater, Florida,

(Nov. 1991).

[57] S. Nishio, M. Araki, K. Shinya, T. Kuroda, M. Sugihara, and Y. Shimomura, "Separatrix Sweeping by In-Vessel Coils on a Fusion Reactor," to be published in *Fusion Engineering and Design*, (1992).

[58] D.E. Post, K. Borrass, J.D. Callen, S.A. Cohen, J.G. Cordey, et al., "ITER Physics," *ITER Documentation Series*, No. **21**, IAEA (1991).

[59] C.H. Wu, R. Behrisch, H. Bolt, et al., "Notes of the Specialist Meeting on Material Data Base, Plasma Facing Materials," ITER-Report, Garching, (Feb. 1990).

[60] J. Kim, "Targets for High Power Neutral Beams," *IEEE Transactions on Nuclear Science*, Vol. NS-28, No. 2 (April 1981) 1326-1330 and also see J. Kim, R.C. Davis, W.R. Gambill, and H.H. Haselton, "A Heat Transfer Study of Water-Cooled Swirl Tubes for Neutral Beam Targets," in *Proc. of the Seventh Symp. on Engineering Problems of Fusion Research*, Knoxville, (1977) 1593.

[61] S.L. Milora, S.K. Combs, and C.A. Foster, "A Numerical Model for Swirl Flow Cooling in High-Heat-Flux Particle Beam Targets and the Design of a Swirl-Flow-Based Plasma Limiter," *Nuclear Engineering and Design/Fusion*, **3** (1986) 301-308.

[62] M. Araki, S. Suzuki, M. Akiba et al., "Development and Testing of Divertor Plates for ITER/FER at JAERI," *in preparation for publication to the 17th Symp. on Fusion Technology*, Rome (Sept. 1992), and also see M. Araki, M. Akiba, K. Yokoyama, et al., "Experimental and Analytical Evaluations of Simulated Sweeping Heat Load on the Divertor Mock-up for ITER," *in preparation for publication to Fusion Engineering and Design*, (1992).

Appendix: Experimental and analytical results of carbon based materials under thermal shock heat loads for fusion application

1. INTRODUCTION

Development of plasma facing components is one of the key issues in the design of the next generation fusion devices such as the Fusion Experimental Reactor (FER) in Japan [1] and the International Thermonuclear Experimental Reactor (ITER) [2]. Plasma facing components will be exposed to the following heat loads: one is a steady state heat load, which is estimated to be 10 - 30 MW/m^2 on the divertor and 0.2 - 0.6 MW/m^2 on the first wall [3]. The other is a pulsed heat load during plasma disruptions. At the plasma disruption, very high heat load is deposited to the plasma facing components. For the divertor, the disruption energy flux is specified as 10 to 20 MJ/m^2 for a duration of 0.1 to 3.0 ms, which gives a heat flux on the order of 10^5 MW/m^2 [3] .

Based on the success of present tokamak experiments, low-Z materials are preferred as armor materials since they minimize the radiation loss from the plasma. Because of their high thermal conductivities and high sublimation temperature, carbon materials have generally been preferred as low-Z materials. Therefore, carbon materials have been selected as a primary candidate for the plasma facing materials during the physics phase in FER/ITER. Recent carbon materials, especially carbon fiber reinforced carbon composites (CFCs), have high thermal conductivity and relatively high fracture toughness compared to an isotopic graphite [4].

Before the experiments, numerical calculations were performed to estimate the erosion damage caused by plasma disruption [5]. They revealed that the erosion damages of carbon materials under the disruption are estimated to be very severe and eroded thickness reaches several hundred microns per disruption. Because only limited data are available on the erosion of carbon materials due to intense heating [5, 6, 7], we have started thermal shock tests on various carbon materials, with special emphasis being placed on newly developed CFCs.

This article describes the experimental results of thermal shock tests and comparison of them with the numerical analysis. Experimental setup and heat flux predictions are summarized in section 2, and the results of thermal shock tests on various carbon materials are presented in section 3, and then discussion and conclusion are given in sections 4 and 5.

2. TEST FACILITY AND TEST SAMPLE

2.1 TEST FACILITY

An electron beam test facility at Kawasaki Heavy Industries (KHI-test facility) [8] which has been developed under collaboration between JAERI and KHI was applied for thermal shock tests. Major performances and a schematic view of the KHI-test facility are shown in Table 1 and Fig. 1, respectively. In the previous experiment (note that its experiment is not in this series), arcing problems occurred in the electron gun due mainly to direct incidence of evaporating materials coming from the specimen. To minimize arcing problems in the electron gun, the KHI-test facility was modified to have an angle between the beam axis at a region of the electron gun and the beam axis normal to the heated surface using deflecting coils as shown in Fig.1. The electron gun was mounted at an inclining angle of 20 degrees from the normal of the heated surface. The electron beam produced at the gun is extracted and focused by the focusing lens system. After that, the electron beam is bent to hit the sample surface. The KHI-test facility can uniformly produce an intense electron beam within a relatively wide area by the beam rastering coil system.

Different heat fluxes and heated areas are easily provided by a combination of beam current and rastering angle of the electron beam. In a range of electron beam current from 0.2 to 0.3 A, heat fluxes and their profiles were experimentally measured by the copper calorimeter [8]. In the present experiment, extended evaluation of heat flux on the test sample is required because 1) the experimental set-up was modified, and 2) the electron beam current is higher than 0.3 A to provide higher heat fluxes. A simple evaluation of the heat flux can be made from a relation between heat flux and the electron beam current. Based on the heat flux measurements, we can introduce the following correlation;

when $0.05\ A \leq I_{acc} \leq 0.5\ A$,

$$q = C_1 \cdot C_2 \cdot V_{acc} \cdot (I_{acc})^{0.8388} \qquad \ldots(1)$$

q : Heat flux (MW/m^2)

V_{acc} : Acceleration voltage (kV : = 100)

I_{acc} : Acceleration current (A)

where C_1 and C_2 are variable constants dependent on the target material and on the heated area, respectively. C_2 was determined by the experimental data at the heated area of 13 mm x 13 mm. Normally, C_2 is 2.71 for the heated area of 13 mm x 13 mm, 7.16 for 8 mm x 8 mm and 0.317 for 38 mm x 38 mm, respectively. C_1 is introduced to consider the following phenomenon: Many electrons are backscattered from the target materials even if electron beam is irradiated to the target material normal to the beam axis. The backscattering ratio depends on the target materials and beam incidence angle. To determine heat flux on various materials, it is very important to evaluate each backscattered power. Deposited power ratio R is defined as the ratio of deposited power P_{dep} to irradiated power P_0. In this experiment, copper was selected as a calorimeter material because the thermal properties are well-known. For copper and carbon materials, each deposited power ratio R is 74.2 % and 93.0 %, respectively [9]. By considering the deposited power ratio for the copper, C_1 of 1.25 is obtained for carbon material. The acceleration voltage can not be changed in the KHI-test facility, and is fixed to 100 kV. In the present experiment, test samples are carbon materials (C_1=1.25) and heated area is specified for 8 mm x 8 mm (C_2=7.16). Therefore, Eq. (1) can be rewritten as follow;

$$q=893.5(I_{acc})0.8388 \qquad \text{[unit: MW/m2]} \qquad \ldots (2)$$

This correlation agrees well with the previous experimental results [8] within an accuracy better than ± 5%. Figure 2 shows typical beam profiles as a parameter of heated area [8]. In the figure, the ordinate represents the ratio of measured heat flux to the predicted average heat flux. Each beam profile is relatively flat over the heated area of smaller than 20 mm x 20 mm. Though experimental set-up was modified, there were no differences in the average heat flux with inclined electron gun and the profile compared to the previous results. Therefore, average heat flux and beam profile on the test sample can be evaluated from Eq. (2) and Fig. 2. Average heat flux evaluated is summarized in Fig. 3 as a function of electron current. At the electron beam currents of 0.33 A and 0.4 A with the heated area of 8 mm x 8 mm, average heat fluxes can be estimated to be 350 MW/m^2 and 410 MW/m^2, respectively.

2.2 TEST SAMPLE

We tested two carbon materials, IG-430U and CX-2002U, which are manufactured by Toyo Tanso Co., Ltd. IG-430U is an isotropic fine grained graphite, and CX-2002U

a 2-D felt type CFC made by chemical vapor impregnation (CVI) process. Major thermal properties of IG-430U and CX-2002U are listed in Table 2. The average thermal conductivity, at room temperature is around 150 W/m.K for IG-430U. CX-2002U has average thermal conductivity of 380 W/m.K perpendicular to the surface, which is parallel to the beam direction, and of 220 W/m.K parallel to the heated surface. Their thermal conductivities drastically decrease with increasing temperature. The specific heat, C_p, also depends on the temperature and gradually increases with temperature. The mass density of IG-430U is higher than that of CX-2002U by several percents because of it's low porosity. Before the experiment, all samples were cleaned and baked at a temperature of around 2000 °C in a halogen gas environment in order to purify them to high purity. In a vacuum environment, the samples are also degassed for several hours at 2000°C and then properly packed after their temperature decrease to room temperature. Typical dimensions of the test samples are 30 mm cube for IG-430U and 25 mm x 25 mm x 10 mm for CX-2002U.

3 THERMAL SHOCK TEST

3.1 TEST AND ANALYSIS PROCEDURES

In the present experiment, heating conditions are as follows: heat fluxes deposited on the test sample surface were selected to 350 and 410 MW/m2 for durations from 20 to 70 ms in order to investigate damages of the material for different heat fluxes due to the difficulty of higher heat flux operations. The heated area was kept at 8 mm x 8 mm, considering beam profile and heat flux. Each test sample was mounted on the test piece table made of stainless steel with a stainless steel bolt as shown in Fig. 1. No active cooling for the test sample was used. Each test sample was irradiated by only one shot to mitigate an influence of thermal cycles on damages of carbon materials. Eroded surfaces were observed with a scanning electron microscope (SEM) and a binocular microscope to investigate the surface morphology and the lifetime of the armor. Weight difference of each test sample was also measured by an electronic balance just before and after heating.

The experimental data were analyzed using a two-dimensional thermal analysis code [10] which takes account of evaporation process. In the analysis, effects of vapor shielding and particle emission on the erosion were not considered because of difficulties for the analytical modelling. Major thermal properties of IG-430U and CX-2002U are summarized in Table 2. Since measured data are limited in their thermal properties as a function of temperature as shown in the table, linearly extrapolated values were used for

temperatures higher than 900 K. Heat of sublimation was assumed to be a constant value of 59.4 MJ/kg for the carbon materials. Mass density was also assumed to be constant, i.e., 1810 kg/m^3 for IG-430U and 1700 kg/m^3 and for CX-2002U, respectively.

3.2 ERODED SURFACE OBSERVATIONS

Photos. 1 and 2 show typical surface morphologies of CX-2002U and IG-430U for heat fluxes of 350 and 410 MW/m^2, respectively. For CX-2002U, the surface morphology at the center region of the heated area is rough because fibers and matrix are found to be preferentially lost, while the impregnated materials, which has originally covered the carbon fibers, is left as seen in Photos. 1 (a) and 1 (c). At the heating boundary region, where the heat flux decreases drastically, only fibers are lost as shown in Photos. 1 (b) and (d). These facts reveal that thermal conductivities of the different phases of the CFC, i.e., the fiber, the impregnated material covering the fibers and the matrix, are slightly different from each other.

For IG-430U, each surface morphology as shown in Photo 2 is relatively smooth compared with those of CX-2002U. These photographs also show eroded surfaces under the heat flux condition of 410 MW/m^2 for different heating durations from 20 to 60 ms (see Photos 2 (c) - (d)). Below heating durations shorter than 20 ms, no difference on the heated surface was confirmed compared with that of the test sample before heating. Though an eroded surface appeared at the heating durations longer than 40 ms, no differences in the surface morphology after heat pulses of 40 and 60 ms could be found as shown in Photos 2 (c) - (d). Longer duration experiments were not performed because of larger evaporation and solid particle emission and of arcing problem in the electron gun. No cracks were observed in all specimens for heat fluxes up to 410 MW/m^2.

The erosion profile has also been measured along the center line of the heated area using a binocular microscope. Figures 4 and 5 show typical erosion profiles of CX-2002U and IG-430U at the constant absorbed energy of 24.5 MJ/m^2. The absorbed energy is defined as the average heat flux multiplied by the heating duration. The erosion depth is larger for higher heat fluxes even if the absorbed energy is kept to be constant. The measured erosion depths of the CX-2002U sample are scattered as shown in Fig. 4, while those of IG-430U are smooth. The reason for this difference is already explained above. The erosion depth of IG-430U is apparently larger than that of CX-2002U at the same heating condition because of its lower thermal conductivity. At the present experiment, each of the measured maximum erosion depths for heat fluxes of 350 and 410 MW/m^2 is

about 0.100 and 0.182 mm for CX-2002U, and is 0.190 and 0.266 mm for IG-430U, respectively. Measured erosion depth at the heated center region of IG-430U is 1.4 to 2.0 times larger than that of CX-2002U. Figure 6 also shows the erosion profile of IG-430U under conditions for heat flux and heating duration of 410 MW/m^2 and 20 to 60 ms. The erosion depth increases drastically with heating durations longer than 20 ms. Figure 7 shows a comparison between the experimental data on the erosion depth and the numerical results. The ordinate indicates an enhancement factor of the experimental erosion depth on the numerical erosion depth, i.e., the ratio of measured data to the analytical result. At the heated center region, only for the heating condition with a heat flux of 350 MW/m^2 and 70 ms duration the measured erosion depth of CX-2002U agrees well with the analytical result. This factor increases and deviates from analytical result with increasing heat flux. In particular, for CX-2002U, a large deviation of measured erosion depth to analytical result is observed for the heat flux of 410 MW/m^2. At the present experiment, the comparison factor is 1.0 to 1.5 for a heat flux of 350 MW/m^2 and is about 2.0 to 2.5 for a heat flux of 410 MW/m^2.

3.3 WEIGHT LOSS

Figures 8 and 9 show specific weight losses of IG-430U and CX-2002U as a function of absorbed energy for different heat fluxes, respectively. The weight loss of CX-2002U is apparently small compared with that of IG-430U at the same heating condition because of the high thermal conductivity. The weight loss increases with the absorbed energy. At constant absorbed energy, the weight loss is larger for higher heat fluxes.

Two-dimensional numerical predictions are also shown in Figs. 8 and 9. These figures can be rewritten as shown in Fig. 10. This figure shows the enhancement factor of the weight loss normalized by the numerical result as a parameter of the absorbed energy for different heat fluxes. For IG-430U, the enhancement factor increases linearly with absorbed energy. No different enhancement factor is found for heat fluxes of 350 and 410 MW/m^2. On the other hand, largely different enhancement factors as shown in Fig. 10 are observed in the CX-2002U sample for different heat fluxes. At an absorbed energy of 24.5 MJ/m^2, their factors are about 1.8 for IG-430U and 2.0 to 2.5 for CX-2002U, respectively.

In our previous papers [6, 11], an enhancement factor by 5 to 6 was reported in the CFCs. The enhancement factors in the present paper are a little bit smaller than that of

the previous data. This reason is that in the previous reports, a factor of 1.25 lower heat flux was applied in the numerical analysis because the heat flux and its profile were also measured with a cooper calorimeter, but were not considered the C_i value.

4. DISCUSSION

When the conventional thermal conduction code is applied for the thermal analysis simulating thermal shock heating conditions, the deviation of the experimental results from the numerical analyses should be caused by a combination effect consisting of solid particle emission, degassing and vapor shielding, which are not considered in the numerical analysis. If much degassing occurs due to intense heating, a large enhancement factor of the weight loss between experimental data and numerical result should be observed, while the enhancement factor of the erosion depth will not change so much. If strong vapor shielding occurs, this effect can be confirmed by the following phenomenon; each measured erosion profile for different heat fluxes should be different from each other because evaporated vapor spreads very fast and then the heat flux profile deposited on the surface changes. In the present experiment, little degassing and vapor shielding from the test sample could be confirmed by considering experimental and analytical results. Strong solid particle emission (including fiber emission) was also observed in all test samples. Therefore, effects of vapor shielding and degassing on the erosion and the weight loss are small in this experiment, and thus the deviation of the weight loss and the erosion depth between the experiment and the analysis is mainly attributable to solid particle emission.

Since the deposited heat flux level in the present experiment has not been simulated to the actual plasma disruption condition and experimental results reveal that higher heat fluxes slightly cause larger erosion depths at a constant absorbed energy, additional thermal shock experiments will be made to provide close simulation for FER/ITER.

5. CONCLUSION

Thermal shock tests were performed on various carbon materials under conditions for heat flux and absorbed energy to be up to 410 MW/m^2 and 24.5 MJ/m^2, respectively. The following results were obtained:

1. For absorbed energy higher than 15 MJ/m^2, each difference between experimental and numerical results in the weight loss and the erosion depth is mainly attributable to the solid particle emission of fibers and matrixes that are not considered in the numerical analysis. Effects of the degassing and vapor shielding on them are small

in the present experiment.

2. Surface morphology depends on the different phases of the CFC and their thermo-mechanical properties.

3. An enhancement factor of 2.0 to 2.5 compared with the erosion depth analysis is obtained for the lifetime estimation of the carbon material armor due to plasma disruption, though this factor increases with the heat flux.

References

[1] S. Yamamoto, et al., Tokamak Reactor Operation Scenario Based on Plasma Heating and Current Drive by Negative-Ion-Based Neutral Beam Injector, in *Proceedings of the 11th Int. Cof. on Plasma Physics and Controlled Nuclear Fusion Research*, Kyoto,1986, IAEA-CN-47/H-I-3

[2] K. Tomabechi, et al., ITER : Conceptual Design, in *Proceedings of the 13th Int. Cof. on Plasma Physics and Controlled Nuclear Fusion Research*, Washington, 1990, IAEA-CN-53/F-1-1

[3] T. Kuroda and G. Vieider, ITER Plasma Facing Components, ITER Documentation Series No. 30, International Atomic Energy Agency, Vienna (1990).

[4] M. Yamamoto, et al., Thermal Characteristic Test of Carbon Materials for PFC of JT-60U, **JAERI-M 90-119** (1990, in Japanese).

[5] C. D. Croessmann, et al., Correlation of Experimental and Theoretical Results for Vaporization by Simulated Disduption, *Journal of Nuclear Materials* **128 & 129** (1984) .

[6] M. Akiba, et al., High Heat Flux Experiments at JAERI, in *Proceedings of the 13th Symp. on Fusion Engineering*, Knoxville (1989) 529 -532.

[7] J. G. van der Laan, et al., Simulation and Analysis of the Response of Carbon-Fiber Composites and Pyrolytic Graphites to Off-Normal High Heat Loads, *Fusion Technology* **19** (1991) 2070-2075.

[8] M. Seki, et al., Improvement of an Electron Beam Facility as a Heat Source for Disruption Simulation Experiments, *Fusion Engineering and Design* **5** (1987) 215-220.

[9] S.Schiller, et al., Electron Beam Technology, John Wiley & Sons, New York, (1982).

[10] S. Yamazaki, et al., Two-Dimensional Disruption Thermal Analysis Code DREAM **JAERI-M 88-163** (1988, in Japanese).

[11] M. Seki, et al., Thermal shock tests on various materials of plasma facing component for FER/ITER, *Fusion Engineering and Design* **15** (1991) 59-74.

Table 1 Performances of the KHI-Test Facility

Acceleration Voltage (kV)	100
Acceleration Current (A)	up to 0.6
Pulse Duration (s)	0.01 - CW
Working Gas	none
Beam Species	Electron
Type of Ion/Electron Source	Solid State Electron Gun
Sweeping Coil	up to 1 MHz in two dim.
Predictable Heat Flux (MW/m^2)	820 at 100 kV, 0.5 A
Maximum Heating Area (m)	0.1 x 0.1
Water Cooling System	$2.4m^3$/hr with 1 MPa

Table 2 Typical Thermal Properties of IG-430U and CX-2002U

	IG-430U (fine grained graphite) Mass Density 1810 kg/m^3		CX-2002U (felt type CFC) Mass Density 1700 kg/m^3	
	Thermal Conductivity (W/mK)	Specific Heat (J/kgK)	Thermal Conductivity (W/mK)	Specific Heat (J/kgK)
at 300 K	155.0	718	381.1/215.0	718
at 400 K	140.0	1000	299.2/180.0	1000
at 500 K	130.0	1300	254.2/150.0	1267
at 700 K	100.0	1500	192.5/116.7	1555
at 900 K	78.3	1700	152.5/93.3	1717

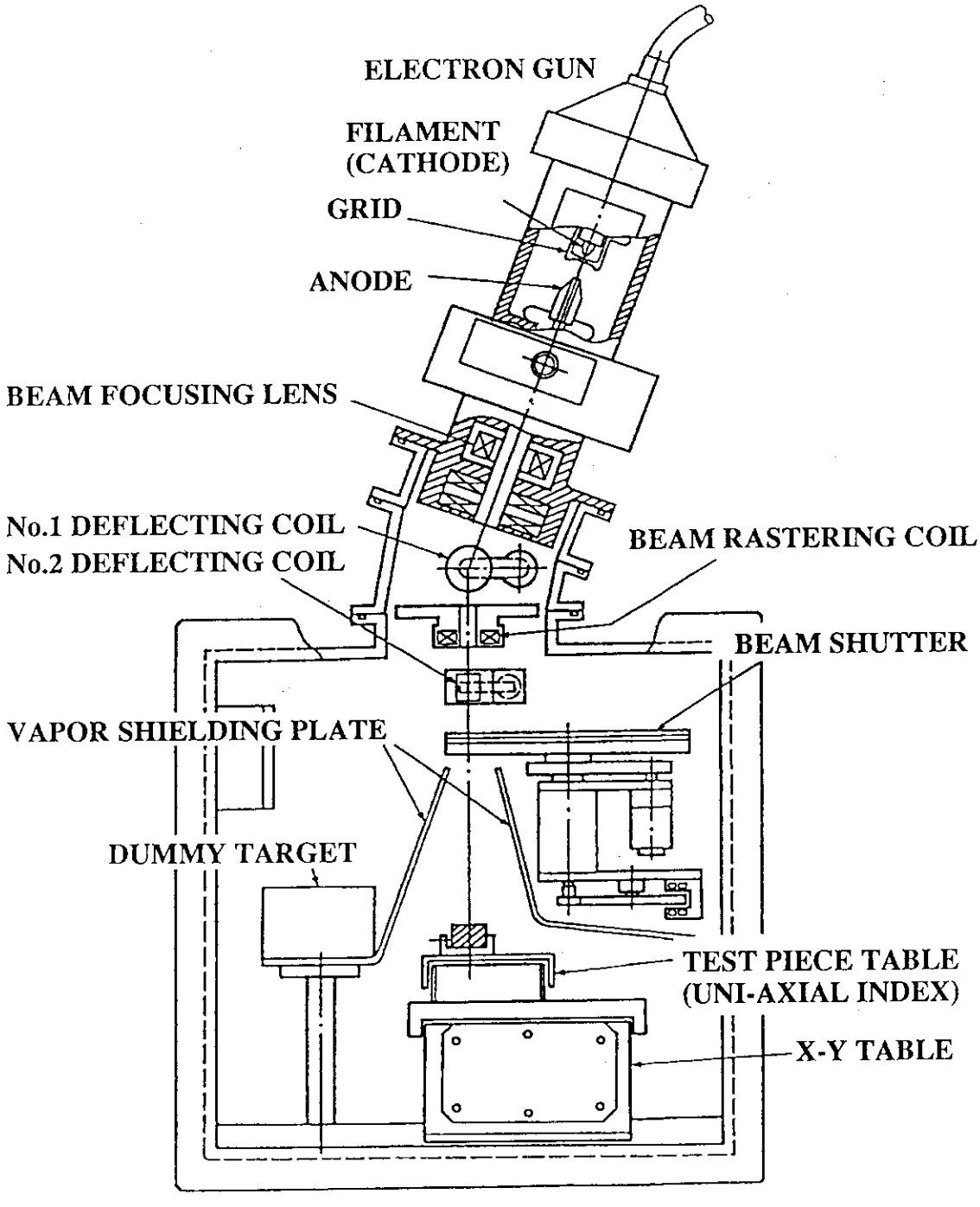

Fig. 1 Schematic View of the KHI-Test Facility

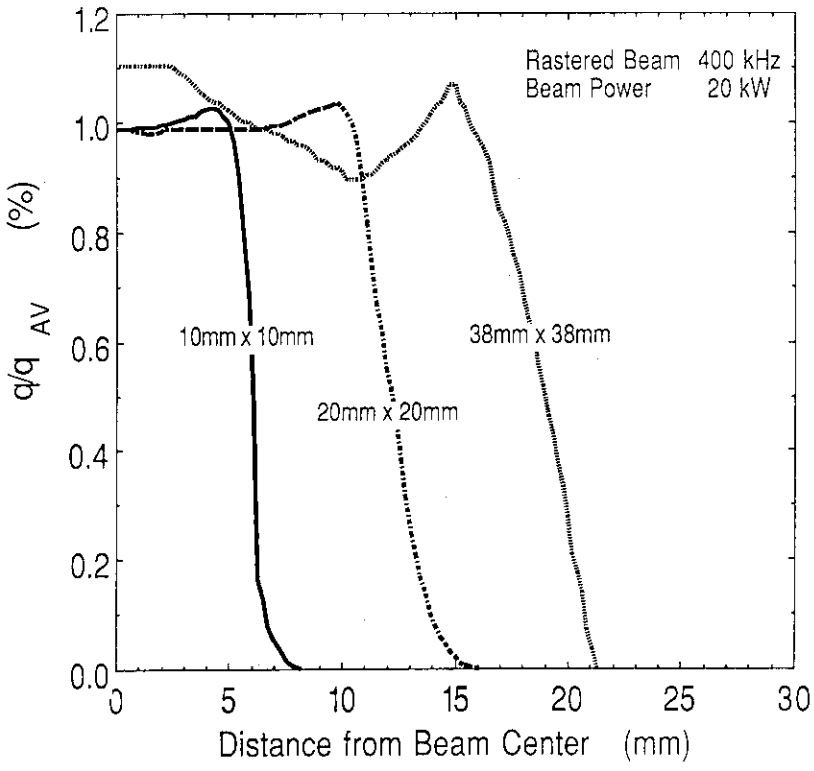

Fig. 2 Typical Beam Profiles as a Function of the Heated Area

The ordinate represents the ratio of measured heat flux to the predicted average heat flux.

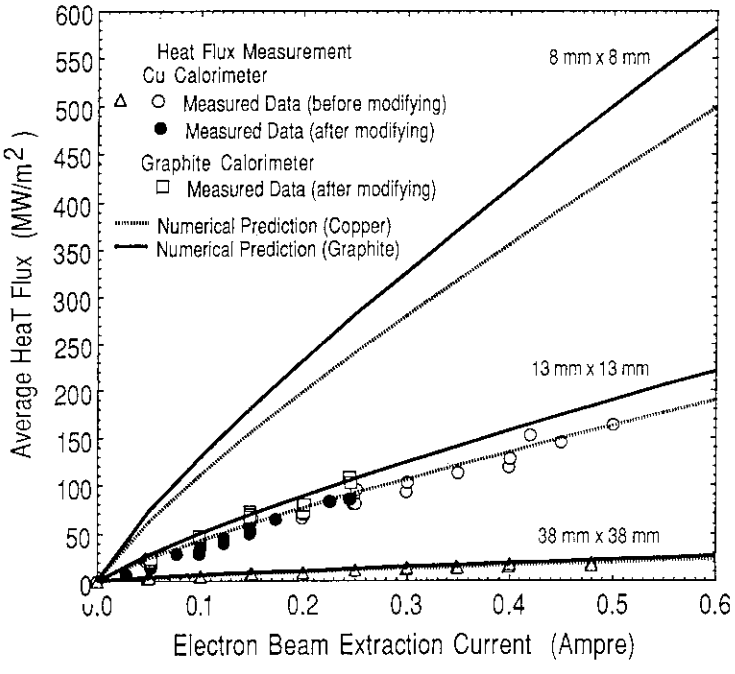

Fig. 3 Average Heat Fluxes as a Function of Electron Beam Current

Analytical heat fluxes for different heated area agree with the previous and the present experimental results within an accuracy better than ± 5%. For graphite material, average heat flux is factor of about 1.17 higher than that for copper material. In the present experiment, although heat fluxes at the heated area of 8 mm x 8 mm were not measured, they are predictable since good agreement between experimental data and numerical result at different heated areas are obtained.

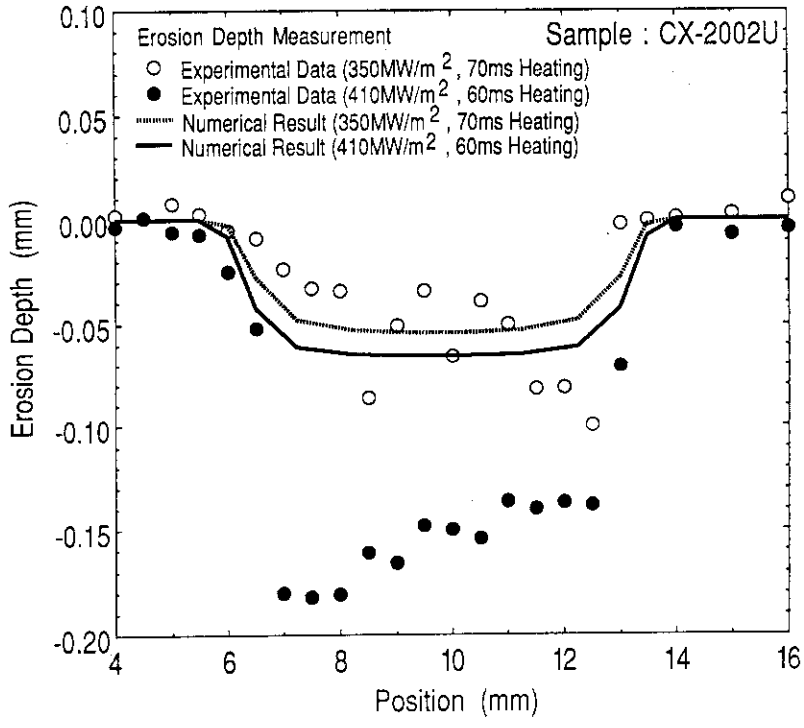

Fig. 4 Typical Erosion Profile of CX-2002U

Experimental data are scattered because fibers and matrixes are preferentially lost, while collapsed impregnated materials are left. At heat flux of 410 MW/m^2, large difference of the erosion depth between experimental and numerical results is observed.

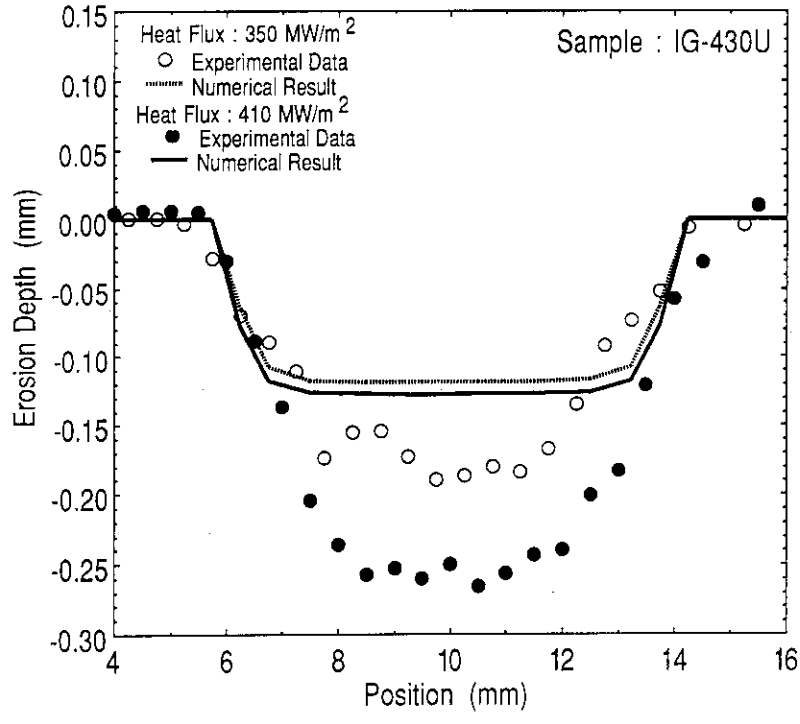

Fig. 5 Typical Erosion Profile of IG-430U

Erosion profile of IG-430U is relatively smooth. Higher heat heat flux causes larger erosion depth at a constant absorbed energy.

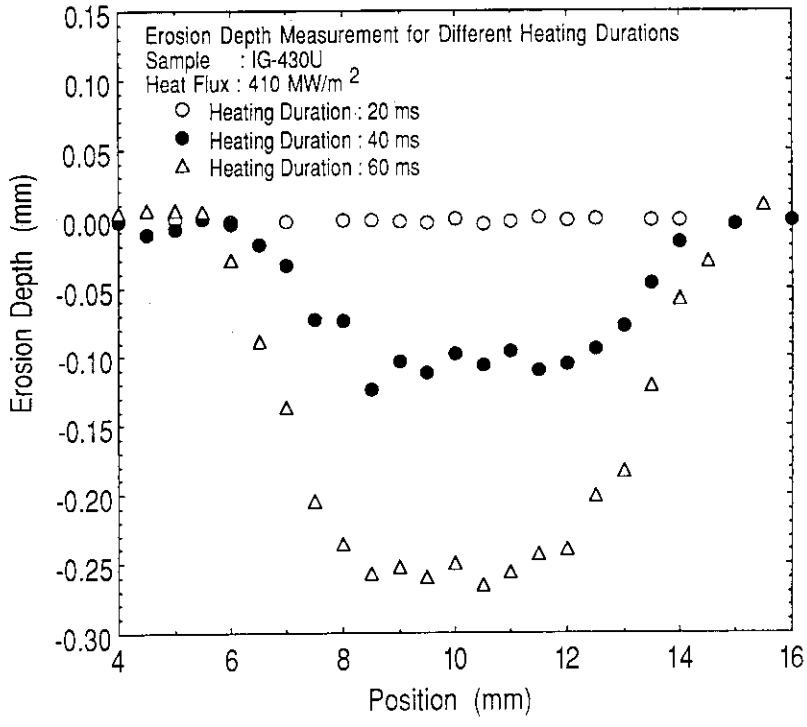

Fig. 6 Erosion Profiles of IG-430U as a Function of Heating Durations

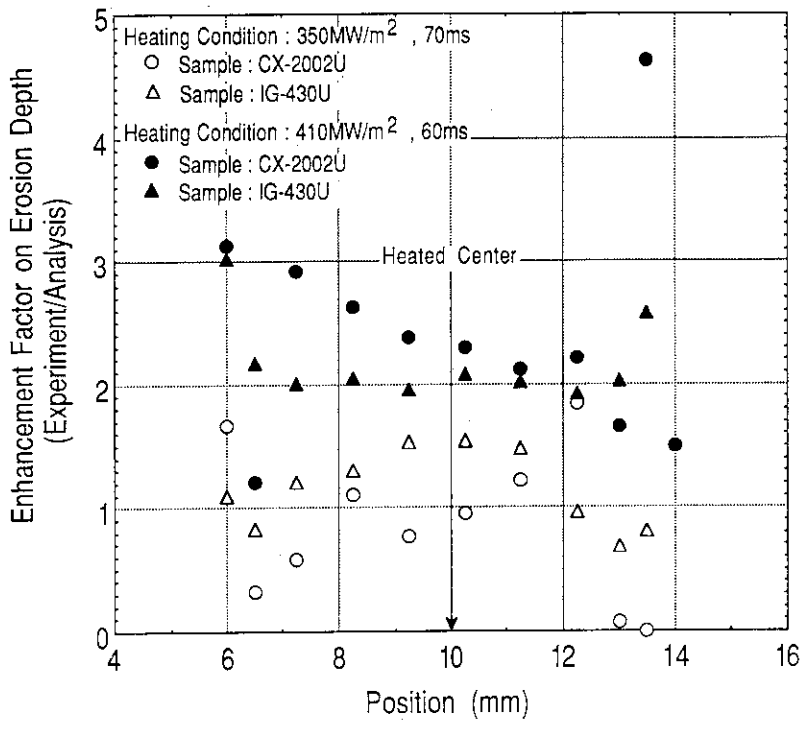

Fig. 7 Comparison of Erosion Depth Between Experiment and Analysis

At the heated center region, an enhancement factor on erosion depth between experiment and analysis increases with heat flux at a constant absorbed energy of 24.5 MJ/m^2.

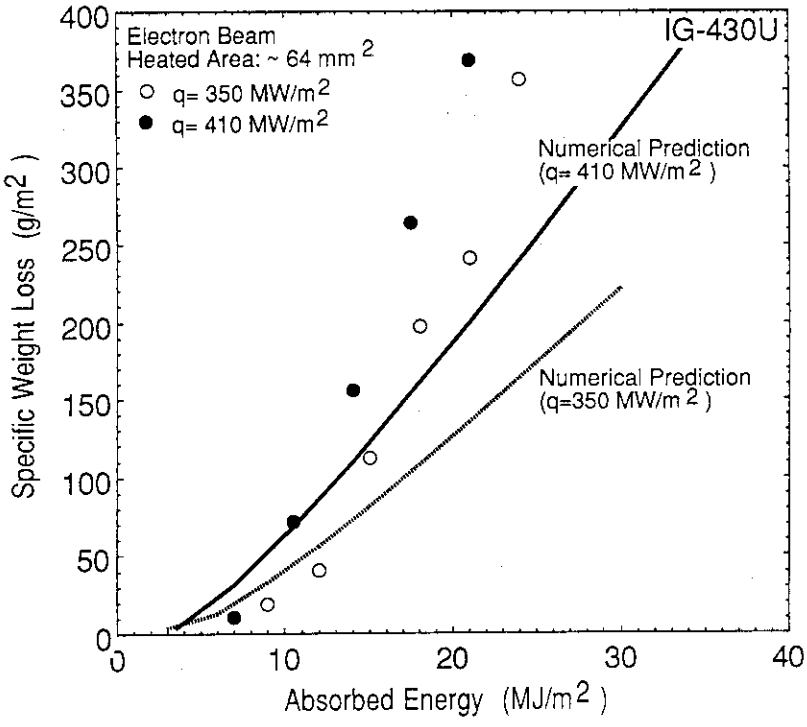

Fig. 8 Specific Weight Loss of IG-430U as a Function of the Absorbed Energy

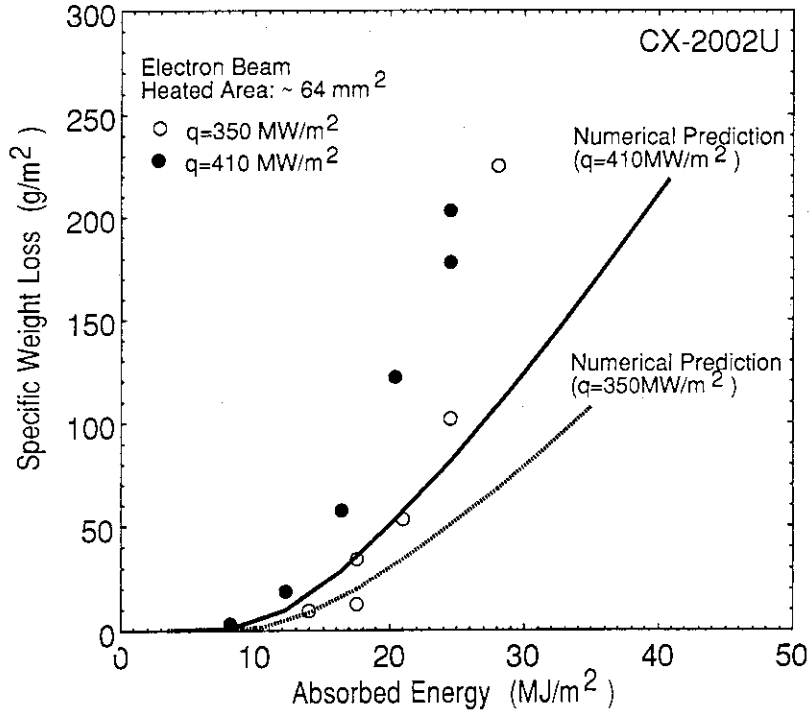

Fig. 9 Specific Weight Loss of CX-2002U as a Function of the Absorbed Energy

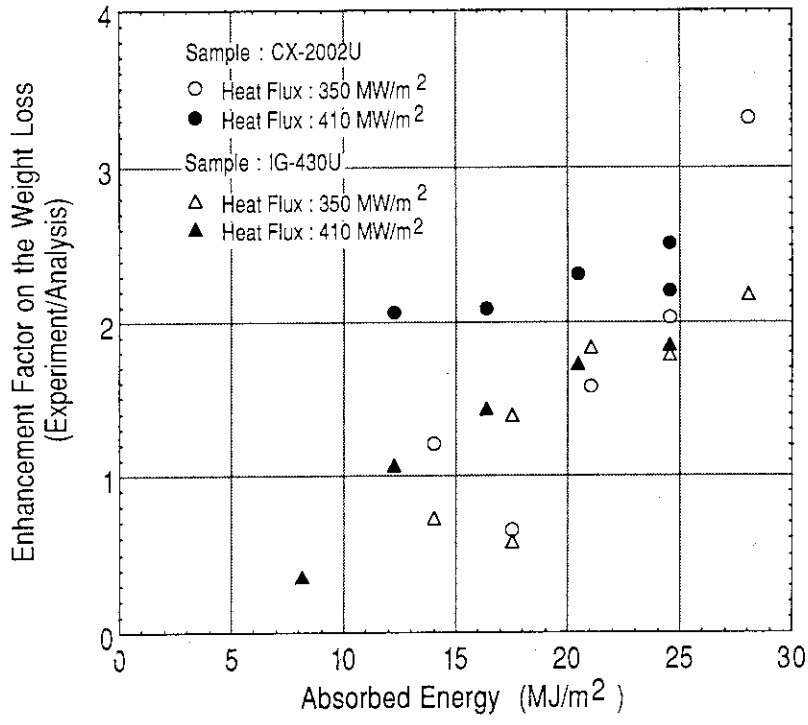

Fig. 10 Enhancement Factor on the Weight Loss Between Experimental and Analytical Results

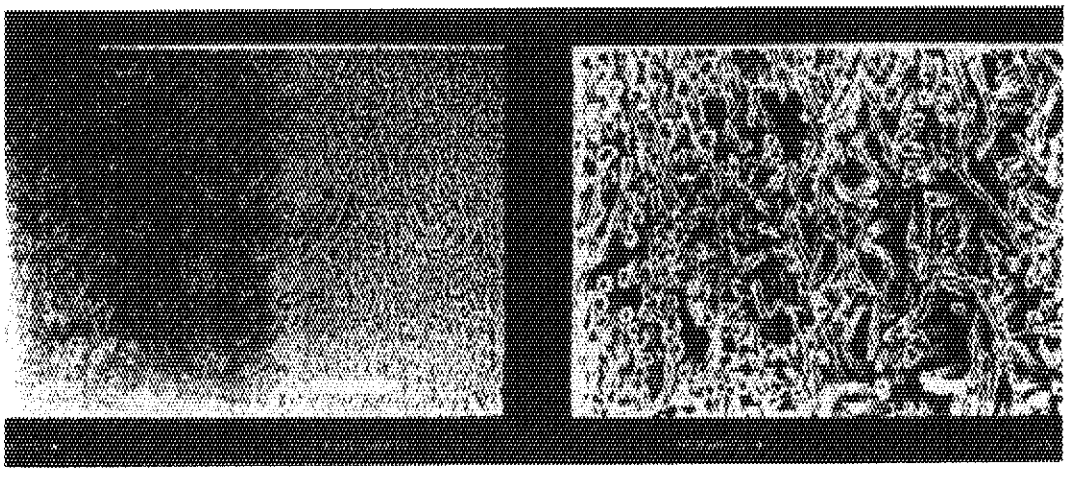

(c) at the boundary region (d) at the center region

q=410 MW/m^2, 60 ms heating

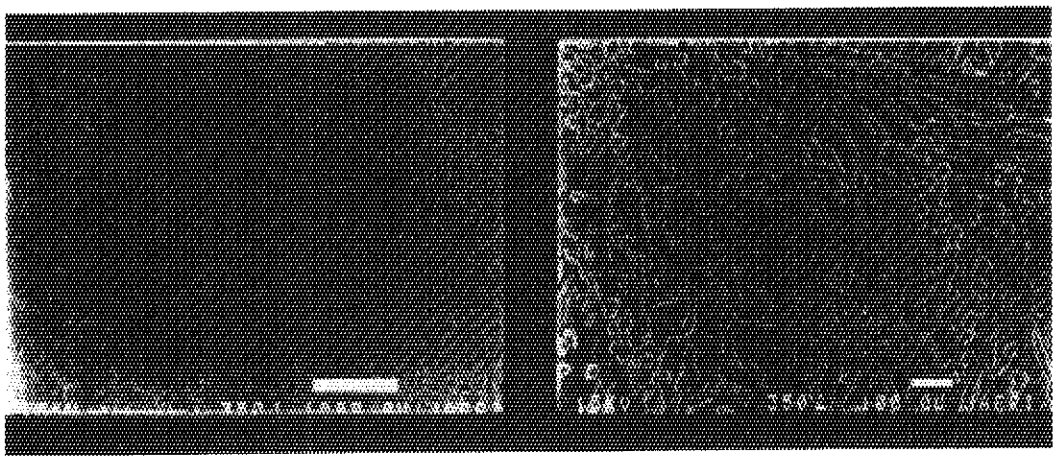

(a) at the boundary region (b) at the center region

q=350 MW/m^2, 70 ms heating

Photo. 1

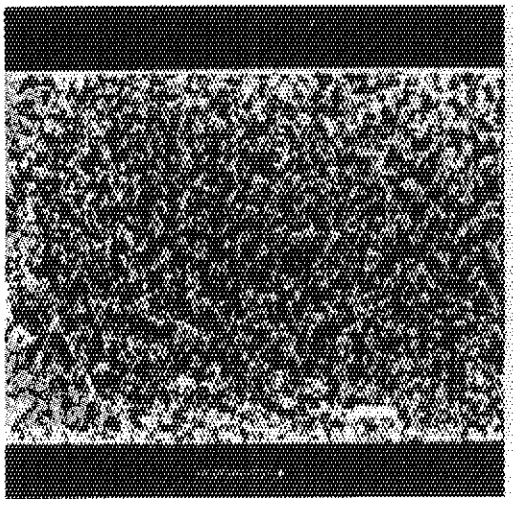

(c) q=410 MW/m^2, 40 ms heating

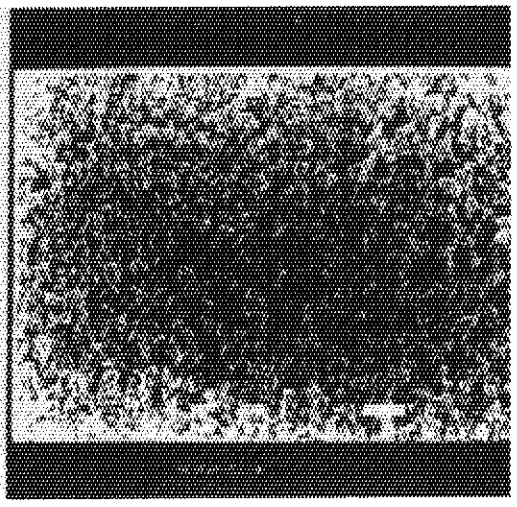

(d) q=410 MW/m^2, 60 ms heating

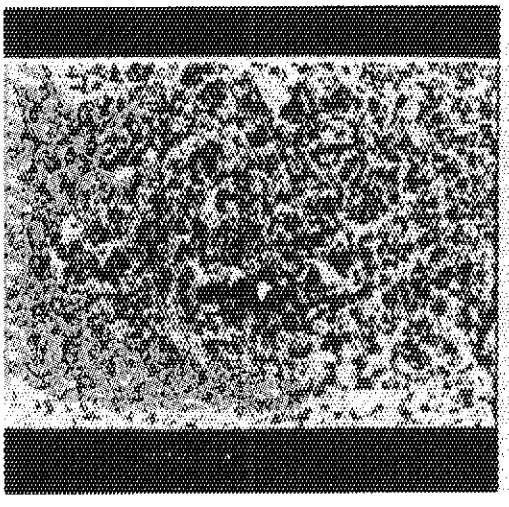

(a) q=350 MW/m^2, 70 ms heating

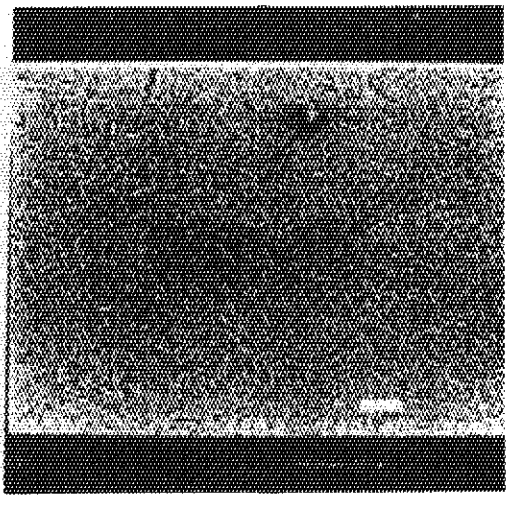

(b) q=410 MW/m^2, 20 ms heating

Photo. 2